University of Southampton

Faculty of Engineering and Physical Sciences

Optoelectronics Research Centre

Study of Partly Quenched Highly Erbium-Doped Fibre Amplifiers

by

Pablo Gerardo Rojas Hernández

Thesis for the degree of Doctor of Philosophy

September, 2019

University of Southampton

Abstract

Faculty of Engineering and Physical Sciences

Optoelectronics Research Centre

Thesis for the degree of Doctor of Philosophy

Study of Partly Quenched Highly Erbium-Doped Fibre Amplifiers

By Pablo Gerardo Rojas Hernández

This thesis reports an investigation of concentration quenching dynamics in the high-power regime and discusses a novel technique to get high-energy pulses with high gain by using short pulses on a short, highly-doped, partly-quenched fibre (referred to as the signal fibre amplifier, or fibre under test). The focus is not on the microscopic details of the concentration quenching, but the effects of quenching in the high-energy regime and to minimize its detrimental effects. As such, the results explore the impact of concentration quenching on amplification of high energy pulses at various pulse durations, in order to suppress the detrimental effects of quenching while keeping a short fibre length to limit optical nonlinearities. Erbium doped fibres are the focus in this thesis, due to their versatility, attractive operating wavelength range (e.g., 1.5 – 1.6 μm) and relative "eye-safety". Some of the work reported in this thesis was carried out in collaboration with Naval Research Laboratory.

The technique discussed in this thesis is based on two key steps: (1) The generation and subsequent absorption of pump energy by the signal fibre amplifier followed by (2) the extraction of energy by the signal pulse. There are two different techniques to optically pump the signal fibre amplifier studied in this thesis, one of them is core-pumping and the second is cladding-pumping, both of which are discussed in detail, including their advantages and disadvantages in the context.

Contrary to the generally held view of poor performance due to quenching dynamics in high concentration erbium fibres, this work demonstrates an efficient extraction of high energy from partly quenched high-concentration erbium doped fibre through amplification of short pulses. Although the quenching degrades the average-power efficiency of the amplifier, the pulse energy can remain high, and the results point to an increasingly promising outcome for shorter signal pulses in the ns to μs-range.

Even at low average-power efficiency, the highest achievable pulse energy is largely unaffected, and reached 9.5 times the intrinsic saturation energy in one erbium fibre, which corresponds to an amplified pulse energy of 0.8 mJ. These results are attributed to the rapid extraction of stored

energy, on time scales faster than the quenching dynamics. This shows it is possible to outperform the typical unquenched silica erbium-doped fibres in generation of energy per unit core area and length as well as gain per unit length. Thus, according to these results, signal pulses can be amplified to high-energies (approaching mJ-level) in short highly-erbium-doped fibres designed to reduce nonlinear distortions, at the expense of average-power efficiency.

Table of Contents

Table of Figures

Research Thesis: Declaration of Authorship

Print name:	Pablo Gerardo Rojas Hernández

Title of thesis:	Study of Partly Quenched Highly Erbium-Doped Fibre Amplifiers

I declare that this thesis and the work presented in it are my own and has been generated by me as the result of my own original research.

I confirm that:

1. This work was done wholly or mainly while in candidature for a research degree at this University;
2. Where any part of this thesis has previously been submitted for a degree or any other qualification at this University or any other institution, this has been clearly stated;
3. Where I have consulted the published work of others, this is always clearly attributed;
4. Where I have quoted from the work of others, the source is always given. With the exception of such quotations, this thesis is entirely my own work;
5. I have acknowledged all main sources of help;
6. Where the thesis is based on work done by myself jointly with others, I have made clear exactly what was done by others and what I have contributed myself;
7. Parts of this work have been published (see Appendix A List of Publications).

Signature:		Date:	

Acknowledgements

I would like to thank my supervisor, Professor Johan Nilsson for welcoming me onboard to his research group, High Power Fibre Laser. Also for his endless support, guidance and patient over the course of this research, which I will constantly repay with my time, work and, above all, loyalty.

In addition, I would like to thank my co-supervisor, Prof. Jayanta Sahu for his advice and assistance.

Furthermore, I would like to thank Dr. Belal Mohammad for his guidance and support in keeping my progress on track and encourage me adapt to explore the research community as a whole, which allow me to grow and achieve my goals. In addition to his companionship and support not only in my research, but also in my overall journey in the University of Southampton.

I am also thankful to work alongside capable researchers and students, who bring me not only their advice, but constant support in all aspects of my life through my studies. I would like to particularly mention Dr. Shankar Pidishety for his time during discussions and work on the lab. As well as fellow research students, with special mention to Angeles Camacho, Norberto Ramirez and Soonki Hong, for enriching my life with their companionship, support and friendship during my studies.

Next, I would like to express my gratitude to Prof. Michalis Zervas for his helpful suggestions and advice regarding the study presented in this thesis, as well as Dr. Kyle Bottrill who provided companionship and support in this research.

My special thanks to Dr. Colin Baker, Dr. Joe Friebele, and their colleagues at the U.S. Naval Research Laboratory for receiving me in their facilities, and more importantly, providing erbium-doped fibres to support this research. My accomplishments and further understanding on the quenching dynamics rely greatly on their invaluable contribution and feedback.

Most importantly, I would like to thank all my family members as well as my dear friends back in Mexico for providing moral support during this ordeal. With special thanks to my parents, Dr. Crisantema Hernandez Gonzalez, Mr. Pablo Rojas Zepeda and my brother Dr. David Rojas Hernandez for their unconditional love, sacrifices and motivation. Without them, this journey would have never been possible.

Finally, I would like to thank the University Research program of Northrop Grumman Mission Systems and National Council for Science and Technology (CONACyT), Mexico for their support in funding this research.

List of Abbreviations

SM	Single-mode
DCF	Double-clad fibre
CW	Continuous-wave
EDFA	Erbium-doped fibre amplifiers
FUT	Fibre under test
TIR	Total internal reflection
NA	Numerical aperture
ASE	Amplified spontaneous emission
EDF	Erbium-doped fibre
PRF	Pulse repetition frequency
EOM	Electro-optic modulator
AOM	Acoustic-optic modulator
SNR	Signal-to-noise-ratio
ESA	Excited state absorption
SRS	Stimulated Raman scattering
SBS	Stimulated Brillouin scattering
SPM	Self-phase modulation
WDM	Wavelength division multiplexing
OSA	Optical spectrum analyser

TLS	Tuneable laser source
EYDFA	Erbium-ytterbium co-doped fibre amplifier
FNE	Frantz-Nodvik equation
MCVD	Modified chemical vapor deposition
YDFA	Ytterbium-doped fibre amplifier
DL	Diode lasers

Chapter 1 Introduction

The field of fibre lasers was born in 1961 when Elias Snitzer first published his famous paper on laser oscillation in glass and then on the possibility of fibre operation [1]. Among the numerous advantages of fibre lasers are, nowadays, established fabrication procedures, low loss, and the possibility of pumping with compact, efficient diode lasers. The fibre itself provides the waveguide and gain media, with a broad gain bandwidth. The availability of various fibre components minimizes the need for bulk optics and mechanical alignment.

Fibre lasers need to be pumped optically, either through core-pumping or cladding pumping, and thus, the properties of the pump source and pump waveguide are crucial for high-power fibre lasers. Practical fibre lasers typically depend on diode lasers for pumping. The power produced by fibre lasers is restricted by the amount of pump light coupled into them. Single-mode (SM) fibre lasers were originally pumped by single-mode pump diodes. However, commercial single-mode diode lasers (DLs) are limited in power to the watt-level, and though a fibre can be pumped by several diodes, the output power from a fibre laser is still limited to one or a few watts with such pump sources.

However, a breakthrough idea, referred to as cladding-pumping, proposed by Maurer for pumping with (non-laser) light-emitting diodes, patented by James Kafka at Spectra Physics for DL-pumping, and demonstrated by Elias Snitzer (2, 3), changed the perspective. In double-clad fibre (DCF), the laser light propagates in a single-mode (or relatively small multimode) core, which is surrounded by an inner cladding in which the pump light propagates. The inner cladding has a significantly larger area than the core, so it can support a large number of propagation modes, allowing the efficient launch of multimode pump diodes. This opened up a vast opportunity to scale output power in devices that combined, at the same time, high efficiency and excellent spatial beam quality for continuous-wave (CW) and pulsed lasers. However, although fibres have a number of beneficial properties for pulse generation, the high nonlinearity severely limits the performance of fibre lasers, particularly in terms of pulse energy and peak power [4]. This is a particular concern with cladding-pumping, since it reduces the pump absorption per unit length and therefore increases the fibre length.

This thesis focuses mainly on erbium-doped fibre amplifiers, which enable versatile and compact optical sources (e.g., [5, 6]), and can be readily cladding-pumped with over 100 W of power from 980-nm diode lasers at relatively low cost. Their emission wavelength range of $\sim 1.5 – 1.6$ µm offers good atmospheric transmission as well as relative “eye-safety”, highly desirable for LIDAR (“light imaging, detection and ranging”), remote sensing, and imaging [7].

However, in terms of performance of power scaling in the high-power regime, numerous limitations regarding fibre laser sources and amplifiers had been encountered. This thesis reports the study of a particular dynamic happening in rare-earth doped fibres (e.g., erbium-doped fibre amplifiers), with a focus on the high-energy pulse regime. Although there are likely to be several quenching mechanisms due to the harmful interaction between Er^{3+}-ions, erbium clustering and especially pair formation are often assumed to be key factors in glasses commonly used for erbium doped fibre amplifiers (EDFAs) [8]. It increases with concentration and is therefore often referred to as concentration-quenching. It is mitigated by lower concentration, but undesirably, this also reduces the absorption. The low absorption in EDFAs is further exacerbated by from the weak absorption cross-sections of Er^{3+}-ions.

1.1 Motivations

The erbium-doped fibre amplifier is one of the most important rare-earth doped fibre amplifiers, as well as one of the most extensively studied. Although EDFAs suffer from low pump absorption, the advantages provided by its operating wavelength (e.g., 1.5 – 1.6 μm) often outweighs this disadvantage, offering relatively "eye-safe" operation and allowing high atmospheric transmission for LIDAR, remote sensing and imaging [7]. Compared to "bulk" laser systems, erbium-doped fibre amplifiers allow for compact systems with performance in many respects comparable or even superior, or at least adequate for applications, at much lower cost of manufacturing and maintenance.

Nevertheless, there has always been the need to reach higher power, and while there have been many improvements over the years, there are still strong limitations that comes with the use of optical fibres. In order to cope with the need for high-power fibre lasers, high doping concentration is required to reach sufficient pump absorption in a cladding-pumped fibre. However, this may lead to concentration quenching effects, inducing excessive losses. This is often quantified in terms of the resulting unsaturable absorption or loss. To solve these issues, the system could rely on longer fibres with lower doping concentration, diminishing the detrimental effects of quenching. However, longer fibres could lead to unwanted optical nonlinear effects exacerbated by tightly confined waveguide modes. This issue can be mitigated by the use of a short fibre, but this requires higher concentrations, and thus possible concentration quenching.

As a possible way to solve this challenge, this thesis presents an investigation of the possibility to extract and supply energy to quenched erbium-doped fibre amplifiers on time-scales that are fast compared to the quenching dynamics, which thus reduces the effects of quenching. Specifically, if it is possible to reach high gain in a fibre then this means that there is significant stored energy,

which may be possible to extract in a short signal pulse even in the presence of absorption that the quenching renders unsaturable under other operating conditions.

In addition to losses as a pulse propagates through an amplifier, there are also losses between the pulses, as the pump builds up the population inversion and thus the energy stored in the amplifier. These losses depend on the details of the pumping. In case of CW-pumping, the losses to quenching may be high during the slow build-up of stored energy. I therefore also consider pumping with high-energy pulses of durations considerably shorter than the pulse period. Note that in contrast to what is typical for so-called QCW-pumped solid-state lasers, the pump duration is also much shorter than the fluorescence lifetime. Pump pulse durations may be in the range of nanoseconds to tens of microseconds, with mJ-level pulse energy. This translates to pump peak powers of at least ~100 W and possibly approaching 1 MW. Unfortunately, diode lasers are comparatively poor for the generation of high peak powers. While the 100-W level may well be realistic and cost-effective, the MW-level pumping is beyond the practical reach of diode lasers. Therefore, the study of pulse pumping system focuses on an architecture known as tandem-pumping [9], in which a signal gain fibre is pumped by a fibre laser configured to generate high-energy pump pulses with suitable peak power and duration.

This thesis presents an in-depth investigation of the quenching dynamics in several highly-doped, partly-quenched (in which it is still possible to achieve amplification) or fully-quenched (amplification not possible) erbium doped fibres and signal transmission (including amplification) characteristics in the high-energy regime. This work quantifies the quenching through the fractional unsaturable absorption present in the fibre under test in amplifier configuration. Having said that, it is worth remembering that this is a simplified description of quenching, and that this thesis does not claim to fully explain the precise details of the quenching dynamics, but rather, show that the results presented in this work demonstrate a novel, optimal method for efficient energy extraction in highly-doped, partly-quenched erbium doped fibre amplifiers, surpassing the conventional methods. Pumping is important. Erbium-doped fibres can be pumped at 0.98 µm or around 1.5 µm (in-band pumping), continuous-wave or with pulses, in the core or in the cladding. These constitute eight distinct options, each with different advantages and achievable parameters such as average power. The complexity, availability, and practicality of different pump sources must be considered, too. I have studied several, but not all, of these options. Even more options can be considered, e.g., the duration of the pump pulses relative to the signal pulses. If, for example, the durations are comparable, then the temporal overlap and timing between signal and pulse becomes important. Most of my work is on relatively long pump pulses and short signal pulses. Co-directional vs. counter-directional pumping can be important, too. This is discussed in the thesis but not comprehensively investigated.

1.2 Thesis Outline

The thesis is structured as follows:

Chapter 2 discusses the rare-earth doped fibre technologies, continuous-wave and pulses laser operation, with focus on erbium-doped fibres. This includes a brief discussion of the issues and limitations regarding fibre lasers and amplifier technologies in the high-power regime, such as quenching dynamics and nonlinear effects. Additionally, it discusses the method in which all the pulse energy measurements were determined in this thesis.

Chapter 3 discusses the initial investigations for pumping options, since there are a wide variety of pump sources regarding their temporal formats, wavelength etc. It includes the discussion of modelling and simulations used to study the pump absorption and the signal gain that can be obtained with tandem pumping with an Er-doped fibre source, including the dependence on signal wavelength. Core- and cladding-pumping are considered, in continuous-wave and pulsed regime, as well as the pump wavelength. Chapter 3 further contains experimental results and discussions on different erbium doped fibres with various doping concentration and different modes of laser operation (such as pulsed or CW-pumping, as well as different pump wavelengths.

Chapter 4 shows the quenching dynamics for different Er-doped fibres-under-test (FUT) in amplifier configurations, using a CW pump source at 980 nm. This chapter also includes an in-depth discussion over the results, and a summary of the most efficient route to obtaining high extractable energy from partly quenched erbium doped fibre amplifiers, up to 0.8 mJ of pulse energy when seeded by 0.2 µs, 23 µJ pulses.

Chapter 5 continues investigating the performance of the fibre under tests (FUTs) through simulations, exploring high energy pulses at 980 nm, using a cladding-pumping configuration. It includes discussion and theoretical results, based on simulations, between pulsed and CW-pumping.

Chapter 6 presents a millijoule-level pulse pump source based on a large core ytterbium-doped fibre amplifier, achieving over 4-mJ of energy extraction and 0.8-kW peak power at 976 nm, with 27% pump conversion efficiency. The amplifier configuration uses a co- and core-pumping scheme, on a 1-meter fibre length, delivering microsecond pulses (e.g., 10-µs) at adjustable pulse repetition frequency (e.g., 1 kHz).

Chapter 7 concludes with a summary of the work presented in this thesis as well as discussing future research directions based on these results and newfound knowledge of the quenching dynamics in the high-power regime.

1.3 References

1. Snitzer E., “Proposed fibre cavities for optical masers”, Journal Applied Physics **32**(1), 36-39.
2. Maurer, U.S Patent 3,808,549 (April 30, 1974).
3. J. Kafka, U.S. Patent 4,829,529 (May 9, 1989).
4. Siegman, A. E., (1986), “Lasers”, University Science Books, pages, 368 (1961).
5. B. Desthieux, R. I. Laming, and D. N. Payne, “111 kW (0.5 mJ) pulse amplification at 1.5 µm using a gated cascade of three erbium-doped fibre amplifiers”, Applied Physics Letters **63**, 586-588 (1993).
6. V. Philippov, C. Codemard, Y. Jeong, C. Alegria, J. K. Sahu, J. Nilsson, and G. N. Pearson, “High-energy in-fibre pulse amplification for coherent lidar applications”, Optics Letters **29**, 2590-2592 (2004).
7. J. W. Nicholson, A. DeSantolo, M. F. Yan, P. Wisk, B. Mangan, G. Puc, A. W. Yu, and M. A. Stephen, “High energy, 1572.3 nm pulses for CO2 LIDAR from a polarization-maintaining, very-large- mode-area, Er-doped fibre amplifier”, Optics Express **24**, 19961-19968 (2016).
8. B. J. Ainslie, S. P. Craig, S. T. Davey, and B. Wakefield, “The fabrication, assessment and optical properties of high-concentration Nd3+ and Er3+ doped silica-based fibres”, Materials Letters **6**, 139-143 (1988).
9. Zhu S., “Pulsed tandem-pumping of ytterbium-doped fibre laser for avoiding photodarkening”, Optical Research Centre, University of Southampton, (2015).

Chapter 2 Background

Scaling the output power from lasers in wide range of operating regimes to meet the needs of new and ever-more demanding applications has come a long way since the first working laser was demonstrated. In this regard, high-power fibre lasers occupy one of the most challenging and demanding place in the field of fibre laser technology. Both continuous wave and pulsed high-power fibre laser systems constantly require technological advances. In order to cope with this, the most prominent approach at present is the development and study of rare-earth doped fibres. However, in terms of performance, the rare-earth doped fibres still have much room for improvement, especially on the suppression of nonlinear effects and other parasitic effects resulting from the properties of the rare-earth ions.

In this chapter, the first section discusses the principles and most important features of the optical fibres and the properties of the rare-earth ions. The second section discusses the characteristics of the CW and pulsed laser regime, as well as describing the main challenges and limitations in the development of high-power fibre lasers.

2.1 Optical Properties and Optical Spectroscopy of Rare Earth Doped Fibres

2.1.1 Principles of Optical Fibres

The main properties of laser (light) propagation in an optical waveguide are determined by total internal reflection (TIR). TIR takes place when light that propagates in a medium with refractive index of n_1, can be reflected from the boundary between this medium and another medium with a refractive index of n_2, which is less than n_1. The condition of TIR takes place for angles-of-incidence larger than a certain angle known as the critical angle.

In the simplest form, an optical fibre consists of a central glass core surrounded by a cladding layer whose refractive index n_c is slightly lower than the core index n_1. If the refractive indices of the core and cladding are constant then the fibre is referred to as step-index fibre. Figure (Fig.) 2.1 shows schematically the cross section and refractive index profile of a step-index fibre [1]. Two parameters that characterize an optical fibre are the relative core-cladding index difference and the so called V-parameter, defined by equation (Eq.) 2.1:

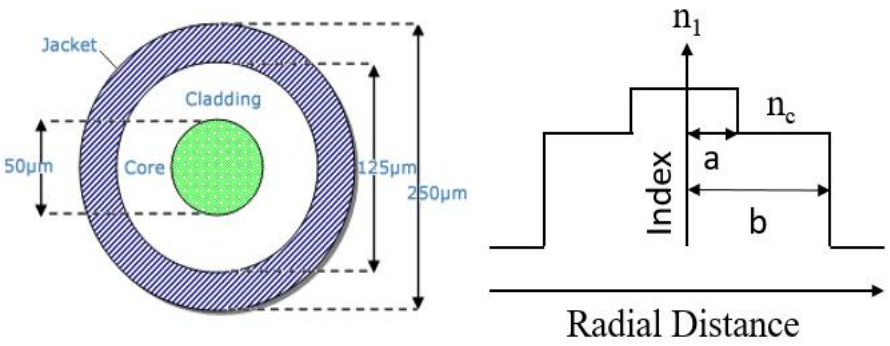

Figure 2.1 Schematic illustration of the cross section of a step-index fibre.

$$V = \frac{2\pi}{\lambda} * a * \sqrt{n_{core}^2 - n_{clad}^2} = \frac{2\pi}{\lambda} * a * NA \tag{2.1}$$

The V-parameter is determined by the operating wavelength (λ), the core radius (a) and the numerical aperture (*NA*), whereas the numerical aperture depends on the refractive index of the core (n_{core}) and the cladding (n_{clad}) respectively, as described by Eq. 2.1.

The V-parameter determines the number of modes supported by the fibre as well as the fraction of the optical power in a certain mode that is confined to the fibre core. For V values below ≈ 2.405 a step-index fibre supports only one mode (this so-called cut-off value is different for different refractive-index profiles). Optical fibres designed to satisfy this condition are called single-mode fibres and fibres with higher V values are called multimode fibres (i.e., able to guide more than one optical mode) [1].

The core-cladding index difference determines the NA of the optical fibre, which determines the range of angles within which the light will be transmitted along it. In a single-mode fibre, the waveguide is strong enough to balance diffraction only for a single mode. As diffraction becomes stronger for smaller modes, fibres with small cores require a larger numerical aperture for proper guiding.

Rare-earth doped fibre lasers dissipate heat because of two main reasons; first, the energy difference between pump and laser photons is lost to the glass host in the form of non-radiative transitions from the absorption band to the upper-lasing level. This constitutes the minimum fraction of absorbed pump power that is dissipated as heat. Second, the quantum efficiency (ϕ) of the laser transition is in practice less than unity because the non-radiative decay rate from the lasing level is non-zero; thus a fraction $1 - \phi$ (λ_{pump} / λ_{signal}) of the pump power is dissipated as heat. The non-radiative decay rate consists of several contributions, including ion-ion energy transfer effects like concentration quenching [2]. However, the thermal stress can be mitigated through the

use of a larger surface area that relieves the heat load in the fibre. In addition to the laser cycle, also propagation losses can lead to heating.

Although heatsinking is a critical aspect of lasers, the fibre geometry with a large surface/volume ratio of the laser-active (doped) region is highly beneficial for thermal management. Therefore, fibre lasers were for a long time considered immune to thermally induced degradation of laser parameters such as beam quality. Although this is no longer true as fibre lasers go far beyond 100 W in large cores, thermal effects are expected to be small at the power levels and core diameters I have used. We note also that also other laser geometries have been developed to better manage with the thermal load, notably disk lasers. [3].

2.1.2 Double-Clad Optical Fibres

Double-clad optical fibres make it possible to use low-brightness, low-cost, and high-power laser diodes as a pumping source for fibre lasers and amplifiers. Cladding pumping technology allows significant scaling of power, currently to over 10 kW in single-mode operation.

A double-clad fibre (DCF) is an optical fibre with two claddings, inner and outer, that are equally important for light propagation. As for a single-clad fibre, there is a core surrounded by a cladding (the inner cladding) that acts as a waveguide for the signal. The main difference between single-clad fibre and double-clad fibre is the value of the refractive index of the layer surrounding the inner cladding, i.e., the outer cladding or coating. This difference allows waveguided propagation of light (i.e., the pump) inside the inner cladding of the double clad fibre. By contrast, the cladding of the single-clad fibre is not designed to be a waveguide. Usually in both cases of single- and double-clad fibres, the outer cladding (or coating) is made of a polymer, which has a lower refractive index in the case of double-clad fibres. Fig. 2.2 shows a schematic and the refractive index profile of a double-clad fibre [4].

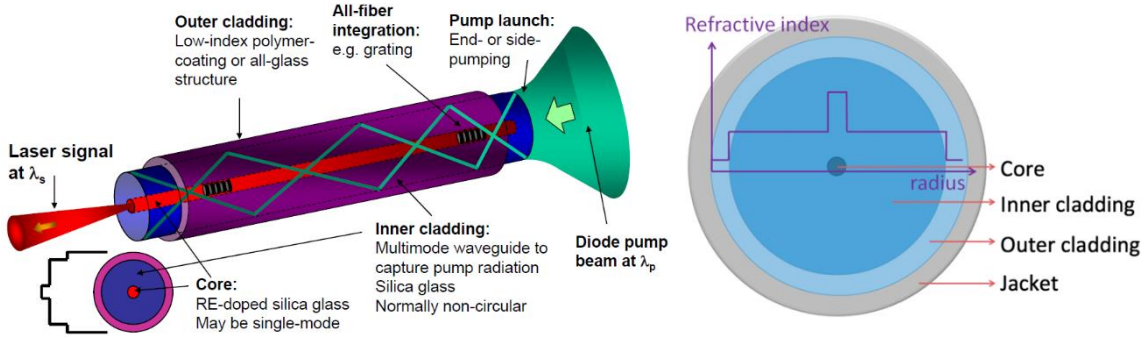

Figure 2.2 Schematic illustration of the cross section, features and the refractive index profile of a double clad optical fibre [4].

One well known advantage of the double-clad geometry is that it facilitates side-pumping by high-power laser diodes [5]. In a typical DCF with polymer outer cladding, the numerical aperture between the core and first cladding is NA_c = 0.1, corresponding to a refractive index Δn = 0.0034; the NA between the first and second cladding is NA_1 = 0.46 corresponding to a Δn = 0.115, thus allowing efficient coupling from laser diodes with relatively large NA.

However, there are many potential limitations with double-clad fibre lasers. The maximum output power that may be generated remains limited from the fibre propagation losses, high-intensity nonlinear effects (Raman and Brillouin gain) and concentration quenching. These limitations are discussed in detail in Chapter 2.2.

2.1.3 Rare-Earth Doped Fibres

Cladding-pumping of rare earth doped fibres can convert pump light from high-power multimode diodes lasers into another light with higher brightness. These rare-earth ions absorb pump light at a shorter wavelength than the laser or amplifier emission wavelength. Power is lost in the conversion, but in addition to the improvement in brightness, the converted light can also be improved in terms of generation of pulses. Both these effects allow for higher intensity on the target, which increases the peak intensity and allows for more efficient light-matter interaction [6,7].

The composition of the glass host has important effects on the rare-earth dopant, silica being one of the most common glass-hosts. Pure silica, however, is not a suitable host for active fibres due to its low solubility for rare-earth ions, leading to quenching even at moderate concentrations. Alumino-silicate, on the other hand, is a much better host in this respect, permitting rare-earth doped fibres with much higher doping concentration, leading to a more efficient pump light absorption (α), as shown in Eq. 2.2.

$$\alpha = N_0 \sigma_{abs} \tag{2.2}$$

The absorption coefficient α is determined by the rare-earth doping concentration (N_0) and the absorption-cross-section (σ_{abs}). Commonly, an erbium-doped fibre (EDF) is pumped at 980 nm. This is further elaborated in Chapter 2.1.4. The cross-section spectra from an Er^{+3}: Aluminosilicate used for the analysis of EDF is shown in Fig. 2.3 [8, 9].

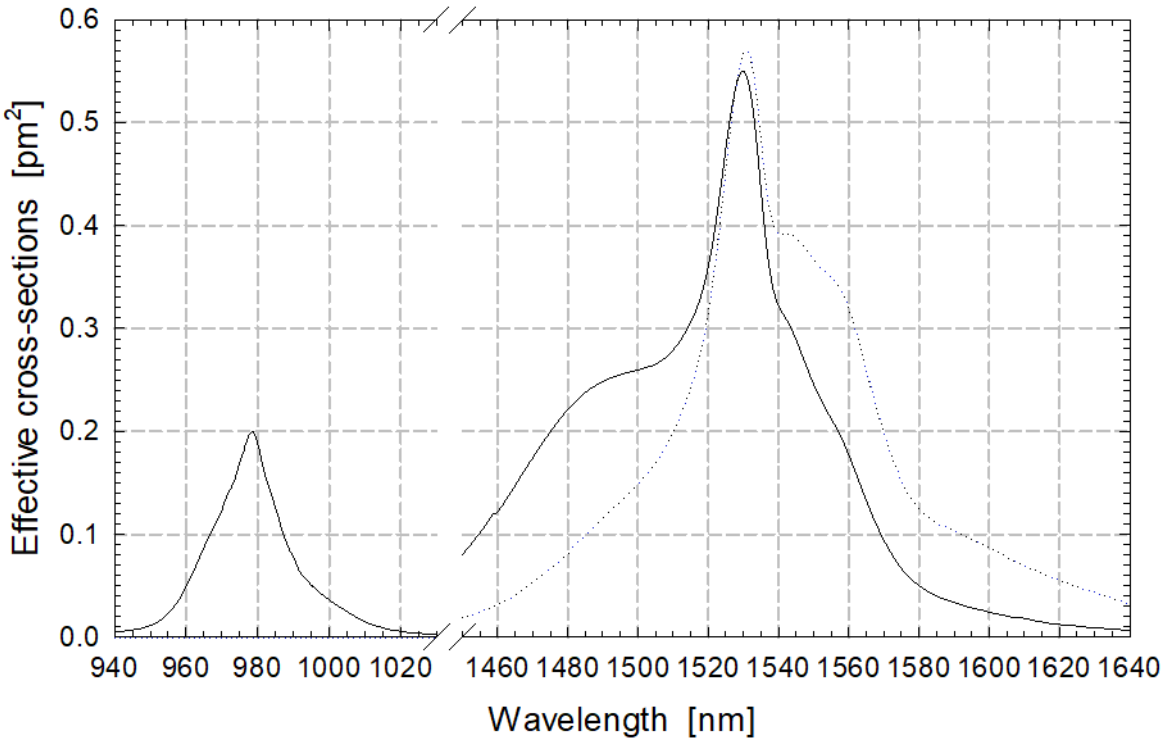

Figure 2.3 Plot of cross-sections vs wavelength [Er^{3+}: Aluminosilicate]

The three fundamental light-matter interaction processes that take place in the rare-earth doped fibre are absorption, stimulated emission and spontaneous emission. First, the rare-earth ions are excited into a higher energy level (upper state level) by absorbing the pump light. The rare-earth ion then is in an unstable state, and it will quickly relax to a lower energy level, and (ultimately) the upper laser level. For the system to work, the upper laser level needs to be a meta-stable state (meaning that the electron will remain excited for a comparatively long time before relaxing). This makes it possible to build up a population inversion, with more ions in the upper laser level than in the lower laser level, so that optical gain can be achieved through stimulated emission [7].

Specifically, when a signal photon interacts with a rare-earth ion in the meta-stable level, it can, through stimulated emission, cause it to emit another photon with a phase, frequency and direction identical to it. The energy provided by this stimulated emission photons constitutes optical gain in the laser cavity. However, electrons in the upper energy level may decay not only through stimulated emission but also through spontaneous de-excitation of the laser ions emitting a photon with no coherence characteristic with respect to the rest.

When the gain in the fibre reaches the level of loss in the laser cavity, then it reaches the pump threshold power. Above the threshold, the laser's output power is dominated by stimulated emission rather than spontaneous emission [7].

2.1.4 Erbium-Doped Fibre Technologies

For erbium-doped fibres (EDFs), the most common laser transition is from the $^4I_{13/2}$ manifold to the level 1 manifold $^4I_{15/2}$ (the ground state) at 1.5 – 1.6 µm. This laser transition is illustrated in Fig. 2.4. The most common pump scheme is based on the transition $^4I_{15/2}$ ➔ $^4I_{11/2}$ with a wavelength of 0.98 µm, although so-called in-band pumping ($^4I_{15/2}$ ➔ $^4I_{13/2}$ at around 1.5 µm) is also frequently used. A multi-phonon relaxation (non-radiative, fast transition) occurs from $^4I_{11/2}$ to $^4I_{13/2}$. The upper-state lifetime of $^4I_{13/2}$ is normally ~10 ms [10], which is exceptionally long. However, at high erbium concentration, energy-transfer upconversion severely reduces the lifetime, degrading the efficiency of the EDF and increasing the pump power required to excite ions and thus store energy in the active fibre [11].

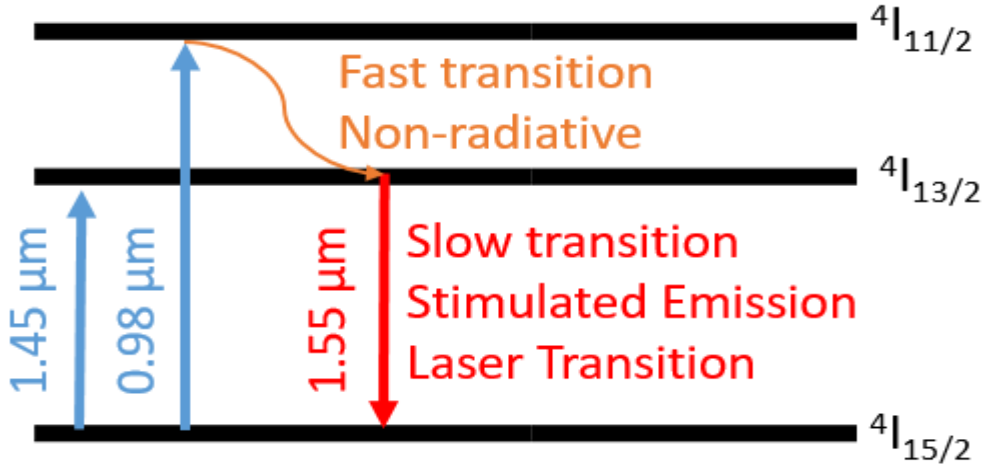

Figure 2.4 Energy level structure of Er^{+3} and some common optical transitions.

One of the most important challenges of Er-doped fibre lasers and amplifiers is a potentially low efficiency. This depends on factors like the excitation level, parasitic absorption processes (e.g., concentration quenching, excited state absorption), optical background losses and pumping technique (including wavelength) [12]. A significant fraction of the coupled pump radiation (e.g., 50%) may dissipate in the form of heat. The potentially low efficiency has motivated researchers to use long wavelength pumping directly into the resonant absorption band of the Er^{+3}-energy level system near 1530 nm. This approach employs 1460 – 1500 nm pump diode lasers. High laser efficiencies have been demonstrated in the core-pumping geometry due to the small quantum defect for resonantly pumped Er^{+3}-fibre lasers in the 1460 – 1530 nm spectral range [12]. Other aspects which may well affect the efficiency include how the pump is launched into the Er-doped fibre. I have primarily used so-called free-space end-pumping, in which the pump is launched into the fibre through a cleaved end. Especially in case of core-pumping, this can easily result in launch losses off more than 50%, although careful mode-matching and alignment can reduce the losses

significantly (e.g., 20%). Note also that whereas a single-clad fibre requires core-pumping, a double-clad fibre can be either core- or cladding-pumped. In case of cladding-pumping. pump launch losses can be much smaller than with core-pumping. Further details on the experimental configurations and results are presented and discussed in Chapter 3.1.

Whereas the launch and lunch losses are of great practical importance, the overlap of the pump and signal with the core is of more fundamental importance. In a typical core-pumped case, the pump and signal overlap with the rare-earth doped core region will be large (> 70%). Especially in case of a multimode core, it is reasonable to approximate the overlap to unity. The high overlap results in a high pump absorption per unit length and a short device length. On the other hand, in a typical cladding-pumped case, the single mode signal is guided by the core of the fibre whereas the multimode pump is guided by the low index inner cladding. Then, the pump absorption is relatively low as the cladding to active core area ratio is quite large, resulting in a relatively low overlap of the pump light with the active core. Yb-doped fibres benefits from the high absorption cross-section of Er and often use an area ratio of 400. Er-doped fibres use much smaller area ratios, typically below 50. Further details, such as computer simulations at different area ratios, pump absorption efficiency, and the experimental configuration are presented and discussed in Chapter 3.2. The absorption as well as the gain of erbium-doped fibre amplifiers (EDFAs), can be written in terms of the overlap and other parameters of the amplifier as follows (Eq. 2.4):

$$G_{dB}(\lambda) = 4.343\Gamma L N_0 \sigma_{ems}^{net}(\lambda) = 4.343\Gamma L N_0 \left[\left(\sigma_{ems}(\lambda) + \sigma_{abs}(\lambda) \right) n_2 - \sigma_{abs}(\lambda) \right] \qquad (2.4)$$

Where the gain (G_{dB}) is determined by the overlap of the launched beam with the rare-earth doped core area (Γ), the fibre length (L), the rare-earth doping concentration (N_0) and the net-emission-cross-section (σ_{ems}^{net}), which is given by the factor in the square brackets. This depends on the emission and absorption-cross-section at the operating wavelength and the excitation level (n_2). This in turn depends on the operating conditions of the amplifier (e.g., the pump power), whereas the other parameters are static and will not change for a given fibre. The parameters can be those of the pump or the signal. In case of the pump, the absorption of the partly excited erbium-ion system is described by a negative value of G_{dB} (λ_p).

As it comes to spontaneous emission, this is not only generated but also amplified by the excited erbium-ions. This leads to so-called amplified spontaneous emission (ASE). Spontaneous emission occurs in all directions, but only the fraction that falls within the numerical aperture (NA) of the optical fibre and is guided inside the core sees significant amplification. The ASE can build up to high power and thus compress (saturate) the gain. Spurious feedback from reflections and backscattering exacerbates this effect, and can even lead to parasitic lasing if the gain becomes too high. It is therefore very challenging to reach more than ~40 dB of gain in a single amplifier stage

(without intermediate isolators) even in the best circumstances. Particularly in fibre lasers, parasitic emission in the form of ASE and unwanted lasing can prevent desired lasing at extreme wavelengths if the gain at other wavelengths is excessive [4, 13, 14]. Parasitic emission also reduces the energy stored in the fibre amplifier by depleting the inversion. Therefore, the extractable energy from the rare-earth doped fibre is strongly limited by unwanted emission, which led to fast self-saturation in the system. Therefore, the spectral shape of the gain is important for energy storage. This is described by Eq. 2.4. First of all, it depends on the absorption and emission cross sections, which depend on the host glass. In addition, the spectral shape is substantially influenced by the average degree of excitation of the erbium ions. Fig. 2.5 shows the gain spectra of Er^{3+}:aluminosilicate, in terms of the net emission cross-section of a single ion; other glass compositions can lead to slightly different gain spectra.

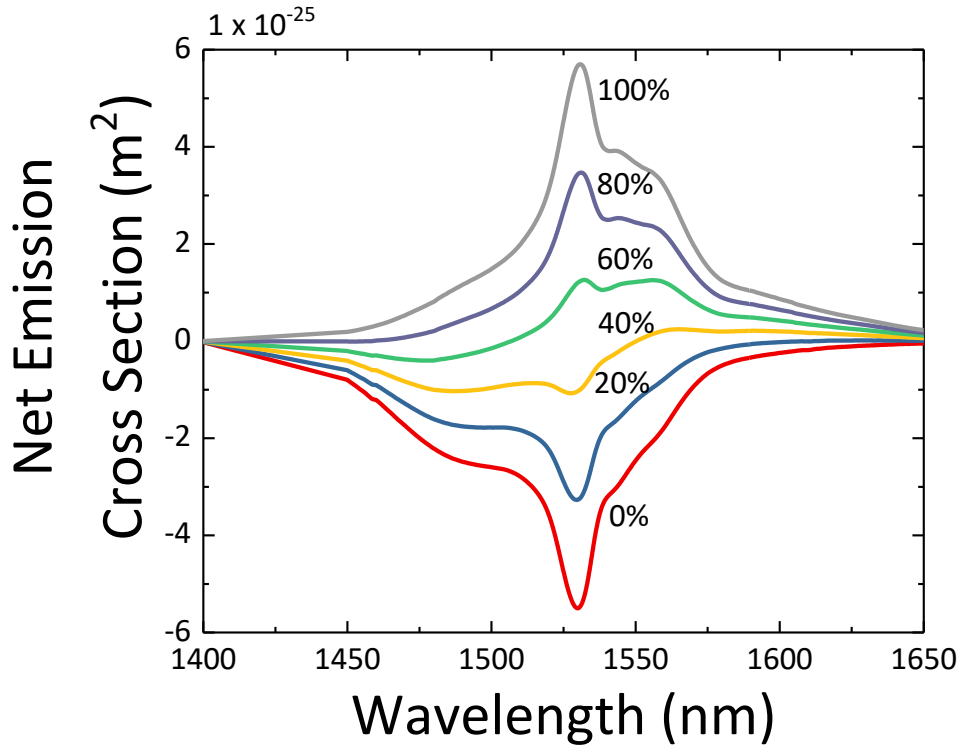

Figure 2.5 Normalized gain spectra at different excitation levels, from 0 to 100% in steps on 20% [Er^{+3}: Aluminosilicate]

In the spectral region of ~1530 nm, the EDF exhibits substantial losses when the excitation level is insufficient, but high gain is possible at higher excitation level (e.g., 60%). At longer wavelengths (e.g., 1560 nm), lower excitation level is required for obtaining gain, but the maximum gain is smaller. Note however that the overall gain depends also on the length, overlap, and concentration. Thus, a small net emission cross can be compensated e.g., by a longer fibre (subject to constraints on nonlinearities, etc.), so it is possible to get high gain also with a small net emission cross-section. In fact, in many practical situations, the gain is saturated. Then, the excitation self-adjusts to the

level that results in the level of saturated gain, which in turn may be decided by parasitic emission, the signal input power, and/or the pump power.

2.2 Pulse propagation and Limitations in Optical Fibre Lasers and Amplifiers

To maximize the performance in the pulse regime, a judicious matching of the various parameters is required. Many parameters are often determined by the application requirements, including the pulse duration and pulse repetition frequency (PRF). However, when the research is more exploratory, such as in this thesis, also those parameters can be varied to find where an amplifier and a specific fibre appears most promising. Furthermore, depending on the pulse duration, pulse energy, PRF and operating wavelength required, very different methods for pulse generation may be most suitable. Thus, Q-switching (for high-energy pulses at lower PRF) and mode-locking (for lower energy at high PRF) are options for generating pulses directly from a laser oscillator. Another option is to modulate the drive current of a laser, typically a diode laser. Finally, and the primary approach of this work, it is possible to create pulses by externally modulating a CW-laser source. Typically, an electro-optic modulator (EOM) or an acoustic-optic modulator (AOM) is used for external modulation. The pulses are then boosted in an amplifier in a so-called MOPA configuration, and it is this amplifier, in the high-energy regime, which is the focus of this work. Compared to Q-switching, the relative merits have not been investigated.

2.2.1 Determination of pulse energy from oscilloscope traces

The PRF of a regular train of pulses is defined as the number of pulses per second. The pulse energy (E_p) is simply the total optical energy content of a pulse. For regular pulse trains, the pulse energy is often calculated by dividing the average power (P_{avg}) by the PRF (Eq. 2.5):

$$E_p = \frac{P_{avg}}{PRF} \tag{2.5}$$

However, this is a valid procedure only if the energy emitted between the pulses is negligible, and thus does not contribute significantly to the average power. The pulse energy together with the pulse duration is often used to estimate the peak power of pulses. Conversely, temporal integration of the instantaneous optical power results in the pulse energy. In principle, this can be done from temporal oscilloscope traces. Indeed, measurements of temporal traces with a detector and an oscilloscope are essential for characterization of optical pulses, and what it is used in this study to determine pulse shape as well as energy. The shape is provided directly by such measurements, and if the average power is measured separately, it is in principle straightforward to calibrate the oscilloscope trace in terms of instantaneous power and then from that determine the peak power

and the pulse energy (through integration). However, although conceptually simple, the trace needs to be measured with high accuracy over a large dynamic range, which may well exceed that directly available from the detector and oscilloscope [15].

For the shape, a dynamic range of 20 dB and a bandwidth of 1 GHz are typically adequate and easily obtainable. I measured pulse shapes a the 15-GHz detector (EOT ET-3500) connected directly to an oscilloscope (Agilent DSO9104H) with 50-Ω termination and 1-GHz bandwidth. The dynamic range of some pulses I measured reached up to ~60 dB in 50-ns pulses. This is much more than the dynamic range of oscilloscopes. There are then various ways to increase the dynamic range, notably measurements with different oscilloscope settings or levels of optical attenuation of a pulse train or a replicated pulse [15]. Although 60 dB is still challenging or even impossible to achieve with nanosecond temporal resolution, a reasonable reproduction of a pulse shape generally requires no more than 20 dB, and 30 dB is more than enough in almost all cases.

The calibration needed for the determination of energy becomes especially challenging at low duty cycle, where the long interval between pulses (e.g., PRF < 3 kHz) leads to significant inter-pulse energy even at low inter-pulse power in the form of ASE and /or leaked signal. Inter-pulse power is difficult to avoid from a high-energy fibre source, because of the high initial gain. This is a problem for the assessment of pulse energy as the average power divided by the PRF (which fails to distinguish energy in the pulses from that between pulses) as well as through the integration of the pulse trace, because of the large difference in instantaneous power in and between pulses. Consequently, given the level of sensitivity and accuracy required to determine the pulse energy at low duty cycle, it is sometimes claimed that "the ASE power cannot be detected by a standard photodetector" [16]. To overcome this problem, an AOM is sometimes used as a time-gate [17] to separately measure the average power during and between pulses. Alternatively, instead of downloading the oscilloscope trace of the instantaneous power for numerical integration in a computer, it is possible to directly integrate the photodetector signal in an analogue electronic circuit [16]. This has been found to work well for 100-ns pulses at 10-kHz PRF (duty cycle 10^{-3}) with a bespoke circuit, although at a relatively small dynamic range (on-off ratio) of ~30 dB [16].

As it comes to the determination of the energy by numerical integration of the temporal trace, it is noted first that the dynamic range required for the measurement is normally determined by the pulse duty cycle rather than the dynamic range of the signal. If the instantaneous powers in and between pulses are P_P and $P_{IP,}$ respectively, the energy between the pulses (E_{IP}), becomes a fraction P_{IP} / (P_P η_P), of the pulse energy (E_P), where η_P << 1 is the pulse duty cycle.

To measure this at, say, the 5%-level requires a dynamic range of $(0.05\ \eta_P)^{-1}$, independently of the power ratio P_{IP} / P_P. It is also worth mentioning that if P_{IP} / P_P > η_P then most of the energy resides

between the pulses. This is not desirable but means that the required dynamic range can be relaxed. For ns-scale pulses, the duty cycle may be as low as 1×10^{-5} or even lower. This would require at least ~60 dB dynamic range for an accurate determination of the pulse energy. This would be very difficult or even impossible with an oscilloscope trace. Although the noise can be reduced to improve the smallest measurable signal if the trace is averaged over a large number of pulses and different oscilloscope gain settings are used to reduce the noise and improve the smallest measurable voltage, this may not be enough to achieve 60 dB. Furthermore, the linearity would also need to be adequate over 60 dB.

Therefore, for energy measurements, the effective duty cycle is reduced, as well as the dynamic range of the signal, by increasing the measurement time constant to a value larger than the pulse duration. This effectively integrates the instantaneous power over an integration time that is longer than the pulse duration. This reduces the dynamic range of the measured trace by a factor τ_P / T_m, where τ_P is the pulse duration and (T_m) is the measurement time constant (equal to the inverse of the measurement bandwidth (f_m)). Furthermore, the effective duty cycle becomes $\eta_{eff} = f_{rep} / f_m$, where ($f_{rep}$) is the PRF. For example, if f_m used for the measurements is calculated to be 400 kHz, and given the smallest PRF used for the work presented in this thesis was 1 kHz, the smallest value of η_{eff} becomes 0.0025 or –26 dB (see Chapter 4).

For this thesis, the pulse peak power was calculated to be as high as 60 dB above the inter-pulse power, for 0.2-mJ, 6-ns pulses (see Chapter 4). In order to determine the pulse energy with such high on-off ratios, I used the large-area detector (Thorlabs DET10C) and reduced the bandwidth (i.e., the effective duty cycle) with a low-pass circuit. Although the integration can be done numerically in a computer, this was done externally with a low-pass circuit comprising a 4.7 nF capacitor in parallel with a 150-Ω resistance, 50 Ω of which was in the oscilloscope's input port. This results in a bandwidth calculated to ~226 kHz, which agrees well with the filter's measured time constant (T_{LP}) of ~682 ns. This has the advantage that it increases the signal voltage, which reduces the impact of the oscilloscope's noise and digitization error, compared to numerical integration in a computer.

Note that for a pulse significantly shorter than the filter's time constant, the peak signal voltage is given by the charge generated by the pulse divided by the capacitance, and is therefore proportional to the pulse energy. On the other hand, although the peak current through the oscilloscope is reduced as the capacitor is charged and discharged, the full charge will still pass through the oscilloscope. Thus, the integral of the trace over the pulse remains the same. Still, even with this reduction, the 0.2-mJ, 6-ns pulse, would generate a voltage as high as 0.2 mC / 4.7 nF = 42.5 kV, if one assumes a detector responsivity of 1 A/W = 1 C/J. I therefore attenuated the light

incident on the detector to yield a peak voltage V_{pulse} of up to around 0.3 V over the oscilloscope's 50 Ω (and another 0.6 V over the 100-Ω resistor in series), so by ~46.7 dB for the pulse. Since the voltage is proportional to the optical power or energy, a multiplier of 10 in the dB scale rather than 20 is normally used for voltages. I attenuated the light reaching the detector by passing it through a multimode patchcord, which collected a small fraction of the output signal. For this, the signal was first passed through a diffuser, so that the collected light is representative of the whole beam. The use of a patchcord also shields the detector from ambient light.

Next, it is considered how the inter-pulse power affects the determination of the pulse energy. Relative to the pulse energy E_P, the inter-pulse energy E_{IP} is given by $(V_{IP} / V_{pulse})\,(T / T_{LP} - 1) \approx (V_{IP} / V_{pulse})\,(T / T_{LP})$, where T is the pulse period and V_{IP} is the average value of the inter-pulse voltage. For a PRF of 2 kHz, $T / T_{LP} = 733$ (28.7 dB). It follows that V_{IP} needs to be measured with an accuracy of around 40 dB relative to V_{pulse} in order to determine the pulse energy to within 10%. This translates to 30 µV in case of a peak oscilloscope voltage of 0.3 V. At the 50-mV/div oscilloscope gain used in this case, the noise level is specified to 641 µV, and the resolution becomes 488 µV with 12-bit digitization. Although these values are in themselves inadequate, I reduced the inter-pulse error through integration (which is equivalent to averaging). With T = 0.5 ms and an oscilloscope setting of 10 MSa/s, there are nearly 5000 samples between pulses, which is expected to reduce the average noise contribution from each sample to the integrated value to 641 $\mu V/5000^{1/2}$ = 9.1 µV. Although this is expected to be sufficient, in addition ensemble-averaged over 256 traces in the oscilloscope. This results in cleaner traces with an expected noise level in each sample of $641\ \mu V/256^{1/2}$ = 40 µV. This averaging also improved the resolution of the oscilloscope to 33 µV through internal data processing. The expected noise averaged over 5000 points becomes 0.67 µV, which is well over an order of magnitude better than needed.

Using averaging and integration as described above, I was able to reduce random errors (noise) to sufficiently low levels for the pulse parameters I investigated, but one must also consider systematic errors. One source is the non-zero reading present in the absence of light (the dark-level). I measured this immediately after the pulses with the same oscilloscope settings and averaging and subtracted it from the pulse traces. At 50 mV/div, the dark-level was ~300 µV. When measured several times within a few minutes, the averaged value varied in a range of around 35 µV. At 1 mV/div, the dark level was ~100 µV and varied over a range of around 8 µV. These values are large compared to the 1.25 µV corresponding to the specified dark-current of the detector of 25 nA or less. Furthermore, the different dark-level characteristics for different oscilloscope settings show that at least some of the characteristics depend on the oscilloscope and are not intrinsic to the detector.

Quantization is also a potential source of systematic errors. A dark-trace that is highly stable with negligible noise leads to a quantization error that is nearly the same in each sample and will not be reduced by integration. This is true also for integration of a mostly-constant inter-pulse trace. In case of 33 μV resolution in the quantization, this can lead to a systematic error in the range of ±16.5 μV in both the inter-pulse trace and the dark trace. However, in the presence of noise or controlled variations with appropriate distribution, the quantization error becomes random with zero mean and can be reduced by averaging [18, 19]. In case of Gaussian noise, a standard deviation of 0.7 or more, relative to the quantization resolution, makes this possible. According to simulations, at that level of Gaussian noise, averaging over 10^8 samples brings the residual quantization error to 40 dB below the quantization resolution, as expected for random errors. Although it had a much smaller number of inter-pulse samples, 5000 samples suffice for averaging the error to around 1% of the quantization resolution, so around 0.33 μV in the given considered example. The results also confirmed that the temporal traces had inter-pulse variations that exceeded 0.7 times the quantization resolution in all traces that I investigated. It is possible that the oscilloscope is designed to satisfy this critical criterion, but it is essential to verify this, and if necessary add variation (e.g., noise), if the quantization error is to be reduced by integration.

Saturation is another possible systematic error. To investigate this, I attenuated the light and investigated the effect on the peak voltage, under representative measurement conditions. The measurements show that the deviations from linearity were around 1 dB in the range from 30 to 300 mV. Linearity was excellent from 3 to 30 mV, and altogether the linearity was found to be within 1 dB (~20%) for 30 dB of dynamic range under representative measurement conditions, if the dark-level is subtracted. Still, this error may seem excessive. However, insofar as the inter-pulse energy is relatively small, it leads to an error in the pulse energy which is much smaller. For example, if the actual inter-pulse energy is 20% of the total energy, the actual ratio of the pulse-to-inter-pulse energy becomes 0.8/0.2, i.e., 6 dB. A saturation of 1 dB reduces this to 5 dB, i.e., 0.76/0.24. The error in pulse energy then becomes 5%. It is only in the limit of negligible energy in the pulses that the error in linearity equals the error in pulse energy that results. Although the inter-pulse energy was quite large and even exceeded the pulse energy in some cases, this was for longer pulse durations with lower peak power. For these, deviations from linearity are expected to be smaller and the overall errors were indeed found to be relatively small.

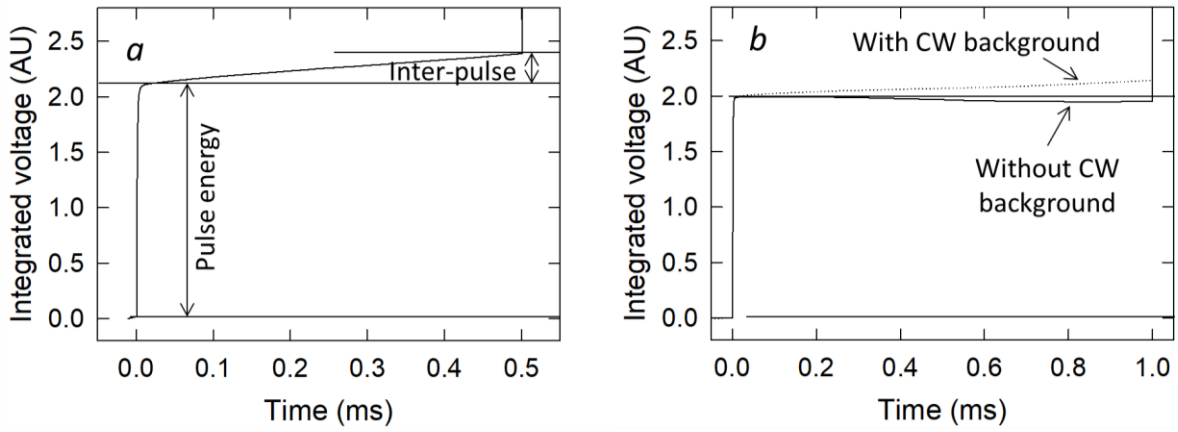

Figure 2.6 Integrated oscilloscope trace measured with the slow detector and low-pass filter and with subtracted dark-trace for (a) the 6-ns pulse at 2 kHz, 0.2 mJ output energy and (b) similar "synthetic" pulses at 1 kHz with and without added background.

The measurement setup was verified by characterizing seed pulses out from the AOM in Fig. 4.1 (see Chapter 4) and mixing in controlled amounts of CW light from a separate light source through a fused fibre combiner at the output of the AOM. The resulting pulses were characterized in the same way as those from the FUT, separately for the CW background and the pure pulses (without added background), as well as combined. Attenuators were used to adjust the power levels reaching the detectors to levels similar to those in the experiments with the FUT. The 64-dB extinction ratio of the AOM ensures that the inter-pulse power is negligible at its output. Thus, it was possible to synthesize similar pulse traces as obtained from the FUT, but with well-known pulse and inter-pulse energy and the option to eliminate inter-pulse light by switching off the CW source. Figure 2.6 shows the integrated voltage for the 6-ns pulse in Fig. 4.5 (a) at 2-kHz PRF (see Chapter 4) as well as for a similar 6-ns "synthetic" case at 1 kHz without and with 0.4 µW of CW background. The average power in the "synthetic" pulses was measured to 10.5 µW. The combined power became 10.9 µW. Thus, the inter-pulse energy was 4% of the total. The synthetic trace without added background has an error of ~6 µV, which results in a decrease in the integrated inter-pulse value of 2.1% of the step (i.e., energy) of that of the pulse. With background, the integrated inter-pulse fraction becomes 6.7%. Although the relative uncertainty in E_{IP} is large, the resulting pulse-energy uncertainty is less than 3% in this case.

Other synthetic pulses were investigated to largely cover the range of parameters encountered in the characterization of the FUTs. The results of this analysis show that for inter-pulse energies below around 20% according to the integrated trace, the error in pulse energy was below 10%. Although the inter-pulse value was larger than that in some cases, those were for pulses of 200 ns or longer. For such long pulses, the error remained at 10% also for inter-pulse energies of 70%. This may be a result of lower peak power and thus lower detector saturation.

In addition, the error was simulated using a simple detection model with a detector affected by saturation, dark-level error, and a low-pass filter for different pulse parameters. Also, according to these simulations, it was possible to reach an error limit of around 10% for these pulses and detection-system parameters. In fact, it was possible to reach this limit for a much wider range of parameters, but this requires that the signal strength is adjusted according to the parameters to a level that seems difficult to know *a priori*. In a similar vein, poorly adjusted measurement parameters such as the power on the detector and the measurement bandwidth can easily lead to large errors. Nevertheless, it seems clear that with appropriate settings, it is possible to determine the pulse energy from most fibre sources of the type I have studied with the approach I have used. Note that the 226-kHz filter bandwidth seems adequate for the range of 1 – 40 kHz. 40 kHz is the highest PRF in my data, and might benefit from a larger bandwidth. On the other hand, for low PRFs, a smaller bandwidth may be preferable. Furthermore, a large detector area may be preferable to mitigate saturation, and saturation as well as dark-trace errors can also be reduced by measuring the same pulses with more than one oscilloscope gain setting, and with more than one level of power onto the detector. Although I did not combine data acquired at different settings or light power levels in order to improve the accuracy, I regularly changed these parameters during the experiments to better understand the pulse characteristics and check for anomalies. The traces from which I calculated the pulse energy were generally measured with up to ~0.3-V peak voltage and ~226-kHz filter bandwidth.

To summarize, my measurement accuracy appears to be limited by ~35 µV dark-level variations for an oscilloscope setting of 50 mV/division. The relative dark level was similar but slightly different for other oscilloscope gain settings that I used. This suggests it arises internally rather than externally to the oscilloscope. Deviations from linearity may be significant when the inter-pulse energy is large. Other identified sources of error are random in nature and become negligible when the signal is integrated (averaged) between pulses. Overall, the errors are estimated in reported pulse energies to roughly 10%, perhaps 15% in some cases, but normally less. This does not consider the error in the thermal power meter used for determining average power nor losses in mirrors and lenses. This investigation has thus shown that with the photodiode and oscilloscope I used, it is generally possible to accurately measure the energy of pulses of around 10 ns or longer at PRF of 1 kHz or more. There are, however, many pitfalls, and care is needed to avoid them.

2.2.2 Limitations in rare-earth doped fibre lasers and amplifiers

Many factors can limit the performance of an amplifier, including those relating to the pump approach and the fibre itself (e.g., quenching and nonlinearities).

For high-energy pulses, the most fundamental limitation relates to parasitic emission that because of the high gain that results at high stored energy. This includes unavoidable ASE. The Eq. 2.6 and Eq. 2.7 estimates the available energy extracted from a fibre amplifier:

$$E_{extr} = U_{sat} * G_{mod}^{Np} \tag{2.6}$$

$$U_{sat} = A * E_{sat} = A\left(\frac{h\nu}{(\sigma_{ems} + \sigma_{abs})}\right) \tag{2.7}$$

The extracted energy (E_{extr}) is determined by the product of the saturation energy (U_{sat}) and the gain modulation (G_{mod}^{Np}). The saturation fluence (E_{sat}) is the saturation energy per unit area (A), the saturation fluence and core area (A) sets a limit in the stored energy, and, consequently, the extracted energy. It depends on the emission and absorption-cross-sections, which in turn depends on the operating wavelength [20].

In Er^{3+}: aluminosilicate (Fig. 2.3), the saturation fluence increases at longer wavelength, e.g., its value is equal to 0.317 μJ/μm^2 at 1565 nm operating wavelength. Assuming a core area of around 100 μm^2, the saturation energy becomes ~32 μJ at 1565 μm. If the fibre amplifier achieves 96 μJ of extracted energy, the gain modulation would be around 3 Np (or 13 dB). It is often desirable to maximize the signal gain, since, most of the time; this also maximizes the stored energy, assuming the pump pulse energy is sufficient. Therefore, the details of the pump source are also important and linked to the signal wavelength, gain and energy.

Eq. 2.6 and 2.7 apply to any optical amplifier. In addition, imperfections of the rare-earth doped fibre can further degrade the performance. Such imperfections include photodarkening (important for ytterbium-doped fibres, YDFs), excited-state absorption (ESA), and energy-transfer upconversion.

In photodarkening, there is a growth of optical loss in the gain medium due to exposure to short wavelengths, inducing excessive transmission loss over time. Those losses can grow during the operation of fibre lasers or amplifiers. The rate with which these losses grow appears to increase with the concentration of excited ions. This means that a fast degradation can appear in highly doped YDFs; the damage may also degrade the lifetime of the Yb-ions inside the fibre [11].

Excited-state absorption involves the absorption of a pump or signal photon of an ion that is already excited (typically to the metastable state). For Er^{3+}, which acts as a three-level laser system (Fig. 2.4), a significant fraction of the ions need to be in the excited metastable state. This exacerbates the problem of ESA. Pump-ESA is not important for ESA pumped art 980 nm or 1.5 μm. However, signal-ESA does occur at long signal wavelengths. Fig. 2.7 indicates the significance of the signal-

ESA at a given wavelength, described also by Eq. 2.8, where the net-emission-cross-section (σ_{ems}^{net}) is calculated, affected by the ESA-cross-section (σ_{ESA}) at different operating wavelengths:

$$\sigma_{ems}^{net}(\lambda) = \left[\left(\sigma_{ems}(\lambda) + \sigma_{abs}(\lambda)\right)n_2 - \sigma_{abs}(\lambda)\right]$$
$$\sigma_{ems}^{net}(\lambda) - \sigma_{ESA}(\lambda) = \left[\left(\sigma_{ems}(\lambda) + \sigma_{abs}(\lambda) - \sigma_{ESA}(\lambda)\right)\right]n_2 - \sigma_{abs}(\lambda)] \quad (2.8)$$

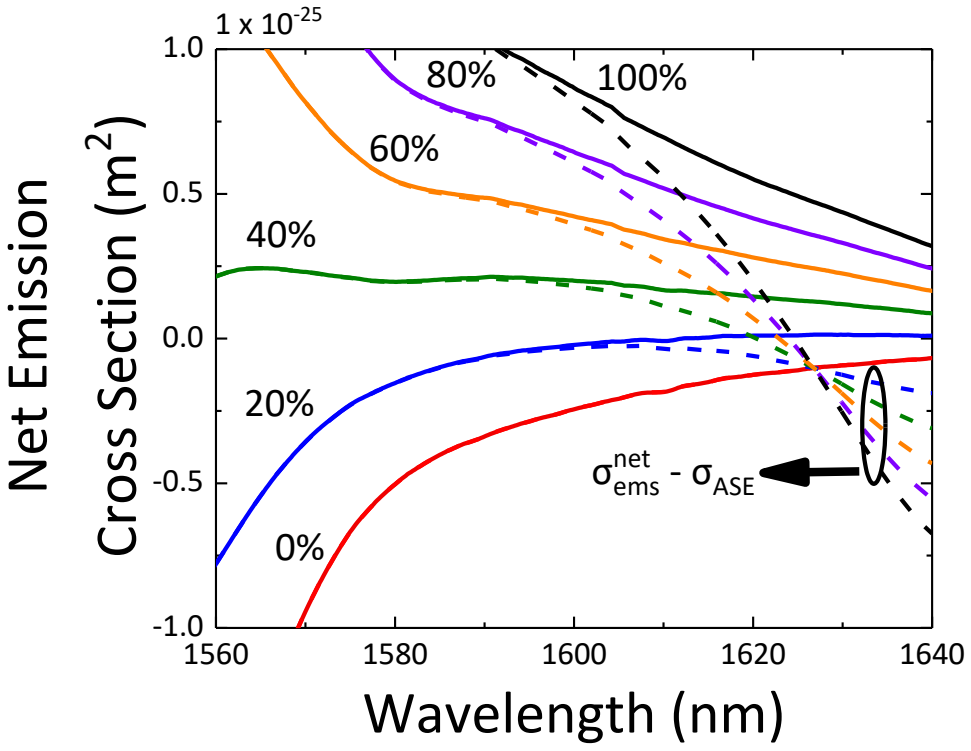

Figure 2.7 Detrimental effects caused by ESA at a given wavelength

The crossing of the curves in Fig. 2.7 correspond to the wavelength where the stimulated emission cross-section is equal to the ESA cross-section. At that point, the gain is independent of the excitation level (including 0%) and thus negative and equal to the small-signal absorption at this wavelength.

Furthermore, and central to this thesis, the weak absorption and emission cross-sections of Er^{3+}-ions lead to low pump absorption [21, 22], to compensate for this, most EDFA systems use relatively long fibres (e.g., 10 m). This leads to nonlinear degradation building up over the fibre length [23, 24, 25].

A high-concentration EDF can increase the pump absorption and gain in a fibre of a specific short length, as well as the energy stored in the excited erbium population. However, at high-concentration, Er^{3+}-ions suffers from harmful quenching due to interactions between neighbouring erbium ions. Although tailored host glass compositions, e.g., co-doped with Al_2O_3, P_2O_5 [26-28], as

well as nanoparticle doping [29, 30], can mitigate this effect, the quenching still reappears gradually at higher concentrations.

Despite the extensive study of EDF systems, the precise details are generally not known .In practice, quenching is often modelled as an unsaturable absorption, often tied to a cluster (e.g., pair) model. A scheme following this model is presented in Fig. 2.8.

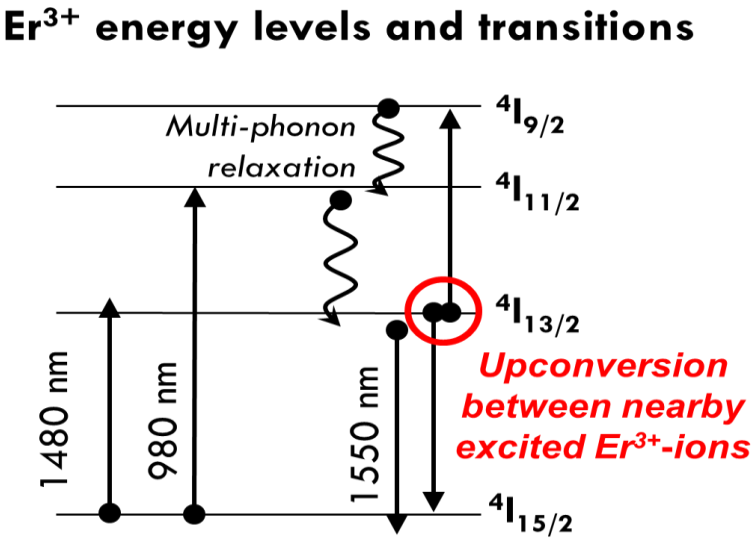

Figure 2.8 Concentration quenching model [31]

As a result of quenching and unsaturable absorption, a signal photon emitted inside the fibre may be lost instead of contributing to the signal output, and an absorbed pump photon may fail to excite an erbium ion. Instead, the interaction between nearby excited Er^{3+}-ions, especially in case of clustered ions, leads to energy-transfer upconversion (ETU), a phenomenon in which rare-earth ions exchange excitation energy among each other. Insofar as this is more likely to happen at high concentrations when the Er^{3+}-ions are closer to each other on average and more likely to cluster, this is also called concentration quenching. If the upper laser level for some laser transition is quenched, the upper-state lifetime is reduced, raising the threshold pump power of the EDF laser and reduce the gain of the fibre amplifier [31]. Although the lifetime shortening can be gradual and continuous, and then modelled as a lifetime shortening that can be modest, for clustered ions the ETU process is often assumed to be instantaneous. The lifetime is then zero and the quenching then modelled as unsaturable absorption. Regardless, it should be appreciated that ETU is a quite complicated process and the description here is simplified.

Note also that the Er^{3+}-ions are partly rather than fully quenched in three respects. Some Er^{3+}-ions are assumed completely unaffected by the quenching.

In the pair model I assume (Fig. 2.8), it is easy to excite one ion in every pair. Note also that 50% excitation leads to gain for wavelengths longer than the zero-phonon wavelength of Er^{3+} of 1.53 µm.

Both ions in a pair can be excited for a short time.

Also note that under the assumption that only one ion per pair can be excited, the fraction of unsaturable absorption becomes $n_q\ \sigma_a$ / (2 σ_a + σ_e). Thus, with our definitions, where $\sigma_a = \sigma_e$ (at ~1.53 µm), the fraction of unsaturable absorption becomes 1/3 even with 100% quenched ions (n_q = 1). At longer wavelengths, the unsaturable absorption fraction becomes smaller, e.g., 26.3% at 1560 nm for n_q = 1. More generally, for a *k*-size cluster in which only one ion can be excited, the fraction of unsaturable absorption is given by n_q (*k* – 1) σ_a / (*k* σ_a + σ_e). Thus, for large *k*, the fraction of quenched ions and the fraction of unsaturable absorption will be the same at all wavelengths, and the same is true if an Er^{3+}-ions is quenched by a trap such as OH (provided also that the absorption cross-sections of quenched and un-quenched Er-ions are the same.

Notably, the unsaturable-absorption model may be too simple for some regimes, and note also that the impact of the unsaturable absorption and ETU depends on the amplifier configuration and operating regime [31-34].

In addition to the unsaturable absorption and ETU in clusters, leading to very short lifetimes, there is homogeneous ETU that leads to much more modest but still distinct reductions in fluorescence lifetime of the upper-state lifetime ($^4I_{13/2}$). This is normally of the order of 10 ms. If this is reduced, it causes a proportional raise of the threshold pump power of a laser and reduction of small-signal gain efficiency of a signal amplifier. For example, a lifetime reduction by 50% doubles the laser threshold. However, the effect on slope and power conversion efficiency, as well as energy storage, is more modest and can be negligible even when the lifetime shortening is significant. See Chapter 4 for further details.

Furthermore, quenching processes such as ETU often create additional fluorescence at other wavelengths [35]. This can be used to detect and analyse quenching. Evidence of the ETU process in highly EDF is shown in Fig. 2.8 and Fig. 2.9. These will be explained in the following, with reference to two Er^{3+}-doped FUTs.

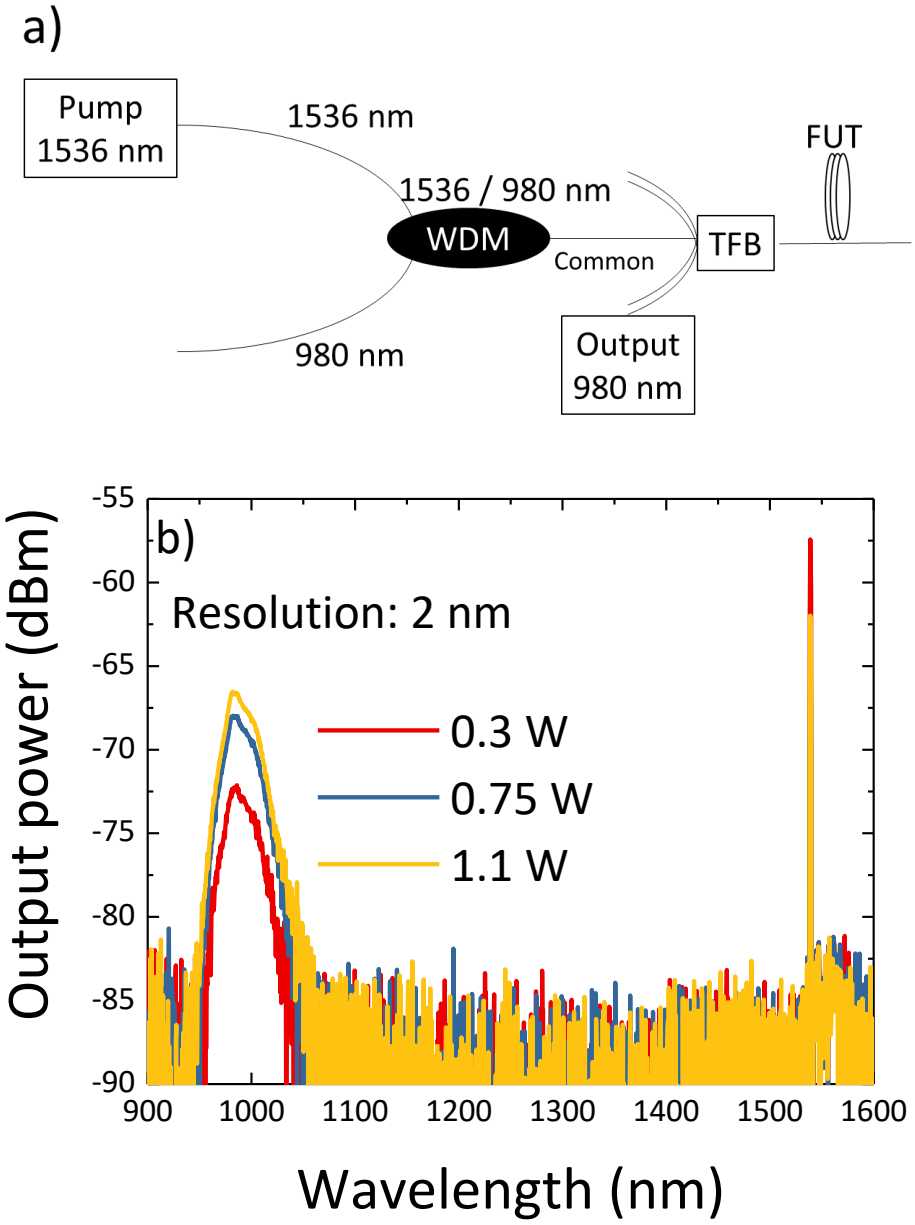

Figure 2.9 a) Upconversion lifetime setup. b) Optical spectrum for different values of CW-pump at 1536 nm.

FUT #1 (NRL-160415) had a 0.13-NA, 20-µm-diameter Er^{3+}-doped aluminosilicate core centred in a 125-µm diameter circular inner cladding, coated by a low-index polymer. The core absorption reached up to 95 dB/m at the 1530-nm peak. FUT #2 (NRL-170525) had a 0.18-NA, 45-µm-diameter Er-doped aluminosilicate core centred in a 264-µm diameter octagonal-shape inner cladding, coated by a low-index polymer. The core absorption reached up to 36 dB/m at the 1530-nm peak. In this measurement, the fibre length is 0.2 m for the FUT #1 and 0.5 m for the FUT #2, conserving the same Er-concentration x fibre length product for both FUTs.

In the setup described in Fig. 2.9 (a), the Er^{3+}-ions are excited at 1536-nm with a high-power CW-pump source (reaching up to 1.1 W). The CW-pump source is spliced to a wavelength-division

multiplexer (WDM) and then to the signal port of a tapered fused-bundle (TFB), the common port pf which is finally spliced to FUT #1. 1536 nm CW-pump light was launched into the FUT through the WDM and TFB. Then, the pump ports (which are normally used to launch additional pump light into the fibre) are used to collect fluorescence at 980 nm. Since the FUT #1 is a double-clad fibre, only a small part of the fluorescence light is captured by the core, while most of it is captured by the inner-cladding. The TFB allows the collection of the fluorescence light propagating in the inner-cladding.

If instead, the FUT was a single-cladding optical fibre, then the fluorescence light would be propagating in the core, rather than in the inner-cladding. Because of the strong absorption at 980 nm wavelength in the EDF, this would have resulted in re-absorption of the 980-nm fluorescence light, making it difficult to detect. Therefore, it is better to have the 980-nm fluorescence light propagating in the inner-cladding, where there is no absorption instead of propagating in the core. Nevertheless, the setup still allows for 980-nm light propagating in the core of the FUT to be measured from the WDM. The fluorescence light at the 980 nm wavelength is attributed to the ETU process expected from a highly EDF.

The assessment targeting such modest lifetime shortening of the fluorescence lifetime was attempted for the fibres under test. This is much easier to measure than the short lifetime of clustered ions. The measurement used pulsed excitation with the 980-nm diode laser, which does not allow to reach high excitation levels. Longer pulses with the same peak power (or even CW-pumping) allow for higher excitation levels, but has the disadvantage of selectively exciting unquenched ions (with long lifetime). Although lifetime shortening could be seen in at least some fibres, it was relatively modest and without obvious pattern. Therefore, it was deemed unfruitful to analyse the results in detail (given also the resulting limited impact). Rather, this thesis is concerned with the much more important impact of the dynamics of the quenched ions (i.e., unsaturable absorption, upconversion fluorescence lifetime).

2.2.3 Limitations from nonlinear effects in the high power regime

Nonlinear processes are particularly challenging for pulsed laser sources compare to CW-lasers, due to their high peak powers. When combined with the optical fibre's tightly confined waveguide mode and length, this readily result in unwanted nonlinear effects [1]. The nonlinear processes of main concern for the system are listed into two main groups:

1) Nonlinear scattering processes: Stimulated Raman scattering (SRS) and Stimulated Brillouin scattering (SBS)
2) Self-phase modulation (SPM)

The nonlinear scattering process can involve elastic scattering (energy is conserved) or inelastic scattering (energy is lost or possibly gained) from the photons. The energy lost to inelastic scattering is absorbed by the molecular vibrations (phonons) in the gain medium. In the process, the scattered photons lose a fraction of their energy resulting in a lightwave at a longer wavelength (lower energy) [1].

Note that the optical wave that drives the nonlinear scattering is normally the signal wave of a system, but this is then called the pump wave in the context of the nonlinear interaction. Although it can be confusing, this is the terminology adopted here.

Raman scattering is an interaction of an incident pump light wave scattered due to intrinsic vibrational modes of molecules in the gain medium. A pump photon is thus downshifted in frequency by the vibration frequency of the molecules. The scattered radiation of the incident light wave is called a Stokes wave. This can occur in all directions. When power grows, so does the Stokes wave, which causes further scattering of other pump photons, insofar as the signal and pump waves overlap over a significant distance. The process thus becomes stimulated (SRS) and is in practice either co-directional or counter-directional with the pump wave. The Stokes wave then grows exponentially with interaction length until the pump wave is depleted. The Raman pump threshold for this process is proportional to the effective area (fibre core area) and inversely proportional to the effective fibre length and the Raman gain coefficient of the material. Once threshold is reached, the rapid build-up of SRS affects most of the pump wave, resulting in severe losses in high-power fibre laser systems [1, 36]. SRS is an ultrafast process with a time constant of a few femtoseconds. Although SRS is a well-known problem for pulsed fibre sources, I have generally managed to avoid it and have not investigated it in this thesis.

Brillouin scattering occurs in optical fibres with high-intensity, narrow-linewidth radiation and involves pump photons being back-scattered into Stokes photons. The large intensity produces compression in the fibre core through a process known as electrostriction. This results in an acoustic wave (i.e., acoustic phonons) with a wavelength that is resonant with the Brillouin scattering. Since the acoustic wave is traveling at the speed of sound (around 6000 m/s in silica), the process changes the frequency of the pump wave. Because of phase-matching requirements, in fibres, conventional SBS occurs only in the backward direction [1, 36], although there are also other types of Brillouin scattering. The time constant of SBS is in the nanosecond regime. I have not studied SBS. Instead, I avoided it by spectrally broadening my signal (acting as a pump for SBS).

For the general case of a stimulated scattering process (SRS or SBS) with an arbitrary pulse duration of excitation (CW; i.e., stationary or pulsed), one can derive an analytical expression for the

scattering process power threshold in a nonstationary regime of excitation. The SRS threshold power is shown in Eq. 2.9, and the SBS threshold is shown in Eq. 2.10:

$$P_{th\,SRS} = \frac{16A_{eff}}{g_R L} \tag{2.9}$$

$$P_{th\,SBS} = \frac{21A_{eff}}{g_B L} \tag{2.10}$$

where the SRS threshold ($P_{th\,SRS}$) and the SBS threshold ($P_{th\,SBS}$) are proportional to the core area (A_{eff}) and inversely proportional to the Raman and Brillouin gain coefficients (g_R,g_B) respectively and the effective fibre length (L) [1, 36]. The power needs to fall within the pump acceptance bandwidth of the process in question. For SRS in silica fibre, this is a few THz, which exceeds the linewidth of typical signals. However, for SBS, it is only a few tens of MHz, which is much narrower than typical signals, especially in the pulsed regime. Furthermore, the length is the effective length. For CW light, this is easy to evaluate with conventional expressions. However with a pulsed pump and a counter-propagating Stokes wave, the effective length is normally limited by the rapid walk-off between pump and Stokes.

Once threshold is reached, optical pulses propagating along in a nonlinear dispersive system will in general experience nonlinear distortion, with stronger effects expected for larger amplitude pulses. Pulse distortion due to linear dispersion such as group velocity dispersion can result in a complex evolution of the optical pulses. The nonlinear effects can combine with or cancel out the linear dispersive effects and will therefore influence the shape and spectrum of the propagating pulses.

Dispersion plays an important role on pulse propagation in optical fibre because different spectral components associated with the pulse will travel at different speeds. This dispersion manifests through the frequency dependence of the refractive index profile. The effect of dispersion with the combination of nonlinearity can cause pulse broadening or self-phase modulation [37]. However, generally with the linewidths and fibre lengths I used, dispersion is negligible.

Self-phase modulation (SPM) is a nonlinear optical effect of light-matter interaction. Light of high intensity, when travelling in a medium, will change the refractive index of the medium, primarily due to the nonlinear Kerr effect. This is an ultrafast process, so in case of a short pulse, the variation in refractive index will produce a phase shift in the pulse, leading to a change of the pulse's frequency spectra which, depending on the requirements, may degrade the performance of the system [37]. The nonlinear phase shift is calculated by Eq. 2.11:

$$\phi_{NL} = \left(2\pi * n_{NL}/\lambda\right) * I * L \tag{2.11}$$

The nonlinear phase shift (ϕ_{NL}) depends on the nonlinear refractive index of the glass host, measured as 2.35 X 10^{-20} m^2/W (n_{NL}) for a silica host, the operating wavelength (λ), the optical intensity (I) and fibre length (L) [33]. I did occasionally observe SPM, but it is a well-known process and I did not study it in detail

In the case of MOPA amplified nanosecond pulses, the effect of gain saturation within the fibre amplifiers is another type of nonlinearity, which directly influences the output pulse shape. The pulse shape is distorted with higher leading edge and an exponentially decreasing trailing edge. The higher the gain extracted from the fibre amplifier, the more distortion suffered by the optical pulse [37]. I often evaluated this effect for my pulses.

2.3 References

1. Agrawal P., “Nonlinear Fibre Optics”, Elsevier, 4th Edition, (2007)
2. Luis Zenteno, “High-Power Double-Clad Fibre Lasers”, Journal of Lightwave Technology **11**, 1435 – 1446, (1993).
3. Apollonov, Victor. (2013). High power disk laser. Natural science. 5. 10.4236/ns.2013.55070.
4. Ter-Mikirtychev, V., “Fundamentals of Fibre Lasers and Fibre Amplifiers”, Springer, Georgia Institute of Technology, USA, page 82 – 90, page 172 – 182, (2014).
5. C. C. Renaud, R. J. Selvas-Aguilar, J. Nilsson, P. W. Turner and A. B. Grudinin, "Compact high-energy Q-switched cladding-pumped fiber laser with a tuning range over 40 nm," in IEEE Photonics Technology Letters, vol. 11, no. 8, pp. 976-978, Aug. 1999.
6. Digonnet, “Rare-Earth-Doped Fibre Lasers and Amplifiers”, Marcel Dekker, page 1, 36 – 43, (2000).
7. J. Nilsson, et al., “Tandem-pumped fibre lasers with low quantum defect”, ASSL 2013, Paris, France
8. Paschotta, R., article on 'silica fibres' in the Encyclopaedia of Laser Physics and Technology (2016).
9. Siegman, A. E., “Lasers”, University Science Books, page 368 – 369, (1986).
10. Paschotta, R., article on ‘erbium-doped gain media’ in the Encyclopaedia of Laser Physics and Technology, 1. Edition, Wiley-VCH, ISBN 978-3-527-40828-3, (2008).
11. Zhu S., “Pulsed tandem-pumping of ytterbium-doped fibre laser for avoiding photodarkening”, Optical Research Centre, University of Southampton, (2015).
12. Dutta N. K., “Fibre Amplifiers and Fibre Lasers”, World Scientific, University of Connecticut, USA, (2015).
13. R. Paschotta, article on 'amplified spontaneous emission' in the Encyclopaedia of Laser Physics and Technology, 1. Edition, Wiley-VCH, ISBN 978-3-527-40828-3, (2018).
14. R. Paschotta, article on 'erbium-doped fibre amplifiers' in the Encyclopaedia of Laser Physics and Technology, 1. Edition, Wiley-VCH, ISBN 978-3-527-40828-3, (2008).
15. J. R. Marciante, W. R. Donaldson and R. G. Roides, "Enhanced-Dynamic-Range, Single-Shot Measurement of Nanosecond Pulses via Optical Replication," LEOS 2007 - IEEE Lasers and Electro-Optics Society Annual Meeting Conference Proceedings, Lake Buena Vista, FL, 2007, pp. 17-18.
16. Leonid Kotov, Mikhail Likhachev, Mikhail Bubnov, Oleg Medvedkov, Denis Lipatov, Aleksei Guryanov, Kirill Zaytsev, Mathieu Jossent, and Sébastien Février, "Millijoule pulse energy 100-nanosecond Er-doped fibre laser," Optics Letters **40**, 1189-1192 (2015)

17. I. Pavlov, E. Dülgergil, E. Ilbey, and F. Ö. Ilday, "Diffraction-limited, 10-W, 5-ns, 100-kHz, all-fibre laser at 1.55 μm," Optics Letters **39**, 2695-2698 (2014)
18. A. B. Sripad and D. L. Snyder, "A necessary and sufficient condition for quantization errors to be uniform and white", IEEE Trans. Acoustics, Speech, and Signal Processing 25, 444-448 (1977).
19. P. J. B. Koeck, "Quantization errors in averaged digitized data", Signal Processing 81, 345-356 (1997).
20. A. Javan, W. R. Bennett Jr., and D. R. Herriott, "Population inversion and continuous optical maser oscillation in a gas discharge containing a He–Ne mixture", Phys. Rev. Lett. 6 (3), 106 (1961).
21. Y. Jaouen, G. Canat, S. Grot, and S. Bordais, "Power limitation induced by nonlinear effects in pulsed high-power fibre amplifiers", Comptes Rendus Physique **7**, 163-169 (2006).
22. G. Canat, W. Renard, E. Lucas, L. Lombard, J. Le Gouët, A. Durécu, P. Bourdon, S. Bordais, and Y. Jaouën, "Eye safe high peak power pulsed fibre lasers limited by fibre nonlinearity", Optics Fibre Technologies **20**, 678-687 (2014).
23. V. Philippov, C. Codemard, Y. Jeong, C. Alegria, J. K. Sahu, J. Nilsson, and G. N. Pearson, "High-energy in-fibre pulse amplification for coherent lidar applications", Optics Letters **29**, 2590-2592 (2004).
24. S. Desmoulins and F. Di Teodoro, "High-gain Er-doped fibre amplifier generating eye-safe MW peak-power, mJ-energy pulses," Optics Express **16**, 2431-2437 (2008).
25. J. W. Nicholson, A. DeSantolo, M. F. Yan, P. Wisk, B. Mangan, G. Puc, A. W. Yu, and M. A. Stephen, "High energy, 1572.3 nm pulses for CO_2 LIDAR from a polarization-maintaining, very-large- mode-area, Er-doped fibre amplifier", Optics Express **24**, 19961-19968 (2016).
26. B. J. Ainslie, S. P. Craig, S. T. Davey, and B. Wakefield, "The fabrication, assessment and optical properties of high-concentration Nd^{3+} and Er^{3+} doped silica-based fibres", Materials Letters **6**, 139-143 (1988).
27. R. Wyatt, "Spectroscopy of rare earth doped fibres", in Fibre Laser Sources and Amplifiers, Michel J. F. Digonnet, ed., Proc. SPIE **1171**, 54-64 (1990).
28. M. M. Khudyakov, M. M. Bubnov, A. K. Senatorov, D. S. Lipatov, A. N. Guryanov, A. A. Rybaltovsky, O. V. Butov, L. V. Kotov, and M. E. Likhachev, "Cladding-pumped 70-kW-peak-power 2-ns-pulse Er-doped fibre amplifier," Proc. SPIE **10512**, Fibre Lasers XV: Technology and Systems, 1051216 (2018).
29. A. Pastouret, C. Gonnet, C. Collet, O. Cavani, E. Burov, C. Chaneac, A. Carton, and J. P. Jolivet, "Nanoparticle doping process for improved fibre amplifiers and lasers", Proc. SPIE **7195**, 71951X (2009).
30. C. C. Baker, E. J. Friebele, A. A. Burdett, D. L. Rhonehouse, J. Fontana, W. Kim, S. R. Bowman, L. B. Shaw, J. Sanghera, J. Zhang, R. Pattnaik, M. Dubinskii, J. Ballato, C. Kucera, A. Vargas, A.

Hemming, N. Simakov, and J. Haub, “Nanoparticle doping for high-power fibre lasers at eye-safer wavelengths”, Optics Express **25**, 13903-13915 (2017).

31. J. Nilsson, B. Jaskorzynska, and P. Blixt, "Performance reduction and design modification of erbium-doped fibre amplifiers resulting from pair-induced quenching", IEEE Photonics Technology Letters **5**, 1427-1429 (1993).
32. P. Myslinski, J. Fraser, and J. Chrostowski, “Nanosecond kinetics of upconversion process in EDF and its influence to EDFA performance”, Institute for Information Technology, National Research Council, 100/ThE3-1 (1995).
33. P. Myslinski and J. Chrostowski, “Effects of concentration on the performance of erbium doped fibre amplifier”, J. Lightwave Technol. 15, 112–120 (1997).
34. E.-L. Lim, S.-U. Alam, and D. J. Richardson, "Optimizing the pumping configuration for the power scaling of in-band pumped erbium doped fibre amplifiers," Opt. Express 20, 13886-13895 (2012).
35. J.C. Wright, “Up-conversion and excited state energy transfer in rare-earth doped materials”, Radiationless Processes in Molecules and Condensed Phases. Topics in Applied Physics, **15**. Springer, Berlin, (1976).
36. S. P. Singh, R. Gangwar, and N. Singh, “Nonlinear Scattering Effects in Optical Fibres”, PIER **74**, 379–405, (2007).
37. Kashyap, K., “Effect of Self Phase Modulation on Optical Fibre”, American International Journal of Research in Science, Technology, Engineering & Mathematics (2013).

Chapter 3 Initial Investigations of Pumping Options

There are a wide range of pumping options, regarding temporal formats, wavelength, beam quality, etc. Thus, the EDFs can be core- or cladding-pumped at 0.98 µm or around 1.5 µm, continuous-wave or with pulses. Each approach with different advantages and achievable parameters such as average power. The complexity, availability, and practicality of different pump sources must be considered, too. I have studied several, but not all, of these options. This chapter presents early work on experiments, simulations, and analysis. Although the experimentally obtained signal energies were unconvincing, this is believed to be for practical rather than fundamental reasons.

3.1 Study of Core-Pumping with Pulsed Er-doped Fibre Source

Core-pumping of EDFAs has the advantage of being able to use shorter fibres, leading to lower optical nonlinearities [1]. Specifically, I investigate pulsed EDFAs in-band pulse-pumped by another Er-doped fibre source, which is deemed to be the most realistic choice of pump source. I also mention that pulsed 0.98-µm core-pumping is unrealistic because of the lack of practical pump sources with sufficient energy fluence.

The experimental layout for this in-band-pumping work is shown in Fig. 3.1. It comprises tuneable-wavelength pulsed seed and pump sources, and a fibre under test.

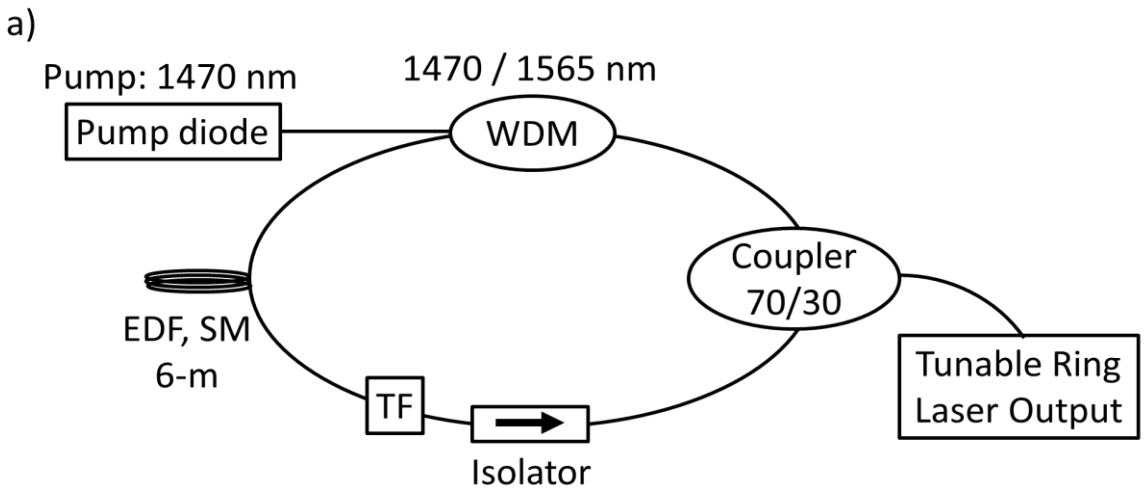

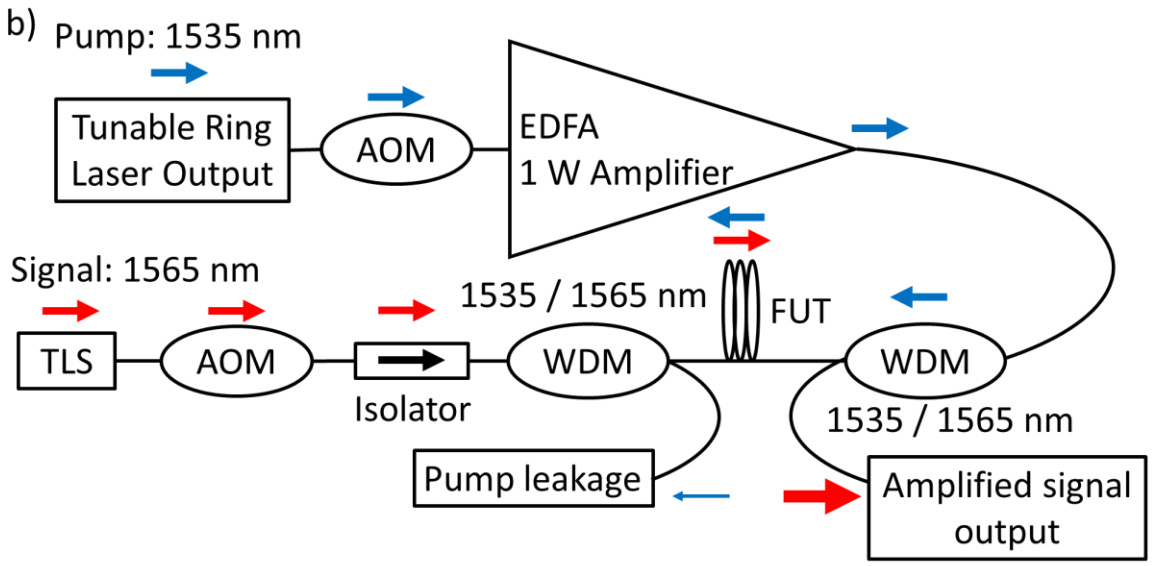

Figure 3.1 Setup for pulsed core pumping. (a) Ring laser (CW) incorporating a tuneable filter (TF) which forms part of the pump pulse generator. (b) Top part of the pump pulse generator; composed of the ring laser (seed), the AOM and an EDFA (~1 W). The bottom part is the signal amplifier setup; composed of a tuneable laser source (TLS), an AOM, an isolator (ISO), two WDM and the signal fibre amplifier. The blue arrows show the direction of the pump pulses and the red arrows show the direction of the signal pulses.

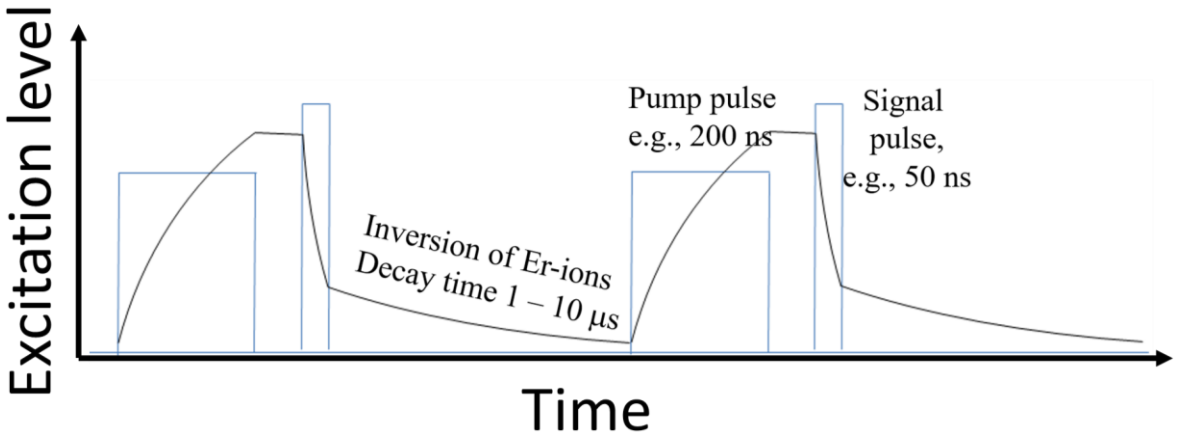

Figure 3.2 Conceptual behaviour of the excitation level for pulse-pumping.

The pulsed pump source is composed of the ring laser (seed), an acoustic-optic modulator (AOM) and an EDFA (~1 W). The ring laser is composed of two polarization-combined pump diode lasers at 1470 nm, a wavelength division multiplexing (WDM) from Gooch & Housego (G&H), a coupler (70/30), an isolator to control the direction of the ring laser output, an EDF as gain medium, and the tuneable filter (TF) which determines the output wavelength. For the signal 'seed' pulsed laser, the setup consists of a tuneable laser diode source as the seed, the device modulating the seed laser (i.e., AOM) and an isolator to protect the equipment from leaked pump pulse energy of the

signal fibre amplifier. For this work, the AOM is preferable over an EOM, due to its much better extinction ratio. Additionally, the WDMs are used for combining and separating pump and signal light.

A laser diode controller drives the diode lasers. Their outputs are combined in a polarization combiner and passed through a WDM into the EDF, to pump it. The EDF is followed by the tuneable filter, which sets the wavelength of the pulses that pump the signal fibre amplifier. A 70/30 coupler is used to couple out light from the ring-laser, through one of the coupler's arms. Another arm is connected to the WDM (G&H), completing the ring.

The absorption of the pump pulse energy by the FUT is an indispensable factor to achieve sufficient fibre laser performance. Aside from the variables stated in Eq. 2.4, the overlap factor (Γ) between the pump and the core further modifies the absorption of the signal fibre amplifier. In the case of core pumping, the overlap factor is usually ignored since it is typically close to unity. Cladding pumping on the other hand has an overlap factor approximately equal to the core/cladding area ratio, which is often of the order of 0.01. Therefore, the pump absorption scales in proportion to the area ratio, so its importance is crucial for cladding pumping [2]. This is further elaborated on in Chapter 3.2. Note also that the operating pump absorption (when the laser ions are partly excited) can differ substantially from the small-signal absorption, and the change in operating absorption can be quite different from what the overlap suggests [3].

Commonly, the fibre amplification of signal pulses employ CW-pumping, due to its simplicity. In CW-pumping of pulsed lasers, the population inversion decreases during the signal pulses as these extract energy stored in the erbium ions. Then the population inversion replenishes between the pulses, allowing the same amount of energy to be extracted once again by the next pulse. CW-pumping benefits from long lifetimes, since then the absorbed pump power can be integrated over a longer time into large amounts of stored energy.

Additionally, Fig. 3.2 shows the conceptual behaviour of the excitation level in a given FUT using pulse pumping configuration. As illustrated, the short lifetime makes CW pumping less appropriate. For a pulse-pumping EDFA, the pump pulses initially excite the ions to higher energy levels (i.e., increases the excitation level in the fibre), and continue increasing until the pump pulse stops. The ions remained excited after the pump pulse. Next, the coming seed signal pulse extracts the energy from the excited ions (i.e., decreases the excitation level in the fibre), increasing the output signal energy. Ideally, the whole storage and extraction cycle is of the order of the lifetime or shorter, to allow for efficient operation also with short lifetimes.

One can also consider temporally overlapping signal and pump pulses, which, when possible, can be advantageous. However, I consider the case where the signal pulse is short compared to the pump pulse. Then, even if the signal overlaps with the tail end of the pump pulse, the pump energy deposited in the overlapping part can be neglected, so that practically all energy is deposited before the signal pulse arrives.

In order to extract the maximum energy at a given wavelength, it is desirable that the signal gain should be as high as possible, while ensuring sufficient absorption of the pump energy pulses, described by Eq. 3.1.

$$T = {}^{1}/_{e^{A_{Np}}} \tag{3.1}$$

The following Figs. (3.3 – 3.5) show the simulations of a typical Er^{3+}-aluminosilicate performance using core-pumping configuration, assuming a relatively high Er-concentration of 5 x 10^{25} m^{-3}. Here, we require an operating pump absorption of 2 Np, in order to allow for efficient operation. Note also that the operating pump absorption changes during the pumping, as the excitation level changes. The 2 Np of absorption is assumed to occur for the excitation level that is reached at the end of the pump pulse, which is also the value at the beginning of the signal pulse. This is the highest value that is achieved. The average excitation is lower, so the average pump absorption will be higher.

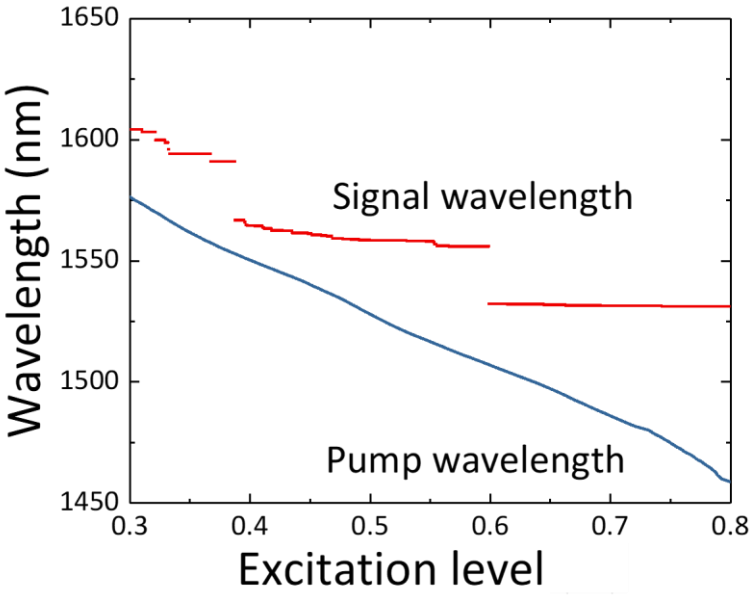

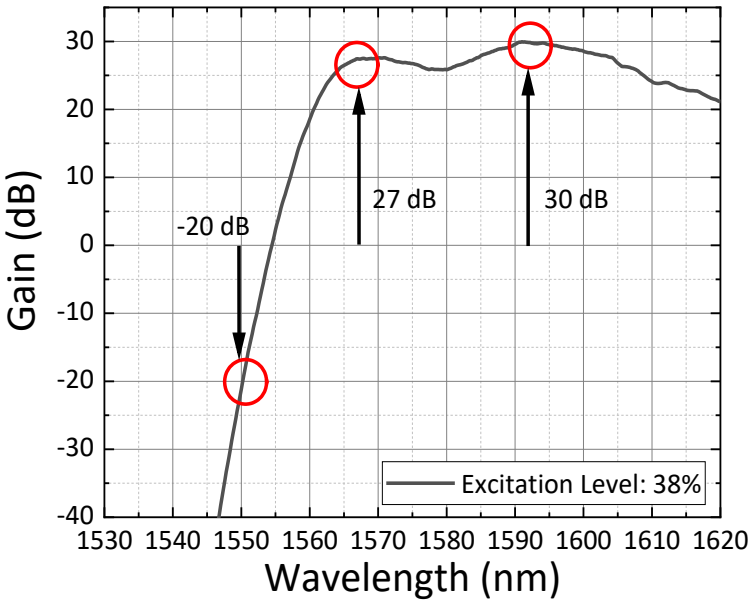

Figure 3.3 (a) Signal gain peak wavelength and maximum pump wavelength that allows for an operating pump absorption of 2 Np vs. excitation level n_2 using typical Er^{+3}-aluminosilicate fibre cross sections. (b) Calculated gain at 38% excitation level at a fibre length adjusted for 7 Np (30.4 dB) peak gain.

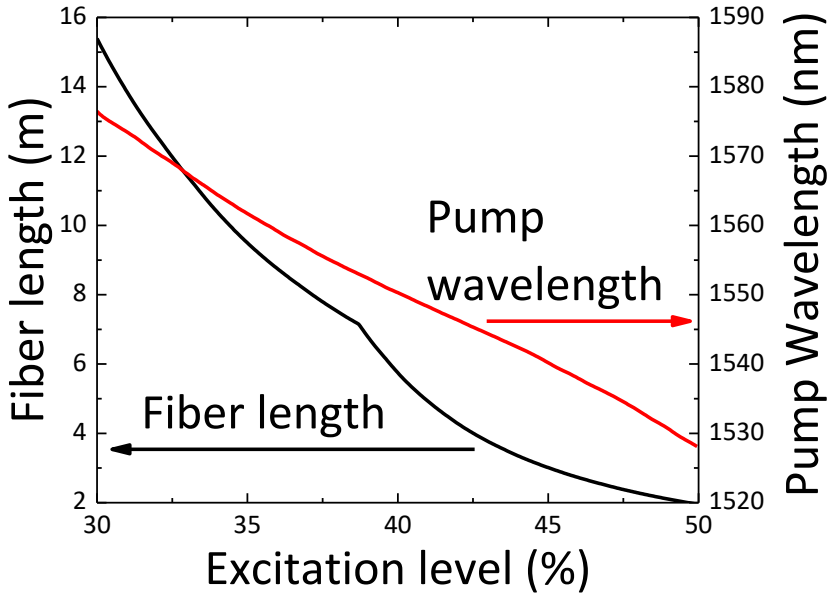

Figure 3.4 Fibre length that leads to a peak signal gain of 7 Np and maximum pump wavelength that allows for an operating pump absorption of 2 Np vs. excitation level.

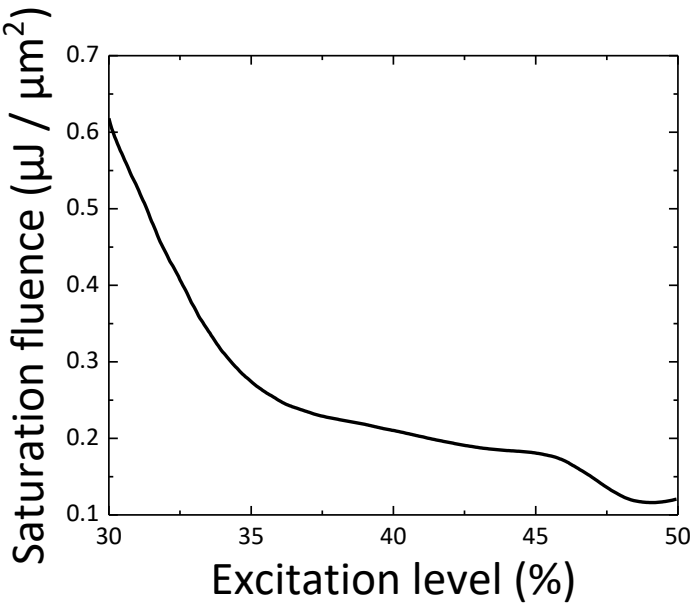

Figure 3.5 Saturation fluence vs excitation level at the pump wavelength given in Fig. 3.2 and 3.3 for an Er^{+3}:aluminosilicate fibre.

A pump absorption of 2 Np corresponds to a transmittance *T* of 13.5%, so 86.5% of the pump power is absorbed by the signal fibre amplifier (FUT), according to Eq. 3.1. Under these conditions, the data shown in Fig. 3.3 revealed the signal gain peak wavelength and the longest pump wavelength that can be used at different excitation levels. The sudden shifts of the gain peak wavelength are a consequence of jumps from one gain peak to the next, as the excitation level changes. In Fig. 3.3 (b), the difference in peak gain from 1590 and 1567 nm is only ~3 dB, and the 1567-nm peak would overtake the 1590-nm peak for a slightly higher excitation level.

While a higher absorption may seem preferable, this requires the pump wavelength to be shorter. In my context of pumping with an Er-doped fibre source, this undesirably lowers the saturation fluence (as seen from Fig. 3.5). It is then more difficult to generate high-energy pump pulses. In principle one can pump with other pump sources, e.g., at 1480 nm, and this would change the analysis. However, an Er-doped fibre pump source offers many advantages, in terms of equipment available to me as well as for possible deployment.

Fig. 3.5 shows that it is easier to generate high pulse energy at lower excitation levels in the pump EDF, but that this requires a longer signal-EDF (Fig. 3.4), which is more susceptible to nonlinear degradation. In addition, ESA becomes a factor at low excitation levels, as the gain shifts to longer wavelengths. This will degrade the efficiency. Fig. 2.6 suggests ESA is largely avoided at a signal wavelength of 1590 nm. Thus an excitation level of 0.4 may be appropriate. Note however that although the gain peak wavelength jumps to longer wavelength for lower excitation levels, the gain at 1590 nm decreases only gradually at lower excitation levels, and it is possible to use a signal wavelength of 1590 nm even when the gain peaks at another wavelength. Furthermore, a pump

wavelength of 1550 nm seems appropriate. Note also that any ASE at longer wavelength from the pump-EDF will be amplified in the signal-EDF and then reduce the stored energy. In principle, this can be avoided with a spectral filter and is not considered in the analysis. In practice, the WDM that combines the pump and signal helps to suppress such ASE, but the suppression was far from complete.

The amplifier used to boost the pump pulses was a protype Er: Yb co-doped fibre amplifier from SPI with parameters that are largely unknown and different from what is assumed in the analysis above. For example, the host is likely to be phosphosilicate rather than aluminosilicate. Through experimental work and results, I found the optimal pump wavelength in the range of ~1535 – 1537 nm (which results in low ASE and high-energy pump pulses). Based on this, assuming that there should be at least 8.7 dB or 2 Np pump absorption at the beginning of the signal pulse and aiming for a 30.4 dB or 7 Np signal gain, the estimation of the excitation level can be achieved. In addition, by knowing the peak absorption, it is possible to calculate the fibre length.

At the operating pump wavelength (1536 nm) and a PRF of 5 kHz, the pulsed pump laser source did not show signs of strong ASE for 2 µs or longer pulses. By going to lower than 5 kHz PRF or shorter pump pulses than 1 µs, it could lead to significant ASE, with, e.g., 5% of the output power or more residing between the pulses at 3 kHz PRF, 1 µs pulse duration. The pump and signal pulses are generated by a dual-channel function generator and the AOMs.

Note that the PRF is significantly higher than the inverse of the fluorescence lifetime of Er^{3+}. Thus, although ASE may be significant, losses to spontaneous emission are relatively minor.

The high-energy pump pulses goes through the WDM (Lightel), which also helps to reduce any ASE from the pump-EDFA in the signal band, and are subsequently absorbed by the signal fibre amplifier. The signal-EDFA is counter-pumped. The residual pump energy is outcoupled from the signal path by a second WDM (Lightel) in order to measure it and to protect the tuneable laser source (TLS). High residual pump pulse energy (e.g., over 15% of the total pump pulse energy) is evidence than the signal fibre amplifier may be too short.

For the signal seed, the TLS CW output is modulated by the AOM into pulses. It travels through an isolator and a fused-fibre WDM (Lightel) and then reaches the signal EDF (FUT). The signal pulses can then extract stored energy, as deposited by the high-energy pump pulses, whereby the signal pulses are amplified.

The pulse energy extractable from a fibre amplifier is strongly limited by unwanted ASE [1]. Furthermore, when the pulse energy reaches saturation, the output pulse will be distorted. This is a result of the direct connection between stored energy and gain. Thus, the leading edge (A1) of

the pulse will see a high gain due to the initially high stored energy. The concomitant high energy extracted by the pulse depletes the population inversion, so the rest of the pulse, at the trailing edge (A2), will decrease in a quasi-exponential fashion [1]. With rectangular input pulses, the gain modulation is described by Eq. 3.2:.

$$\Delta Gain\ (Np) = Ln\left({}^{A1}/_{A2}\right) \tag{3.2}$$

Both the pump and signal pulses will be the affected by distortion as well as the limited pulse energy. However, assuming that the core composition and area of the pump fibre and the signal fibre amplifier are equal, the saturation energy calculated in the signal wavelength will always be higher than at the pump wavelength. The reason is that the saturation energy decreases monotonically from longer to shorter wavelengths, until the cross-section peak at 1.53 µm. Operation at shorter wavelengths than 1.53 µm is not realistic, since the gain quickly becomes smaller and the ASE at the gain peak becomes severe. (This is quite different from operation at wavelengths longer than 1.53 µm, since at shorter wavelengths, the emission cross-sections are smaller than the absorption cross-sections.) Therefore, it will be difficult to generate pump pulses with enough energy for the signal amplifier to reach high enough gain for ASE to become significant, when pumped by those pulses. Thus, the limited pump energy sets an upper limit on the signal energy that can be extracted from the fibre under test (FUT).

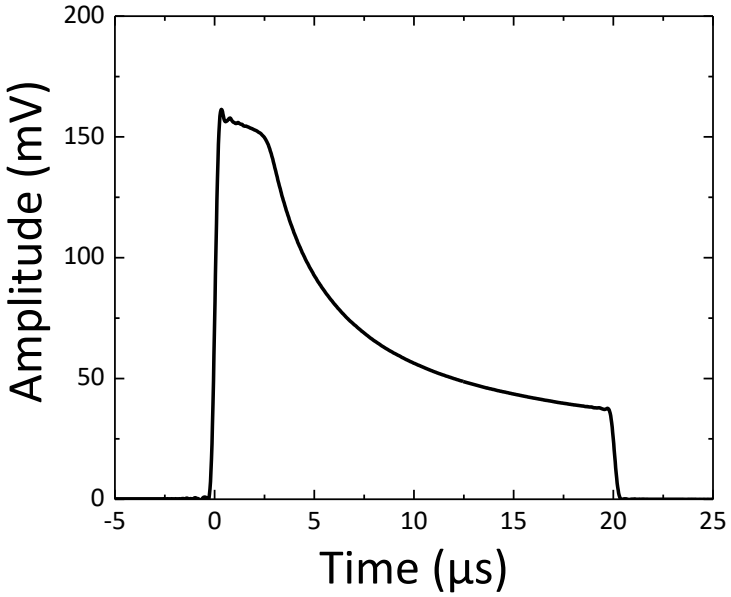

Figure 3.6 Temporal trace of the pump pulse at 20 µJ energy, 20 µs pulse duration and 5 kHz repetition rate

Fig. 3.6 shows the pump pulse, which confirms the strong distortion of the shape as the pump pulse extracts energy from the erbium-ytterbium co-doped fibre amplifier (EYDFA). It is also worth mentioning that more than 95% of the total output energy remains within the pulse, and continue to do so at energies below 25 µJ. Thus, ASE (primarily occurring between pulses) is less than 5%. By

using Eq. 3.2, the gain modulation between the leading edge and the trailing edge is ~1.48-Np, at the extracted energy of 20 μJ. This suggests that the saturation energy is ~13.5 μJ at the pump wavelength. However, the pump fibre is Er/Yb co-doped fibre, leading to different cross-sections compare to EDF. The calculated saturation fluence at 1536 nm (assuming an aluminosilicate host) is equal to ~0.093 $\mu J/\mu m^2$, which corresponds to an effective core area of the pump fibre equal to ~145 μm^2.

Next I describe my investigations with two different signal fibres (see Appendix B for details):

1) ORC fibre: A0735-L10420 (FUT #3)
2) Commercial fibre (Fibrecore): I-12 (980/120)HC (FUT #4)

Depending on the characteristics of the fibres (including the pump fibre), a judicious selection of the pulse duration and PRF of pump pulses is required to maximize the performance of the pulse energy extraction from the signal fibre amplifier. Most effort in this investigation was spent on exploring this parameter space. In the process, the pump pulses extract energy from the pump fibre and transfer it to the signal fibre amplifier. In the pulse pumping system, when the pump pulses passes through the signal fibre amplifier, at the beginning of each pulse, the excitation level in the signal fibre rises quickly, then suffers a sudden short loss of excited ions at the end of the pump pulse as any short-lived (quenched) ions relax. After that, the excitation decreases more slowly as normal ions relax. The signal pulse should arrive before most of the fast relaxation has occurred. When the next pump pulse arrives and the excitation levels will quickly rise once again, repeating the process [1].

The first selected fibre under test (FUT #3, EDF A0735-L10420) is fabricated in the ORC. The fibre has a core diameter is 14.4-μm, 0.13-NA aluminosilicate core centred in a 125-μm-diameter cladding, which was coated by a high-index polymer. The core absorption reached 130 dB/m at the 1530-nm peak. V = 3.84 at 1530 nm, so the fibre is multimoded.

The second FUT, #4, is a commercial fibre I-12 (980/125) HC, fabricated by Fibrecore, which has a core diameter of 5.2-μm, 0.25-NA aluminosilicate core centred in a 125-μm-diameter cladding, coated by a high-index polymer. The core absorption reached 20 dB/m at the 1530-nm peak.

Diagnostics for this work include an optical spectrum analyser (OSA, ANDO AQ6317B), a 1-GHz oscilloscope (Agilent DSO9104H), InGaAs photodetectors (Thorlabs DET10C, 35-MHz and EOT ET-3500, 15-GHz). Pulse energies are determined from the average power and oscilloscope traces and spectra are checked for inconsistencies (e.g., excessive ASE) with the OSA in CW and different pulsed measurement modes. Average optical powers were measured with thermal and semiconductor power meters.

3.1.1 A0735-L10420 (FUT #3)

In this section, the performance of in-band pulsed core-pumping of a fibre with a high degree of quenching is shown. The estimated erbium doping concentration of FUT #3 is 5.65 × 10^{+25} m^{-3}, calculated through Eq. 2.4, and with an estimated absorption cross section (σ_{abs} (1530 nm) = 5.3 × 10^{-25} m^2). The advantages presented for FUT #3, in the context of this research, lies in the large core area, sufficient to avoid nonlinear effects and also leads to higher extractable energy and saturation energy on the FUT. In addition to this, the fibre has a 130 dB/m core absorption at 1530 nm. Fig. 3.7 shows CW unsaturable absorption measurements at 1536 nm.

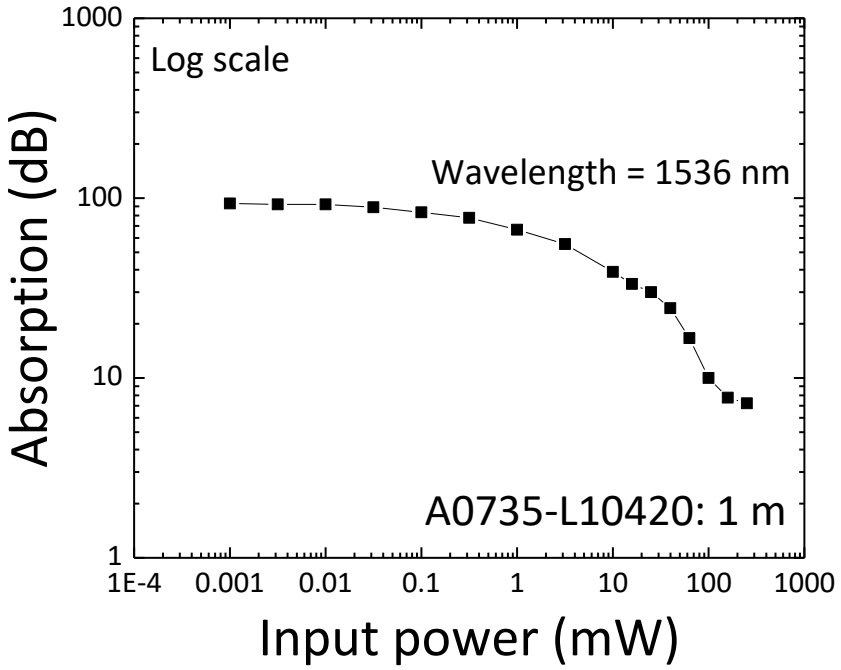

Figure 3.7 Unsaturable absorption measurements from FUT #3.

Based on experimental data for different fibre lengths and signal wavelengths, a signal wavelength of 1565 nm and a fibre length of 0.17-m are selected. The summary of the research regarding the core pulse-pumping in highly EDF using the FUT #3 is presented in Fig. 3.8

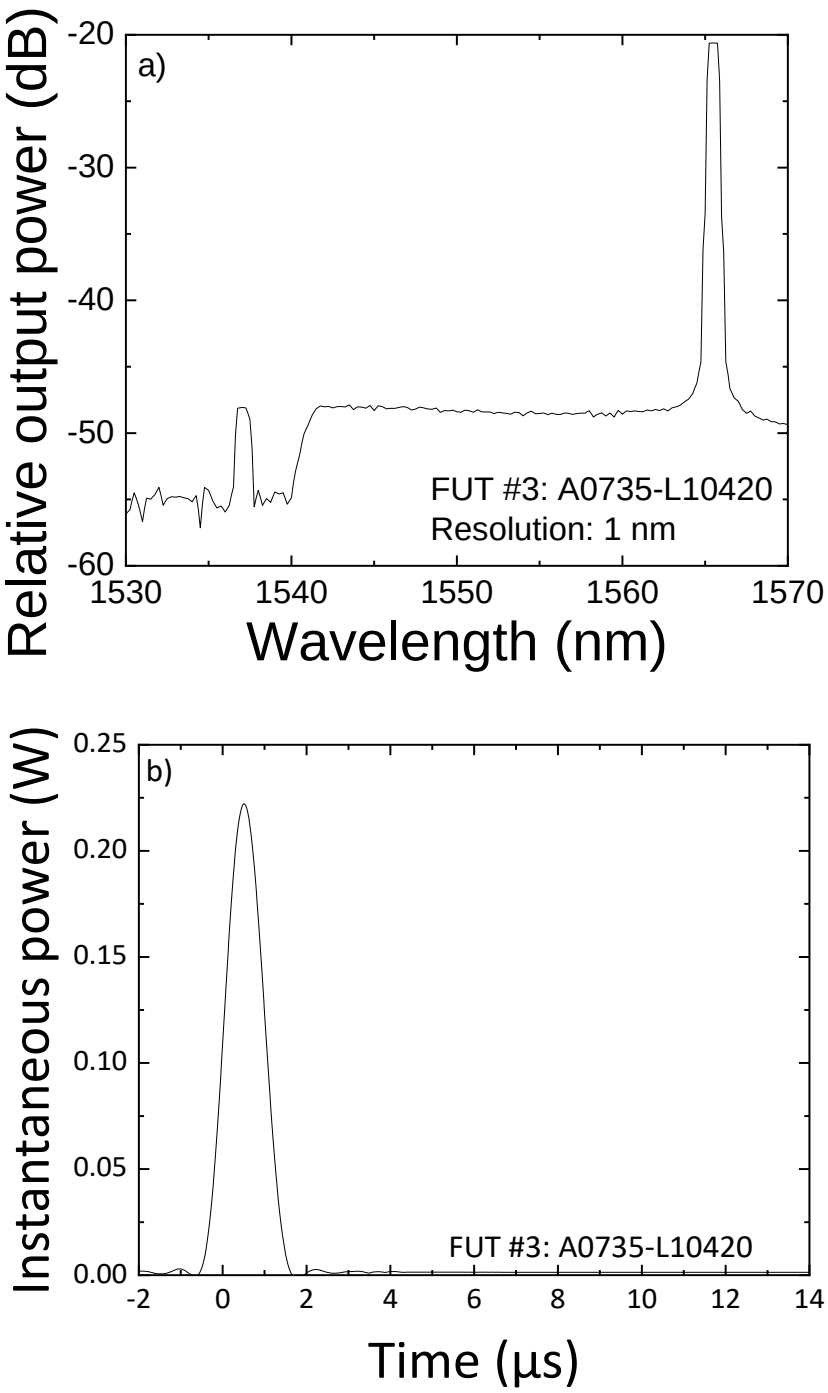

Figure 3.8 (a) Optical spectra from the signal pulses at 1 µs, 5 kHz and output pulse energy of 224 nJ. (b) Temporal trace from the signal pulses.

The counter-directionally core-pumped amplifier configuration used pump pulses at 25 µJ pulse energy, 25 µs pulse duration, and signal pulses at 162 nJ pulse energy, 1 µs pulse duration, both at 5 kHz PRF. Through the pulse generator, it was possible to control the position of the signal pulse, moving it through the pump pulse. The experimental data shows that the signal pulse extracts the energy more efficiently at the beginning of the pump pulse, decreasing by a factor of 0.02 mW when the signal pulse moves farther away from the leading edge of the pump pulse. The reason for the lower performance as the signal was shifted from the leading edge of the pump pulse is likely

to be the higher instantaneous pump power in the leading edge. This also implies that the pump pulse duration is too long, i.e., better results may be achievable with shorter pump pulses with higher peak power. Note also that the 25-µs pump pulse duration is much larger than the transit times through fibre. This is ~5 ns/m. For 1-µs pulse durations the length of cables, fibres and beam paths can normally be neglected, but for durations below 100 ns this is not necessarily the case.

The highest peak signal power measured is ~225 mW, corresponding to a pulse energy of 225 nJ, shown in Fig. 3.8. A 20% of the pump energy is leaked from the FUT #3. This means that approximately 20 µJ of energy was stored within the fibre. Fig. 3.9 shows the results at a constant 20 µJ stored pump energy at different avg. seed power, with a constant 5 kHz PRF, comparing these results with the CW-regime (i.e., avg. signal input power = CW signal input power).

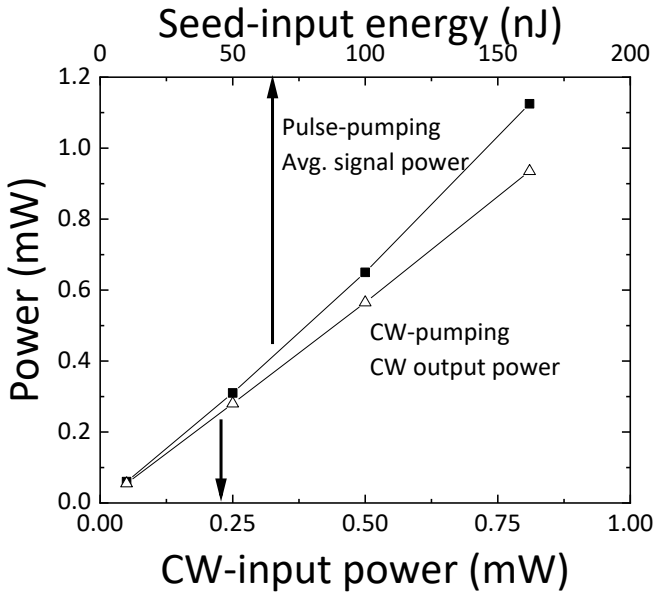

Figure 3.9 Gain vs pump energy at 10-µs (pulse duration) and CW-power. In the case of pulse pumping, the pulses have a 25-µs pulse duration and 5-kHz PRF.

The highest achievable gain using the FUT #3 is 1.45 dB, which corresponds to 1.12 mW avg. output power. When compare to CW-pumping (i.e., 0.6 dB gain), the gain is 0.85 dB higher in the pulse-pumping regime. This is attributed to the rapid energy extraction from the Er^{3+}-ions. On the other hand, the saturation energy from the fibre FUT #3 at 1565 nm is calculated to be 42 µJ. Unfortunately, the highest extractable energy obtained is only 0.225 µJ, giving the indication that strong parasitic effects (i.e., concentration quenching related effects) are hindering the performance of the FUT #3.

In conclusion, the results have shown that in this highly-quenched EDF, pulse-pumping is more efficient than CW-pumping (if only marginally in this case) . The system obtained 1.45 dB gain by pulse-pumping a 0.17-m EDF, compared to 0.6 dB with CW-pumping. Unfortunately, it seems that

the detrimental effects on a highly-quenched EDF were more severe than anticipated, at least with the pump pulse duration considered here.

In the context of pump energy, assuming the stored energy in the fibre is 20 µJ, yet only 0.1% of said energy is being extracted, the question now becomes if it is worth it to work with a large core area. Using a smaller core area will limit the saturation energy on the fibre, which in turns limits the extractable energy that can be achieved from it. However, using a larger core increases the pump threshold in the fibre, which means that higher pump energy will be needed to achieve gain in the signal fibre amplifier (i.e., FUT). Therefore, if it is not possible to improve the pump energy, then the easier way to address this is to reduce the core size of the signal amplifier.

To verify that it is possible to reach high gain with my pulse-pumping setup I therefore next investigated a smaller-core EDF with low quenching, i.e., FUT #4, which is a commercial fibre, and used that as a baseline from which the impact of quenching could be assessed.

3.1.2 I-12 (980/120) HC (FUT #4)

The FUT #4, a commercial EDF from Fibrecore (I-12(980/120) HC), is investigated by the counter-, core-pumping scheme (as described in Fig. 3.1). Due to the low absorption peak at the pump wavelength (i.e., 1536 nm), as seen in Fig. 3.10, the operating fibre length of ~14.5 m in order to keep the same operating pump absorption as FUT #3 (i.e., 80%). The estimated Er-concentration from the FUT #4 is 8.7 × 10^{+24} m^{-3}, calculated by Eq. 2.4. The saturation energy for FUT #4 is calculated to be 6.23 µJ, which is 7 times smaller than the FUT #3.

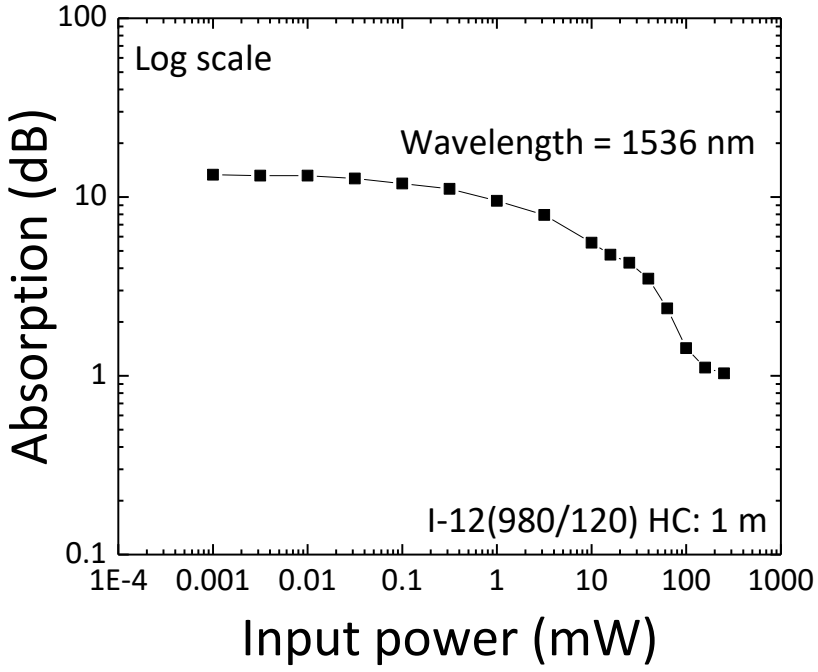

Figure 3.10 Absorption measurements from the FUT #4.

At 14.5 m fibre length, the pump leakage measured from the FUT #4 was 20%, which seems to indicate that the stored energy within the fibre is the same as the stored energy in FUT #3 (i.e., 20 µJ). Furthermore, Fig. 3.11 shows the optical spectrum (a) and temporal traces (b) using pump pulses at 25 µJ pulse energy, 25 µs pulse duration and signal pulses at 170 nJ pulse energy, 5 µs pulse duration, both at 5 kHz PRF. This amplifier configuration reached up to 13.5 µJ of output energy, which is 2.17 times the estimated saturation energy from the FUT #4, and corresponds to a pump energy conversion efficiency of 54%. Shorter pulses at 1 µs, as well as changing the relative timing between the pump and signal by 0.1 to 0.5 µs, were also tested but did not show any significant difference in regards of the extractable energy.

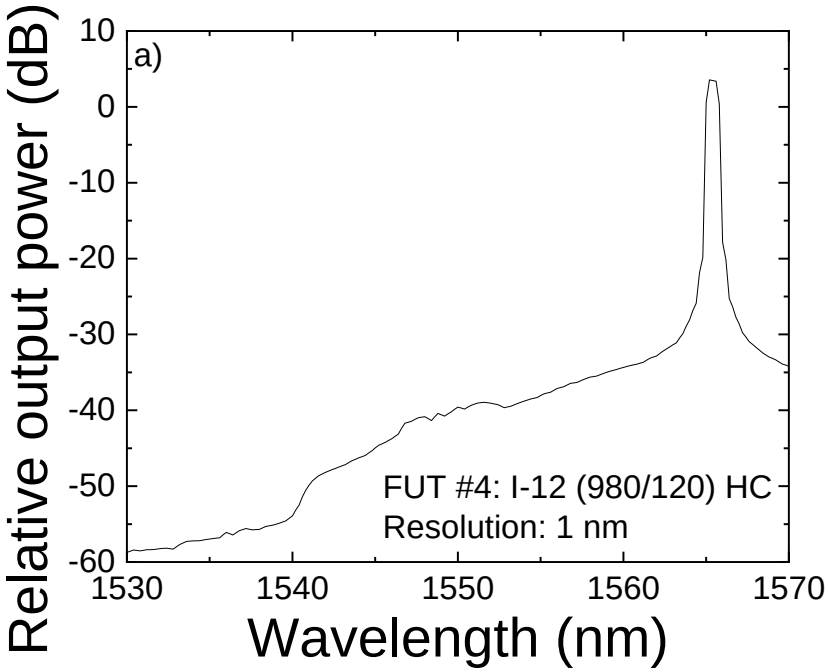

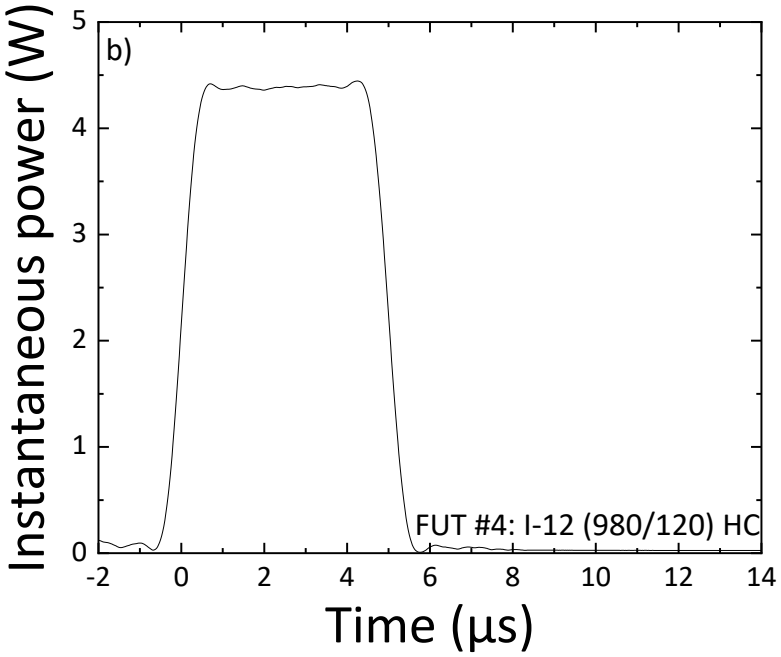

Figure 3.11 (a) Optical spectra from the signal pulses at 5-µs, 5-kHz and output pulse energy of 13.5-µJ. (b) Temporal trace from the signal pulses.

To reiterate, the aim of this project is to convert pump energy to signal energy, and in order for this to work, the first step is to launch the pump pulse energy into the signal fibre amplifier and then extract that energy with the signal pulses. However, there is a limit of how much pump energy one can store within the signal fibre amplifier. Saturation energy is one of the main factors that determines the limit of the stored energy, which in turns depends on the core area. Therefore, Fig. 3.8 and 3.11, the FUT #3 can have much higher stored energy capacity compared to FUT #4. Nevertheless, the pump pulse energy currently available (i.e., 25 µJ pump pulse energy) can still be fully stored within the commercial fibre, and because of that, there is no need for such a high saturation energy provided by the FUT #3.

In other words, there is a limit of how much energy can be stored within both signal fibre amplifiers, but because it is not possible to reach that limit in the case of the FUT #3, that advantage becomes irrelevant.

Rather, in this situation, the ability to store more energy may be a disadvantage, since it means that pump energy needed to reach a certain gain becomes higher, and, equivalently, the gain achieved for a certain pump energy, becomes lower. Therefore, it is not possible to create as much gain on the FUT #3 (even disregarding the quenching). This makes it harder to extract the energy from it, compared to FUT #4.

In conclusion, while the FUT #3 has a higher limit of stored energy, the system cannot take advantage of it, and unfortunately, it is still taking the penalty of having a harder time extracting the energy from that fibre and being more strongly quenched..

In the context of pulse duration, one need to remember that this commercial fibre will not suffer from concentration quenching as much as a highly doped fibre, so it is easier to avoid this detrimental effect, even at longer pulses (e.g., above 5 µs). The primary idea is to overcome concentration quenching by using short pump pulses to store the energy efficiently within the fibre, before the Er^{3+}-ions quenched, and their lifetime is reduced, reducing the gain of the signal fibre amplifier. Therefore, a highly doped fibre does require short pump pulses (shorter than the 25 µs I used), whereas the commercial fibre does not necessarily require these shorter pump pulses (e.g., 1 to 10 µs) to achieve high energy extraction (but would have definitely help in achieving much higher peak powers).

Thus, it is concluded that core-pumping configuration may not be ideal to pursue with the current pump energy available at 1530 nm. This issue is also crucial in the cladding-pumping configuration. A solution for this is to verify if CW-pumping may be a viable way to store the energy in a highly quenched erbium fibre.

3.2 Cladding-Pumping Study

This section considers cladding pumping at 0.98 µm as well as 1.5 µm, pulsed as well as CW.

The use of a double-clad signal fibre amplifier removes the need to launch the pump pulses into the core, which is instead launched into the inner cladding. This opens up for pumping with much higher energy pulses from multimode laser sources of relatively low energy fluence. However, cladding pumping reduces the pump absorption. A question then is if it is possible to absorb the pump pulses in a signal fibre that is sufficiently short to avoid excessive nonlinearities.

For cladding pumping of the signal fibre amplifier, the same general principles as for core pumping applies, taking into account the lower pump absorption. For a given value of n_2, there is a value of the operating (net) absorption cross section, which depends on wavelength. The operating pump absorption for the double-clad fibre is calculated according to Eq. 9, Eq. 10 and Eq. 11:

$$\alpha_p = N_o * \sigma_{net}^{pump} * L * \Gamma_{clad} \tag{9}$$

$$\Gamma_{clad} = \left(\frac{r_{core}}{r_{clad}}\right)^2 \tag{10}$$

$$\sigma_{net}^{pump}(\lambda) = \big(\sigma_{ems}(\lambda) + \sigma_{abs}(\lambda)\big)n_2 - \sigma_{abs}(\lambda) \tag{11}$$

Thus, the pump absorption coefficient (α_p) depends on the rare-earth doping concentration (N_o), measured in ions / m^3, the net absorption cross section (σ_{net}^{pump}), which varies depending on the absorption and emission cross sections at a given wavelength, the fibre length (L) and the overlap core / cladding ratio (Γ_{clad}). Because of the low absorption cross-sections of erbium, it is necessary to use a large pump overlap and thus a relatively small inner cladding (area ratio typically below 50). In addition, Eq. 10 represents a best-case scenario. By contrast, circular symmetry in double-clad fibre (DCF) is known to lead to poor overlap between pump modes in the inner cladding with the rare-earth-doped region in the core, and thus low effective pump absorption [2]. Techniques such as noncircular inner cladding and offset signal core are used to deviate from the circular symmetry and thus improve the pump absorption per unit length [3-6]. However, non-circular geometries can be difficult to realize with EDFs for two reasons. If the inner cladding is small (e.g., below 80 µm diameter), the fibre becomes difficult to handle. Furthermore, for pumping at 1.5 µm, the coating absorbs the light. For both reasons, all-glass guiding structures are preferable, which however makes it more difficult to fabricate fibres with shaped cladding. I have not considered this important practical aspect in any detail. Although I improved the pump absorption of circular fibres by bending them, this is difficult in case of low-NA cores. Furthermore, that approach is rarely, if ever, used in commercial products.

3.2.1 Analysis of In-Band Cladding-Pumping with Pulsed Er-Doped Fibre Pump Source

Fig. 2.5 shows that for Er: aluminosilicate, the operating absorption peaks at around 1530 nm, for the anticipated range of excitation levels (up to 40%). Thus, this would be the pump-wavelength-of-choice, if the absorption was the only concern. However, we must also take the energy that can be reached at different wavelengths into account. In case of pumping with an EDF source, this increases for wavelengths longer than 1.53 µm. Therefore, there will be an optimal choice of pump wavelength, as well as fibre length, signal wavelength and core/cladding area ratio for the signal fibre amplifier. I next analyse this, under the assumption that the peak gain is limited to 7 Np, to avoid excessive ASE and spurious lasing. As before, the excitation level n_2 is a critical parameter. Two fibres with the same n_2 will have the same spectral gain shape (including peak gain wavelength), and it they also have the same concentration-length product, they will have the same peak gain, whether they are core-or cladding-pumped. Thus, the gain details are the same for the equivalent core-pumped case, and here the focus is on pump absorption.

Considering the overlap factors and the Er-doping concentration as constants for a given fibre, the net-absorption cross section is the only variable in the calculation of the absorption (and gain). The maximum achievable pump pulse energy ('effective energy') is assumed proportional to the

product between the net absorption cross-section and the saturation fluence at the pump wavelength, described in Eq. (12) and by Fig. 3.12:

$$Effective\ energy \propto \sigma_{net}^{pump} * U_{sat}^{pump} \quad (12)$$

Effective energy = Value proportional to the achievable pump pulse energy stored at the signal fibre amplifier

Equation (12) can be understood as follows. For a given fibre, for each value of n_2, the length is determined by the 7-Np peak gain. Thus, the absorption per unit length is fixed for a total operating pump absorption (e.g., 2 Np). Furthermore, at this n_2-value, the pump absorption per unit length is proportional to the resulting net operating pump absorption cross-section divided by the pump area (equal the inner-cladding area of the signal-EDF). Thus, the pump area is inversely proportional to the net absorption cross-section. Then, insofar as the fluence that can be obtained from the pump source is proportional to the saturation fluence, the total pump energy that can be launched into a signal fibre with inner-cladding area chosen to allow for 2 Np pump absorption follows Eq. 12.

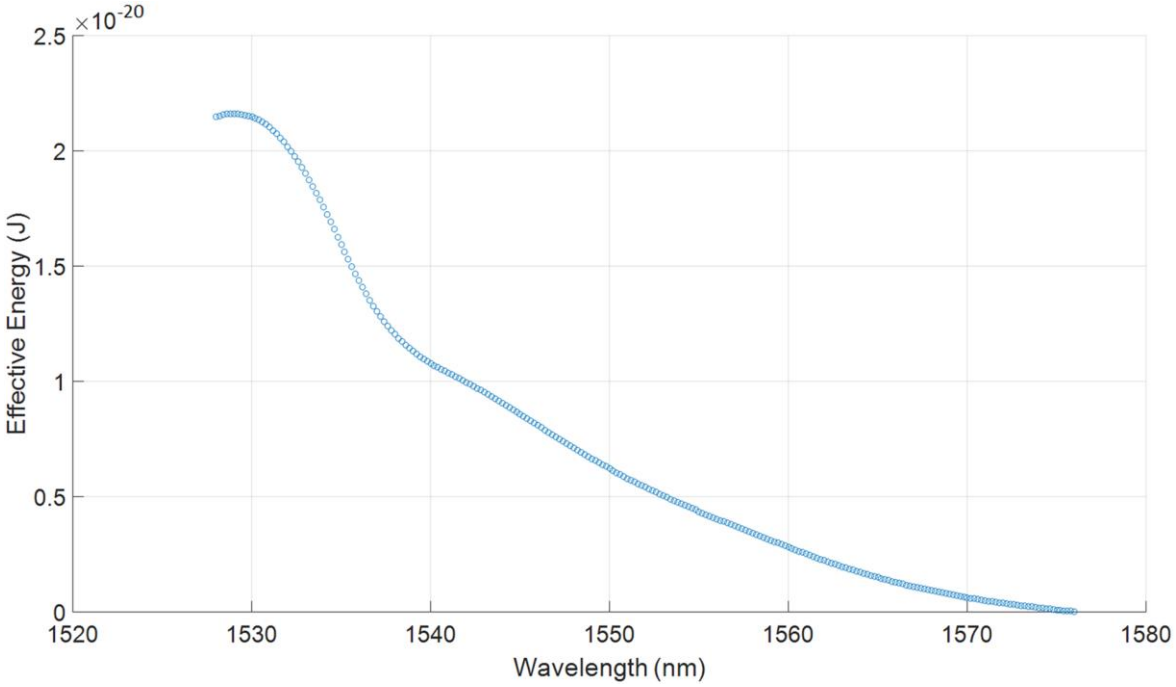

Figure 3.12 Pump wavelength vs effective energy $\sigma_{net}^{pump} * U_{sat}^{pump}$ at the excitation level of 0.3 [Er^{+3}: aluminosilicate].

Although those deliberations are rather complicated, in practice the outcome is quite simple, namely, pumping at the 1530-nm absorption peak is best for cladding-pumping. From the graph in Fig. 3.12, the 'effective energy' decreases for pump wavelengths longer than 1530 nm. This remains true for $n_2 \leq 0.4$. Also worth mentioning is that for $n_2 \geq 0.5$, 1530 nm is no longer absorbed, so shorter pump wavelengths would be needed. However, a there is no attractive pump source for

pulsed in-band pumping at shorter wavelengths than 1530 nm. Therefore, in practice, the shortest operating pump wavelength with the highest achievable pump pulse energy is 1530 nm.

The precise pump energy that can be extracted from an appropriate pump-EDF and launched into the signal-EDF is given by:

$$k\ U_{sat}^{pump}\ (\sigma_{pump}^{net}\ /\ \sigma_{signal}^{net})\ A_{core}^{SF}\ (NA_{clad}^{SF}\ /\ NA_{pump})^2\ (G_{operating})\ /\ \alpha_{operating})\ /\ \Gamma_{signal}^{SF}$$

$$= 5 \times 2.2\times10^{-20}\ \text{J}\ (1\times10^{-26}\ \text{m}^2)^{-1} \times 1000\ \mu\text{m}^2\ (0.3/0.06)^2\ (7\ \text{Np}\ /\ 2\ \text{Np})\ /\ 1$$

$$= 0.96\ \text{J}. \text{ (Eq. 13)}$$

Here, the superscript "SF" is used for quantities relating to the signal fibre. The factor k = 5 represents how many times the saturation energy can be extracted from the pump fibre, and the product $U_{sat}^{pump}\ \sigma_{pump}^{net}$ (the effective pump energy) is taken from Fig. 3.12 as 2.2×10^{-20} J, which assumes n_2 = 0.3. The NA of the pump beam on the exit of the pump fibre is assumed as NA_{pump} = 0.06. The signal overlap is assumed to be unity. The net emission cross-section for the signal (peak wavelength ~1605 nm) is 1×10^{-26} m^2. This is close to the value for n_2 = 0.3, but note that it increases to ~2.3×10^{-26} m^2 for n_2 = 0.4 at the 1565-nm peak.

The energy thus assessed for cladding-pumping is astonishing, and there are certain to be additional limitations, including damage, thermal, and nonlinear limitations. From Fig. 3.4, the length of the signal-EDF for n_2 = 0.3 becomes 15.4 m even for a relatively high concentration of 5×10^{25} m^{-3}, although it decreases to 5.8 m for n_2 = 2. Furthermore, the energy can be stored in the signal fibre is much smaller than 0.96 J. Such high energy can be expected to provide a lot of design flexibility, but further optimization for specific scenarios is needed to make the most of this.

It is also interesting to see how cladding-pump system compares to core pump. As previously discussed, the main issue with cladding pumping is the lower absorption compare to core pumping. Based on Eq. (2), the pump absorption coefficient is proportional to the net-absorption cross-section. For cladding pumping, the best pump wavelength is 1530 nm for all excitation levels below 40% in order to keep high effective energy. Therefore, the next step is to know how much the absorption coefficient decreases with cladding pumping compared to core pumping. This is equal to the area ratio that is used in case of cladding-pumping, or more precisely, the ratio ($\Gamma_{pump}^{core\text{-}pumping}$ / $\Gamma_{pump}^{cladding\text{-}pumping}$) in the signal fibres. Eq. (13) calculates the ratio between the net-absorption coefficients for the cladding pumping and core pumping (referred to as 'effective absorption coefficient'). This is an important factor in Eq. 13 and is shown in Fig. 3.13:

$$Effective\ absorption\ coefficient = \frac{\sigma_{net,clad}^{pump}}{\sigma_{net,core}^{pump}} \quad (14)$$

$\sigma_{net,clad}^{pump}$ = Net-absorption cross section in cladding pumping

$\sigma_{net,core}^{pump}$ = Net-absorption cross section in core pumping

This amounts to trading a reduced pump absorption rate through the use of cladding-pumping at 1530 nm against a reduced pump absorption rate through the use of a longer pump wavelength, where the saturation energy is higher. This can be thought of as comparing the performance in (nearly) opposite ends of the curve in Fig. 3.12, drawn for $n_2 = 0.3$.

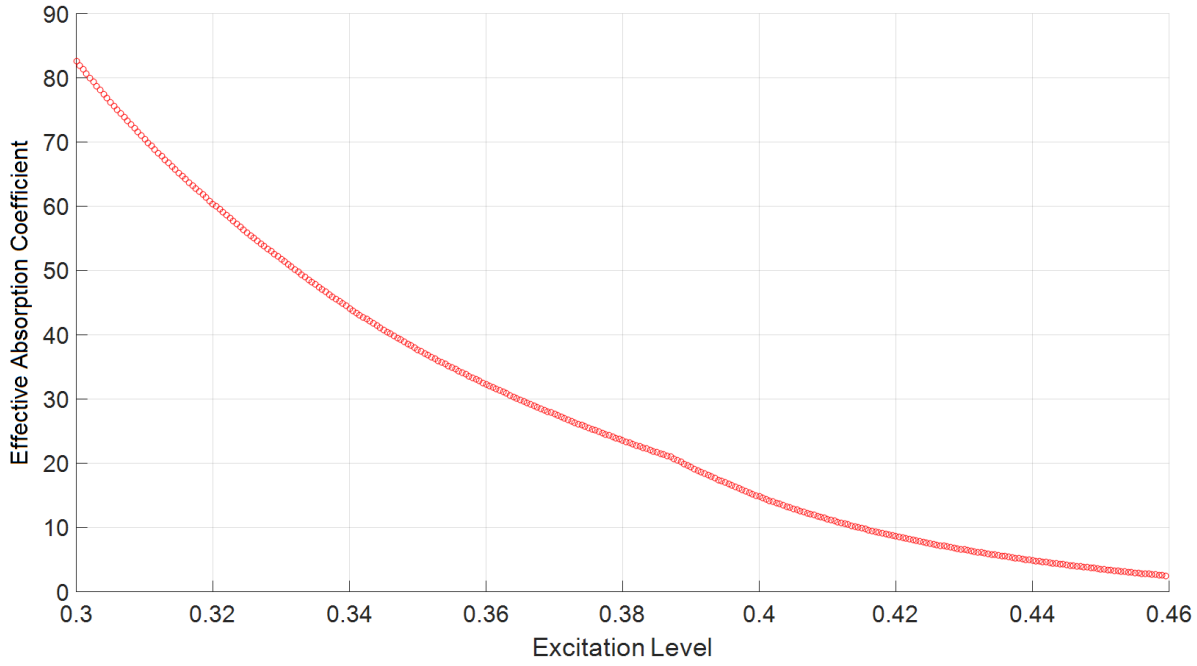

Figure 3.13 Excitation level vs effective absorption coefficient [Er^{+3}: Aluminosilicate] according to Eq. 14. This is the same as the area ratio that can be used in case of cladding-pumping.

Finally, for comparing cladding pumping and core pumping, we introduce a quantity 'effective saturation fluence' as shown in Eq. (15):

$$Effective\ saturation\ fluence = \left(\frac{\sigma_{net,clad}^{pump}}{\sigma_{net,core}^{pump}}\right) * U_{sat,clad}^{pump} \quad (15)$$

$U_{sat,clad}^{pump}$ (J/m^2)= Saturation energy at 1530 nm (cladding pumping system)

Effective saturation fluence (J/m^2)= Achievable saturation fluence stored in a double-clad signal fibre amplifier

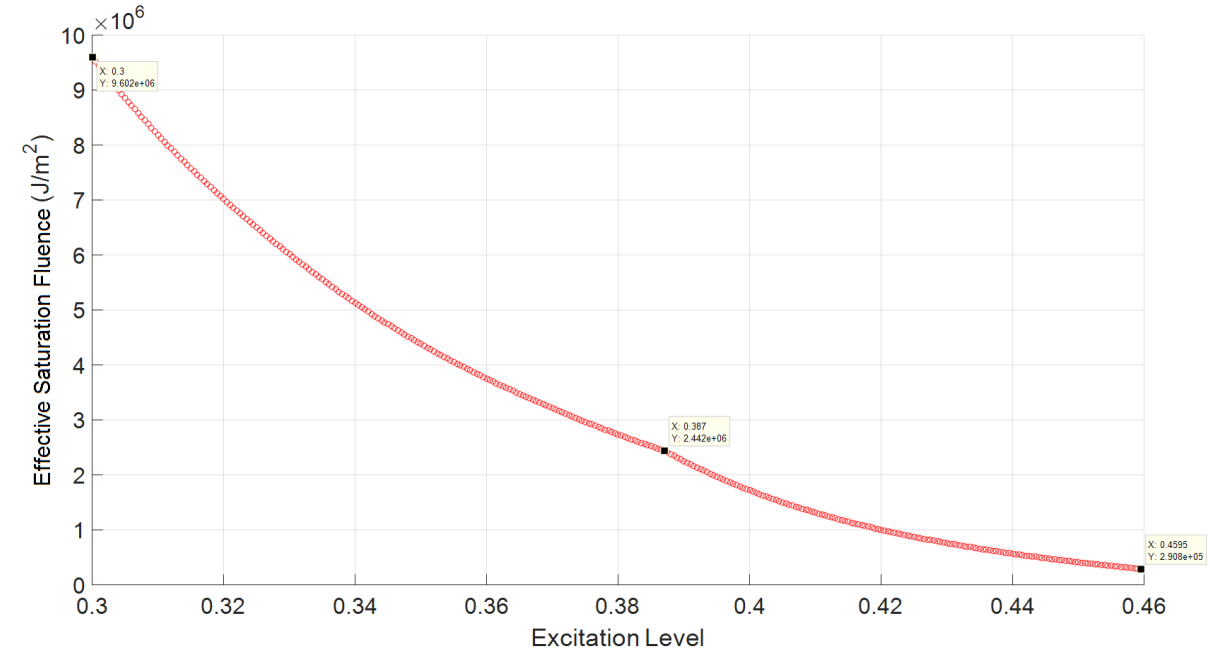

Figure 3.14 Excitation level vs effective saturation fluence [J/m^2]) [Er^{+3}: Aluminosilicate].

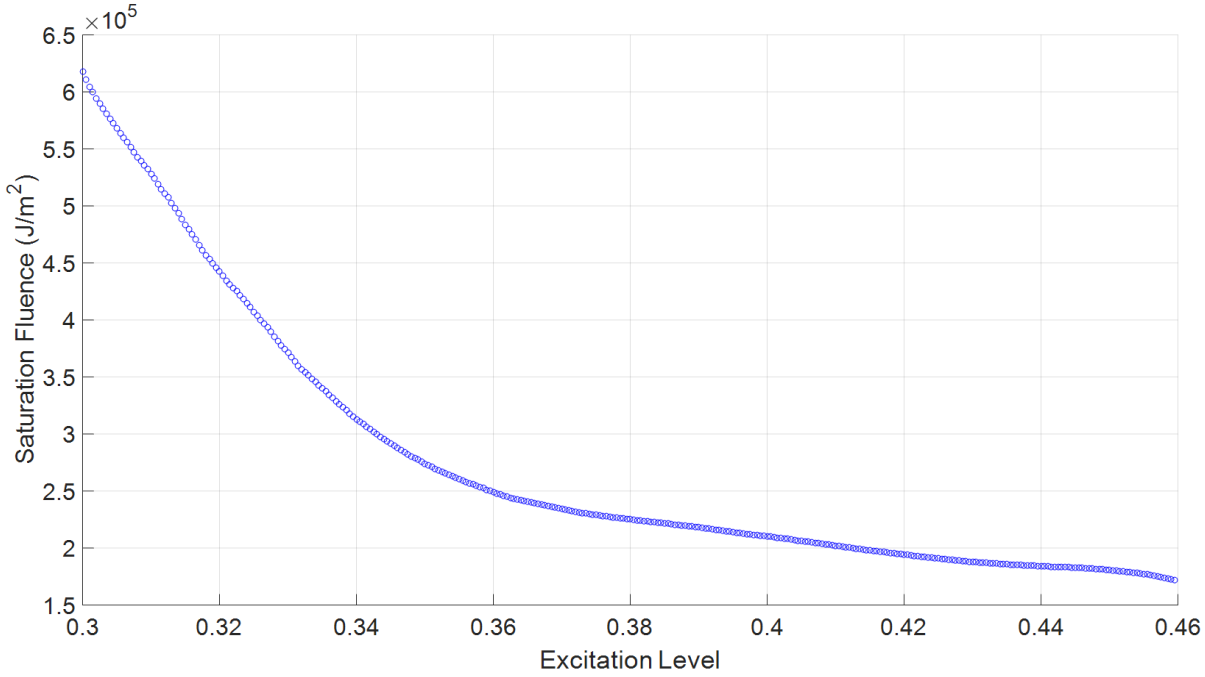

Figure 3.15 Excitation level vs saturation fluence for the core-pumping system [Er^{+3}: Aluminosilicate].

By comparing Fig. 3.14 (cladding pumping) with Fig. 3.15 (core pumping with a longer wavelength that leads to the same pump absorption), the effective saturation fluence is approximately 15 times larger, which means that cladding pumping leads to approximately 15 times higher saturation fluence compare to core pumping. Note that this still disregards the NA-scaling that is available with cladding-pumping, i.e., $(NA_{clad}{}^{SF} / NA_{pump})^2 = 25$ in Eq. 13.

Although it seems very promising, this approach requires advanced fibre designs which were not available. Therefore, it was not pursued.

3.2.2 Simulations of 0.98-µm Cladding-Pumping

The promising analysis for in-band cladding-pumping motivated an analysis of cladding-pumping at 0.98 µm, where suitable fibres and pump sources may be more readily available. Here, the analysis is restricted to CW-pumping, whereas pulse-pumping is considered in future chapters. For this work, the investigations revolve around the amplification of high-energy pulses of 0.1 – 10 µs duration in a counter-directionally cladding-pumped Er-doped fibre amplifier. The quenching timescale for these simulations is in the range 50 ns – 10 µs [7]. Amplified spontaneous emission (ASE) is neglected. Whereas significant ASE can be avoided at the low signal gain, it can still be a factor if the gain peak wavelength is different than the signal wavelength, or the gain is locally unsaturated, e.g., at the edge of the core [8].

The simulations assumed a 60 W CW cladding-pumping at 980-nm, and a signal pulse of 25 µJ pulse energy at 1560 nm. For the pump fibre, it is assumed a CW multimode fibre coupled laser diode at 980 nm, with a core diameter of 110-µm. For the signal fibre amplifier, the simulations considered the D-shaped inner cladding, on a double-clad EDF with a 0.13-NA, 20-µm-diameter Er-doped aluminosilicate core centred with an inner cladding / core area ratio of 16 – 81. In addition, an Er-concentration of $5 \times 10^{+25}$ ions / m^3 and with 100% of pair Er^{3+}-ions detrimental effects at 1560 nm (i.e., fully quenched). The results of these simulations are shown in Fig. 3.16:

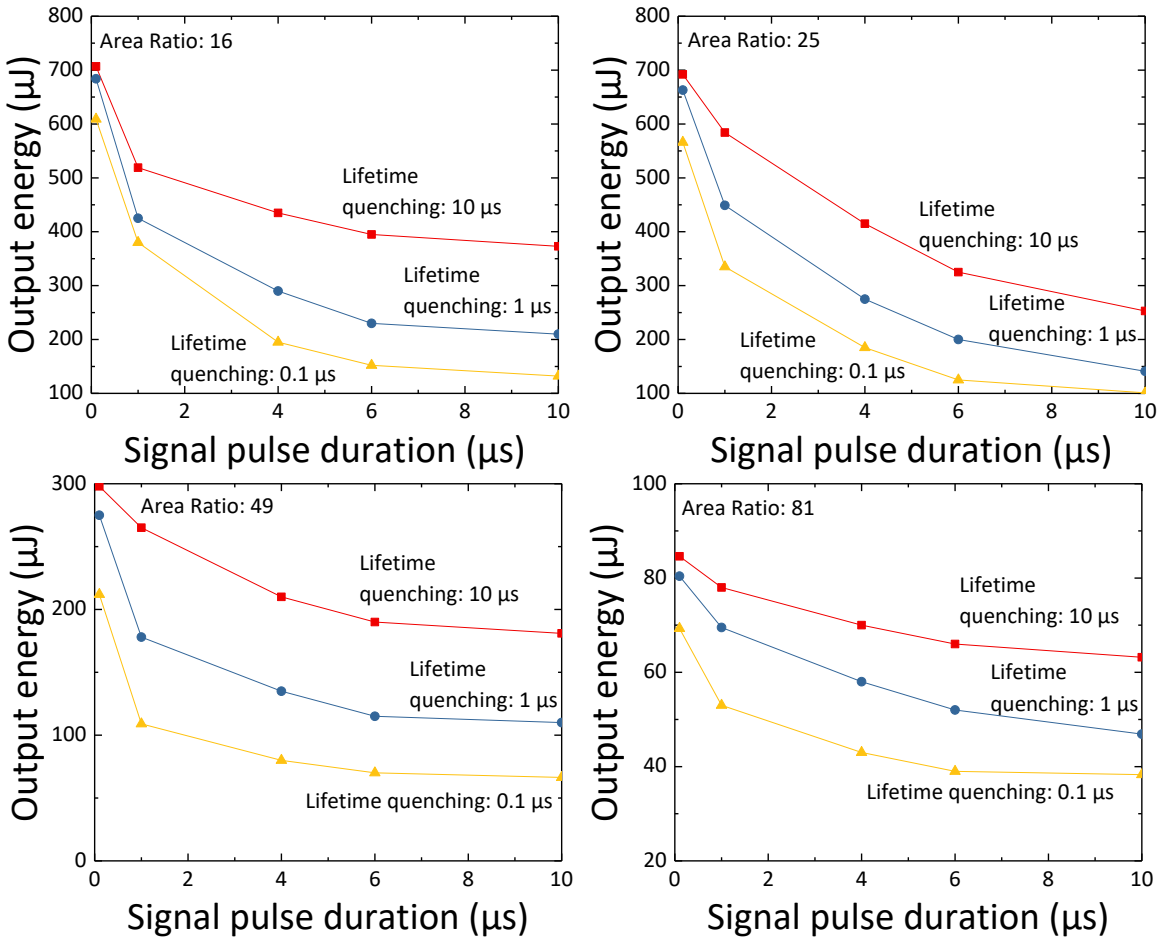

Figure 3.16 Study of the performance on a cladding-pumping configuration for various fixed pulse durations but at different area-ratio, with 100% unsaturable absorption.

Fig. 3.16 shows the output energy for a 60 W CW cladding-pumped EDF, with a 25 µs launched signal pulse energy. The fibre length is optimized depending on the area ratio, keeping a fixed pump absorption (e.g., 80%), at different area-ratio, at a fixed CW pumped power and signal pulse energy. These results show that it is possible to achieve over 15 dB signal gain despite the use of CW-cladding pumping configuration. In addition, the optimal area ratio appears to be in the range of 16 – 25 under this regime, at 3 m operating fibre length.

The lifetime quenching (i.e., quenching time scale) is an important factor in the simulations, which significantly changes the extractable energy at different pulse duration. The shorter the lifetime quenching, the more important it is to operate with a signal pulse duration shorter than, or comparable to, the lifetime quenching.

An Er-concentration of $5 \times 10^{+25}$ ions / m^3 is understandably quite high, and also leads to relatively high unsaturable absorption, although assuming that 100% of pair Er^{3+}-ions is a bit unrealistic, but not impossible.

3.3 Conclusions

The system with the homemade fibre A0735-L10420 (i.e., FUT #3) proved to work as a signal fibre amplifier for the signal seed, despite its significant degree of quenching. However, the increase of 1.45 dB gain could hardly be considered adequate. Much better results were demonstrated by the commercial fibre (i.e., FUT #4). The results demonstrate the efficacy of pulse pumping, when the parameters of the FUT and pump source are appropriate.

In conclusion, the pump pulse energy and the signal fibre core area need to be reasonably well match. In this regard, the FUT #4 was a better match to the system than the FUT #3. And while one of the aims of this work is to overcome the disadvantages of quenching effects, it is worth reminding that an unquenched fibre always win in terms of extractable energy. However, the final goal is not only overcoming quenching effects, but also keeping the fibre short enough to prevent optical nonlinearities that can appear in high-power fibre amplifiers. At the end, with this method, the signal fibre amplifier may still win thanks to also avoiding optical nonlinearities in contrast with the other systems.

There are currently two ways to improve the system; the first is the use of a pump fibre with a larger core area. As said before, the saturation fluence at the pump fibre will always be lower than the signal fibre, setting an upper limit on the signal pulse energy in the core-pumping configuration. However, the saturation energy at the pump fibre can increase by using a larger core area, compensating or that limitation. For the signal fibre amplifier, it might be better to work with a highly doped fibre, while retaining a similar core area to the commercial fibre, matching as well as possible with the current pump pulse energy available with the core size.

The second way is to consider the use of a double-clad fibre amplifier. Preliminary investigations suggest that in-band pulsed cladding-pumping with an EDF source can allow for pump energies well over 100 mJ. However, this would require development and fabrication of new types of fibres, and therefore this avenue was not pursued. CW in-band cladding-pumping would be simpler, but without any clear advantage over 0.98-µm pumping in the simplest of configurations, cladding-pumping directly with diode lasers. Its attractions, was further strengthened by the simulations presented in this chapter, which proved that cladding-pumping with a CW high-power diode laser at 980 nm is a viable way to store the pump energy within the signal fibre amplifier, despite being affected by concentration quenching. Furthermore, it is far easier to obtain high average-pump power from a 980-nm diode laser, than with high-energy pulses at 1.53 µm.

3.4 References

1. Desurvire, E., (2012), “Erbium-doped Fibre Amplifiers”, Department of Electrical Engineering Columbia University, Wiley-Interscience, page 320 – 330.
2. S. Bedö, W. Lüthy, and H. Weber, “The effective absorption coefficient in double-clad fibres,” Optics Communications **99**, 331–335 (1993).
3. Yutong Feng, Pablo G. Rojas Hernández, Sheng Zhu, Ji Wang, Yujun Feng, Huaiqin Lin, Oscar Nilsson, Jiang Sun, and Johan Nilsson, “Pump absorption, laser amplification, and effective length in double-clad ytterbium-doped fibers with small area ratio”, Opt. Express 27, 26821-26841 (2019).
4. A. Liu and K. Ueda, “The absorption characteristics of circular, offset, and rectangular double-clad fibres,” Optics Communications **132**, 511–518 (1996).
5. A. Liu and K. Ueda, “Propagation losses of pump light in rectangular double-clad fibres,” Optical Engineering **35**, 3130–3134 (1996).
6. M. H. Muendel, “Optimal inner cladding shapes for double-clad fibre lasers,” in Conference on Lasers and Electro-Optics, vol. **9** of OSA Technical Digest (Optical Society of America, Anaheim, California, 1996), p. CTuU2.
7. P. Myslinski, J. Fraser, and J. Chrostowski, "Nanosecond Kinetics of Upconversion Process in EDF and its Effect on EDFA Performance," in Optical Amplifiers and Their Applications, Vol. **18** of 1995 OSA Technical Digest Series (Optical Society of America, 1995), paper ThE3.
8. M. K. Davis, M. J. F. Digonnet, and R. H. Pantell, Journal of Lightwave Technology **13**, 120 (1995).

Chapter 4 Efficient High Pulse Energy Extraction from Partly Quenched Erbium-Doped Fibres

The experimental results in the previous chapter with in-band pulse pumping, as well as available equipment, motivated a shift of focus to 980-nm CW cladding-pumping. This was further supported by simulations in this regime. Thus, the work in this chapter demonstrates experimentally efficient pulse-energy extraction from a partly-quenched erbium-doped aluminosilicate fibre amplifier. The EDF used, FUT #1 (see Appendix B), has a high erbium-concentration, which allows for short devices with reduced nonlinear distortions, but which also results in partial quenching and thus significant unsaturable absorption, even though the fibre is still able to amplify. Although the quenching degrades the average-power efficiency, the pulse energy remains high, and these results point to an increasingly promising outcome for short pulses.

As discussed in previous chapters, in the context of high energy extraction on a partly-quenched EDFA, the signal pulse duration may be shorter than, or comparable to, the quenching time scales, reported to be in the range 50 ns – 10 µs [1]. By contrast, the quenching process is often assumed to be instantaneous, but this may exaggerate the impact of the quenching on such pulses. Thus, in this regime, a finite quenching time may allow for high-energy pulse amplification at higher quenching-levels than normally considered. Indeed, refined simulations with 2-µs quenching time showed a modest pulse-energy penalty of ~10% in an EDFA core-pumped with 10-200 mW at 980 nm [2], but there was no experimental investigation. The fractional unsaturable absorption was not stated, but I evaluated it to 1.7%. This is a quite low level of quenching even compared to commercial low-concentration EDFs [3].

In this chapter I use signal pulses of 6 ns - 20 µs. The signal EDF (FUT #1) is a high Er^{3+}-concentration, partly-quenched with 16.3% unsaturable absorption at 1536 nm. The key finding is that despite this quenching, it was possible to amplify pulses to high energy in the primarily investigated FUT #1. Even though the unsaturable absorption was at a level where it severely compromised the power conversion efficiency, the attainable pulse energy was comparable to that expected from an unquenched EDF.

4.1 High-energy pulse amplification in unquenched fibre amplifiers

In the absence of quenching, high-energy pulse amplification in rare-earth-doped fibre amplifiers, including EDFAs, is well understood [4-14]. In the unquenched case, amplified spontaneous emission (ASE) or spurious lasing limits the energy that can be extracted ($E_{extractable}$) in a high-energy

signal pulse to a few times the intrinsic saturation energy (E_{IS}), or say, at most 10 times [15-17] if the stored energy and the extraction efficiency are both at their practical limits. Specifically, the extractable energy is related to the gain according to [16].

$$E_{extr} = U_{sat} * G_{mod}^{Np} = E_{IS}\, G_{Np}^{initial}, \qquad \text{(Eq. 2.6)}$$

where $G_{Np}^{initial}$ is the initial gain in nepers when the pulse arrives. The extractable energy (which is a fraction of the energy stored in the EDFA) and thus the gain build up between pulses and generally reach their highest values when the pulse arrives. The small area of a typical core leads to low intrinsic saturation energy, so high-energy amplification in fibres requires high initial gain. However, ASE and spurious lasing limit the gain to at most ~10 Np (or ~43 dB), and thus the extractable energy according to Eq. (4.1) even in an unquenched amplifier. The extracted energy can be evaluated more precisely with the Frantz-Nodvik equation (FNE) [17], but the limit set by the achievable initial gain remains. Damage and nonlinearities can further limit the pulse energy as well as the peak power (e.g., [10, 18]).

4.2 Concentration quenching

Since EDFs for high-energy pulses are often highly doped to reduce the fibre length and thus the nonlinear degradation, they are likely to suffer from some degree of concentration quenching. Even if the EDF is not fully quenched and is able to reach net gain when pumped sufficiently hard, the quenching still impairs the amplification and may well limit the build-up and extraction of energy. Also quenching has been treated in many publications but there are still considerable uncertainties in the details, and considerable variations between different fibres, even if these are similar in other respects. Generally, non-radiative electric or magnetic multipolar coupling or in extreme cases even so-called direct exchange between neighbouring Er^{3+}-ions in the metastable upper laser level ($^4I_{13/2}$) lead to quenching through energy-transfer upconversion [1, 3, 19-39]. The strengths of these types of parasitic interactions depend on the distance between the Er^{3+}-ions in different ways, and at low concentrations, the separation between Er^{3+}-ions can be large enough to make quenching negligible. Tailored host glasses, e.g., co-doped with Al_2O_3 or P_2O_5 [14, 19-21, 40], as well as nanoparticle doping [38, 39, 41-44] can also counteract quenching, but it still reappears gradually at higher concentrations.

Quenching can be understood as a nonradiative lifetime shortening of the upper laser level from the unquenched value of ~10 ms. This leads to a distribution of lifetimes depending on the local environment of individual ions, but for simplicity, the ions are often grouped into two classes, clustered ions, which typically exhibit severe lifetime shortening, even to the point where it is

difficult to measure, and isolated ions. Whereas also isolated ions can experience some lifetime shortening, e.g., due to so-called uniform or homogeneous upconversion (HUC) involving nonradiative energy-transfer over relatively large distances, the effects are relatively modest [3, 19, 20, 29, 30, 33, 36, 40]. Fluorescence decay measurements showed no lifetime shortening when a 25-cm piece of FUT #1 was cladding-pumped at 980 nm with pulses of 10 µs duration and 21 W peak power at 12 Hz pulse repetition frequency (PRF). Such excitation is only expected to probe isolated ions. Still, even for those, this leads to no more than around 2% excitation, so the likelihood of finding two excited ions close enough to interact non-radiatively is quite small. Furthermore, the detector's response to scattered pump light masked the initial 5 ms of the fluorescence decay. Since lifetime shortening is most pronounced in the initial part of the fluorescence decay and at high Er-excitation levels, I cannot rule out modest lifetime-shortening associated with isolated ions. However, although that could perhaps be significant in the low-power regime, such reduction in lifetime can be fully compensated for by an increase in pump power, and the resulting pump power penalty is less significant at the powers that were used. I rarely used less than 10 W of pump power, and never used all the available pump power. Therefore, I disregard the possible effects of HUC, including the measured modest lifetime-shortening in this chapter.

Instead, the quenching and its impact is often more strongly tied to Er^{3+}-clusters (e.g., pairs) [19-21, 30-36, 40]. In those, the nonradiative energy transfer between excited Er^{3+}-ions and the resulting quenching through so-called inhomogeneous upconversion is rapid, orders of magnitude faster than the fluorescence decay of unquenched ions. This makes it difficult or practically impossible to excite more than one ion in a cluster, even if the pump power is increased. Therefore, most of the clustered ions remain in the absorbing ground state, and such a cluster (or pair) forms a quenching centre, or a trap. A higher Er^{3+}-concentration increases the fraction of clustered Er^{3+}-ions. It is possible to measure directly the dynamics of the quenching process, by measuring the weak and short-lived fluorescence they emit. Quenching timescales have been reported to lie in the range of 50 ns – 10 µs [1], and later, by the same authors, restricted to sub-microsecond [36]. However, both the excitation and the detection used in my fluorescence measurements were inadequate for this. Note that other traps such as OH^- are also possible [45], which also make it difficult to excite the Er^{3+}-ions. Even in cases when the relative or even absolute concentration of traps does not depend on the Er^{3+}-concentration, the quenching can still increase at higher Er^{3+}-concentrations due to increased rates of energy migration to traps [45, 25-27, 46].

Regardless of the details of such rapid quenching, it is often described in terms of a resulting unsaturable absorption [3, 31-35, 39]. Unsaturable-absorption measurements directly probe the fraction of ion that are (strongly) quenched and directly quantify the unsaturable absorption, which, in this context, is more important for the performance of high-power EDFAs than the much more

modest lifetime-shortening characteristic of HUC (e.g., already 10% unsaturable absorption is highly significant, whereas even 50% fluorescence lifetime shortening is negligible in simulations of a representative high-power EDFA). A signal photon emitted inside the EDF may then be lost to unsaturable absorption instead of contributing to the signal output, and an absorbed pump photon may fail to excite an Er^{3+}-ion. A non-zero quenching time means that the saturation characteristics become less distinct, and at sufficiently high probe power density, also the "unsaturable" absorption can saturate, if quenched ions become excited. Similarly, when the fibre is used to amplify pulses of duration shorter than, or comparable to, the quenching timescale, the pulses may be able to partly saturate the normally unsaturable absorption, if the peak power and energy of the pulses are high enough. In particular, and central to this chapter, an ion in the ground state that absorbs a signal photon does not have time to return to the ground state and can therefore not absorb a second signal photon in the same pulse, irrespective of whether the ion is quenched or not. Then, Eq. (1) applies to the ion collective as a whole, and the key question becomes if it is still possible to reach a high initial gain, despite the quenching. As proposed in the introduction, this may reduce the impact of the quenching and allow for high-energy pulse amplification at higher levels of unsaturable absorption than normally considered. I emphasize that the finite quenching time is essential for this hypothesis, whereas other details of the quenching process may be less important.

4.3 Experimental setup

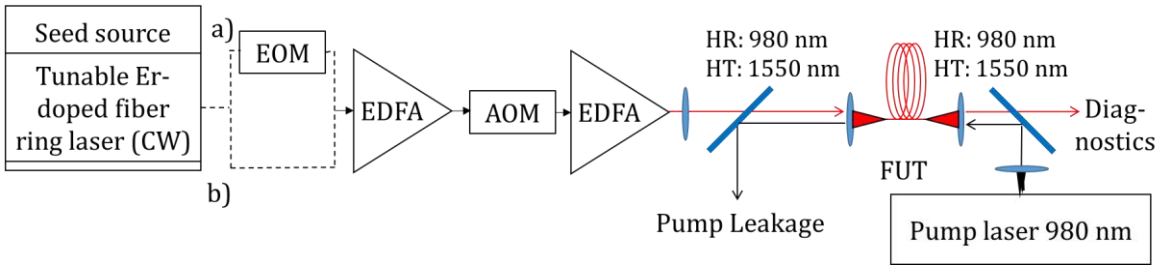

Figure 4.1 Amplifier test rig for the FUT. Path (b) is used for signal pulses longer than 50 ns and up to 20 µs, defined by an acoustic optic modulator (AOM). Path (a) introduces an electro-optic modulator (EOM) to define pulses of 6 – 50 ns duration. The AOM is then set to 50 ns.

My experimental layout is shown in Fig. 4.1. This comprises an amplified wavelength-tuneable pulsed single-mode signal seed source, a pump laser, and dichroic mirrors and lenses for coupling signal and pump light into and out of the Er-doped fibre-under-test (FUT #1). The pump laser was a pigtailed diode laser (IPG PLD-70-974) with up to 57 W of output power at ~975 nm. The launch efficiency was ~85% into the FUT, which had both ends angle-cleaved at ~12° to suppress feedback.

Counter-pumping from the signal output end was chosen for its higher efficiency in quenched EDFs [6, 31, 38].

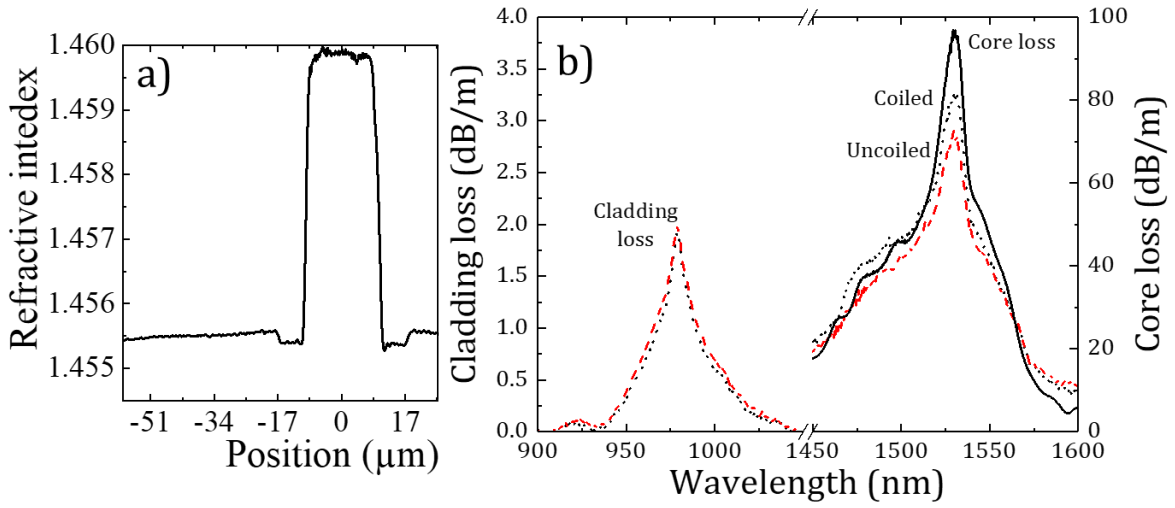

Figure 4.2 (a) Refractive index profile and (b) white-light absorption spectra for the FUT (NRL-160415) showing core loss around 1530 nm in a short fibre (black solid curve) as well as pump waveguide (i.e., cladding) loss around 980 nm and 1530 nm for a tightly coiled (black dotted curve) and uncoiled (red dashed curve) 2.6-m-long fibre.

FUT #1 is fabricated by Naval Research Laboratory (NRL) using MCVD and solution-doping [20, 41] and is designated NRL-160415. It has a 0.11-NA, 20-μm-diameter Er-doped aluminosilicate core centred in a 125-μm-diameter circular inner cladding, which is coated by a low-index polymer. Figure 4.2 shows the refractive-index profile of the core together with white-light absorption spectra for the core as well as the pump waveguide (i.e., largely the inner cladding). The core absorption spectrum was measured on a short fibre to avoid errors from saturation and re-emission [47]. It reached 95 dB/m at the 1530-nm peak. Based on preliminary experimental data for different fibre lengths, signal wavelengths, and pulse parameters, I used a signal wavelength of 1560 nm in most amplification experiments, and an optimal length of 2.6 m. The emphasis was on high pulse energy, but this fibre length and wavelength performed well across the range of pulse parameters I used. Thus, the pump-waveguide absorption spectrum in Fig. 4.2 (b) was measured on a 2.6-m long fibre. The circular symmetry of the FUT can lead to poor pump absorption. Therefore, the FUT was coiled to promote mode scrambling and thereby pump absorption [48, 49] in one case in Fig. 4.2 (b) as well as in the amplification experiments. The FUT was wound into a triangle-shaped coil around three 2.5-cm-diameter cylinders, 8 cm apart from each other. This improved the white-light absorption in the pump waveguide of the 2.6-m piece from ~6.7 to 7.4 dB at the 1530-nm peak. These values can also be compared to the value of 95 dB/m × 2.6 m × (20 μm / 125 μm)^2 = 6.3 dB calculated from the core absorption and the area ratio. The values are relatively similar. The lower value calculated from the core absorption is unusual. It is possible that this is a result of imperfect overlap (i.e., below unity) of the different core-guided modes with the Er-ions. Through simulations,

the V-value is calculated as 4.38 at 1560 nm, so the core is expected to support LP-modes 01, 11, 21, and 02. Out of these, the modes with the lowest overlap and thus the highest transmission may dominate the output, leading to a lower measured core-absorption. Note here that even though modes with low overlap with the core are weakly guided and are susceptible to bendloss, the fibre was nearly straight for the core absorption measurements. Alternatively, there are also factors that affect the pump-waveguide absorption measurements. For example, the probe light in the inner cladding may be disproportionately located to the centre of the fibre (including the core). One possible reason for this is that the coating absorbs at 1530 nm. As it comes to the absorption at 980 nm, this reaches a peak value of 5.2 dB both with and without coiling. It is concluded that the pump absorption is satisfactory, and does not exhibit any significant mode-selective pump depletion effects, which would be detrimental. I calculated a saturation energy of 84.5 μJ from the core area and standard absorption and emission cross-sections at 1560 nm for aluminosilicate EDFs (1.69×10^{-25} m^2 and 3.04×10^{-25} m^2, respectively).

To quantify the quenching, I measured the unsaturable absorption fraction to 16.3% with a probe at 1536 nm with up to 1 W of power, continuous-wave (CW). At longer wavelengths, the saturation power increases, and at shorter wavelengths, the available probe power was smaller. These factors hamper unsaturable-absorption measurements, and 1536 nm was the best compromise. The fibre length was 0.3 m, which gives 20 dB of small signal absorption and allowed for a maximum transmitted probe power of over 400 mW. This is well above the saturation power of unquenched ions of ~3 mW at 1536 nm, so their absorption is well saturated. For the 16.3% unsaturable absorption at 1536 nm, assuming that this is caused by ion pairs, the corresponding pair fraction was calculated to almost exactly 50% of the ions, whereas the other 50% of the ions would be isolated. The fractional unsaturable absorption with 50% paired ions becomes smaller at longer wavelengths, e.g., 13.3% at 1560 nm. Note that I use standard Er^{3+}:aluminosilicate cross-sections also for the quenched ions for all calculations in this chapter, although deviations have been reported [37].

The seed source comprised a tuneable CW Er-doped fibre ring-laser with 25 mW of output power (same as in Fig. 3.1), an optional pigtailed electro-optic modulator (EOM, Lucent 2623NA, path *a* in Fig. 4.1), a pigtailed acousto-optic modulator (AOM, NEOS, shortest time duration 70 ns to reach maximum transmission; 50 ns duration possible with slightly reduced transmission, extinction ratio measured to 64 dB), and two EDFAs. Optionally, the EOM was by-passed (path *b* in Fig. 4.1). The pulses produced by the seed source had duration of 6 ns – 20 μs and energy of 3 – 60 μJ at 1 – 40 kHz pulse repetition frequency (PRF). Path *a* was used for pulse durations of 50 ns and shorter, with the EOM running at 12 MHz. The AOM was set to 50 ns duration at the target PRF, to down-sample the pulses and suppress inter-pulse ASE. Path *b* was used for longer pulses, up to 20 μs in this

chapter. A dual-channel waveform generator (Tektronix AFG3252) connected to the EOM and the AOM controlled the pulse duration and PRF. The bias of the EOM was regularly adjusted to maintain an extinction ratio (ER) of ~20 dB or more.

The first EDFA (IPG EAD-5K-C) in the seed source was operated at constant current for the data I present. It yielded 900 mW of output power with 25 mW of CW-seeding at 1560 nm (path *b*), but lower output power for pulsed seeding (path *a*) with low average input power, e.g., ~5 mW with 7.2% duty cycle. Two different EDFAs were used for the second EDFA. In case of path *b*, I used an engineering prototype from SPI Lasers. In case of path *a*, I used an in-house un-packaged EDFA pumped at 1480 nm and based on 3 m of a 5-µm core EDF from Fibrecore (I-15(980/125)HC). Compared to the prototype from SPI Lasers, this was better suited to the low input power to the 2nd EDFA that resulted with path *a*, which could be as low as 10 µW. For both path *a* and *b*, after all other parameters had been adjusted, the drive current to the second EDFA was set to produce the desired pulse energy. Whereas I focus on the useful signal energy and average power in the pulses, there was also unwanted energy between the pulses from ASE and leakage through the modulators. This includes unwanted inter-pulse energy in the seed, which limited the maximum seed pulse energy. Table 1 lists key characteristics of selected seed pulses. In the pulse energies and average powers I report in this chapter, the intra-pulse contributions have been subtracted and are quoted separately. The signal launch efficiency into the core of the FUT was ~90%.

Table 1 Characteristics of selected seed pulses at 1560 nm as launched into the FUT and resulting gain and output from the FUT.

Notes (case)	(*a*)	(*b*)	(*c*)	(*d*)	(*e*)	(*f*)
Seed pulse energy	3.5 µJ	3.5 µJ	22.5 µJ	4.5 µJ	1.13 µJ	22.5 µJ
Pulse duration	6 ns	20 µs	1 µs	1 µs	1 µs	0.2 µs
PRF	2 kHz	2 kHz	2 kHz	10 kHz	40 kHz	2 kHz
Energy between seed pulses	0.25 µJ	0.05 µJ	1 µJ	0.01 µJ	2.5 nJ	1.5 µJ
Inter-pulse energy fraction in seed	0.067	0.014	0.043	0.0022	0.0022	0.063
Duty cycle	1.2×10^{-5}	0.04	0.002	0.01	0.04	4×10^{-4}
Seed pulse extinction ratio (*g*)	61 dB	32 dB	40 dB	47 dB	40 dB	46 dB
Path (*cf*. Fig. 4.1)	Path *a*	Path *b*	Path *b*	Path *b*	Path *b*	Path *b*
FUT output pulse energy	200 µJ	76 µJ	770 µJ	243 µJ	53.7 µJ	800 µJ
FUT output extinction ratio (*g*)	60 dB	18 dB	29 dB	31 dB	27 dB	36 dB
Resulting energy gain in FUT	17.6 dB	13.4 dB	15.3 dB	17.3 dB	16.8 dB	15.5 dB

Resulting gain for total average power in FUT	17.6 dB	14.7 dB	17.3 dB	17.6 dB	17.0 dB	17.4 dB
FUT pump power	25 W	25 W	50 W	50 W	50 W	50 W

(*a*) Used in Fig. 4.4 (shortest pulse duration), and in Fig. 4.5.
(*b*) Used in Fig. 4.4 (longest pulse duration).
(*c*) Used in Fig. 4.6 (point with highest output energy).
(*d*) Used in Fig. 4.6 (point with highest average signal output power).
(*e*) Used in Fig. 4.6 (point with highest PRF).
(*f*) Used in Fig. 4.7 (point with highest output energy), and in Fig. 4.8 and 4.9.
(*g*) Ratio of average instantaneous power (energy/duration) in a pulse to that between pulses.

Diagnostics include an optical spectrum analyser (OSA, ANDO AQ6317B). This was used in CW measurement mode with sufficiently low measurement bandwidth to measure the time-averaged spectrum. For temporal measurements, I used a 1-GHz oscilloscope with 12 bits of vertical resolution (Agilent DSO9104H) and InGaAs photodetectors (Thorlabs DET10C, 35 MHz, detector area 0.8 mm^2, bias voltage 5 V, and EOT ET-3500, ~15 GHz, area 8×10^{-4} mm^2). Since the leakage through the modulators in the seed occurs largely at the seed wavelength, the pulse energy is determined from the average power and oscilloscope traces and checked there were no inconsistencies in the optical spectrum (e.g., excessive ASE). See Chapter 2.2.1 for details. Average optical powers were measured with thermal and semiconductor power meters.

4.4 Continuous-wave characteristics

Figure 4.3 shows the gain for a CW seed with 1 mW of launched power at 1560 nm. This reaches 34 dB = 7.8 Np. The pump leakage was ~30% (–5.2 dB) at high gain. Thus, the pump absorption is similar to the white-light absorption at the 980-nm peak, despite the significant excitation of Er^{3+}-ions, and any non-ideal spectral overlap between the pump and the absorption. A possible explanation is that the spatial overlap with the Er^{3+}-ions is larger for the pump light than for the white light used in Fig. 4.2. The gain slope in Fig. 4.3 drops at high pump power due to gain saturation, as the signal output power exceeds 2 W. Lower seed power reduces the saturation, but 1 mW is reasonably representative of the seed's parasitic inter-pulse power, so the measured gain is an indication of what initial gain may be achievable (i.e., $G_{Np}^{initial}$ in Eq. (4.1)). Note however that during high-energy pulse amplification, the instantaneous gain varies continuously in time, and the precise initial gain was not measured in the pulsed experiments. The differential conversion efficiency from pump to signal power in the saturated regime becomes 12% with respect to absorbed pump power for the data in Fig. 4.3. In simulations with 50% of paired ions and the signal gain deeply saturated, the signal output power increases linearly with the pump power with a slope (i.e., differential conversion efficiency) of 18%. Here, the quenching of pairs was assumed to be instantaneous, since it is expected to be much faster than Er^{3+} absorption and stimulated-emission

rates in the CW case. For example, in Fig. 4.3, typical transition rates correspond to a time scale of, e.g., 0.1 ms. Without quenching, the simulated differential conversion efficiency was at the quantum limit of 63%, which is ~7 dB higher than the experimental value, and 5.5 dB higher than the simulations with 50% of the Er-ions in pairs. This underlines the strong detrimental impact of quenching in the CW regime. Nevertheless, the high gain that I reach may allow for high pulse energies, according to Eq. (4. 1).

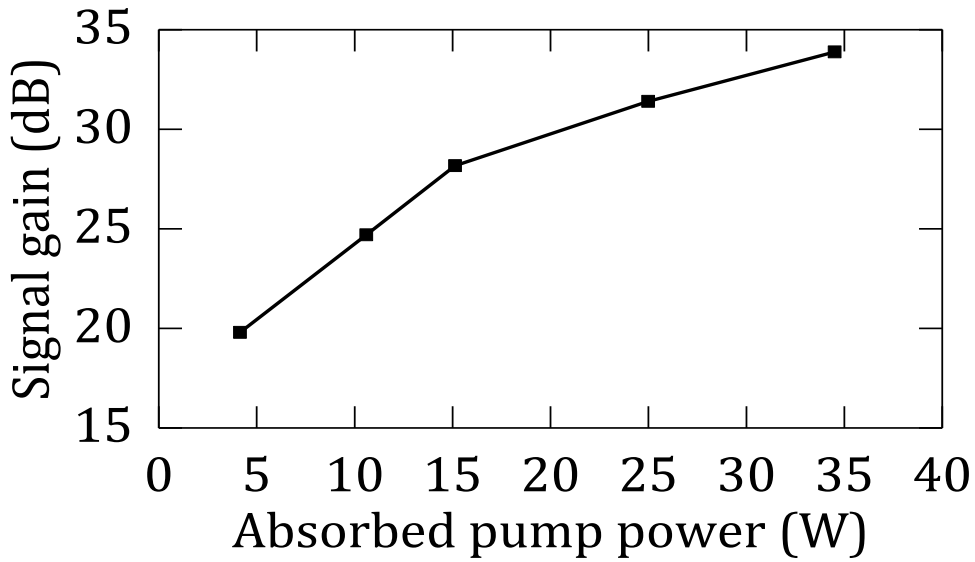

Figure 4.3 Gain *vs*. absorbed pump power for 1 mW of CW input signal at 1560 nm.

4.5 Pulse amplification results and discussion

Figure 4.4 shows the output signal pulse and inter-pulse energy *vs*. pulse duration for 2-kHz PRF, 3.5-μJ seed energy (average seed power 7 mW), and 25 W of launched pump power (17 W absorbed). The pulse duration varies from 6 ns to 20 μs, and the seed's peak power from ~580 W down to ~0.17 W. The EOM (path *a*) is used only for durations of 50 ns and less. The total output power as measured with a thermal power meter is also shown, in terms of the total energy during the pulse period, i.e., the average power divided by the PRF. For the longest pulses (20 μs), the output energy reaches 68 μJ, so the energy gain becomes 13 dB. The total average output power becomes 190 mW. The ER becomes 18 dB in terms of the power during the pulses relative to the average power between pulses. The stimulated-emission rates induced by the input and output signal pulses become ~1290 s^{-1} = (770 μs)$^{-1}$ and ~25,100 s^{-1} = (40 μs)$^{-1}$, respectively, if one assumes that the pulses are rectangular. All these values then increase for shorter pulses. Thus, for 6-ns pulses, the energy gain increases by 5 dB from that of the 20-μs pulses and reaches 18 dB. The ER becomes 60 dB, and the total average output power becomes 450 mW. The output pulse energy reaches 0.2 mJ energy (~2.4 times the saturation energy). For comparison, the FNE yields 0.27 mJ of output pulse energy with standard cross-sections for an unquenched EDF and 28 dB of initial

gain, obtained from Fig. 4.3 for 17 W of absorbed pump power. This is only 1.5 dB higher than the experimental result for 6-ns pulses. The stimulated-emission rates induced by the input and output signal pulses become ~4.3×10^6 s^{-1} = $(230\ ns)^{-1}$ and ~250×10^6 s^{-1} = $(4.1\ ns)^{-1}$, respectively, if one assumes that the pulses are rectangular. This is comparable to, or faster than, reported quenching rates [1, 36].

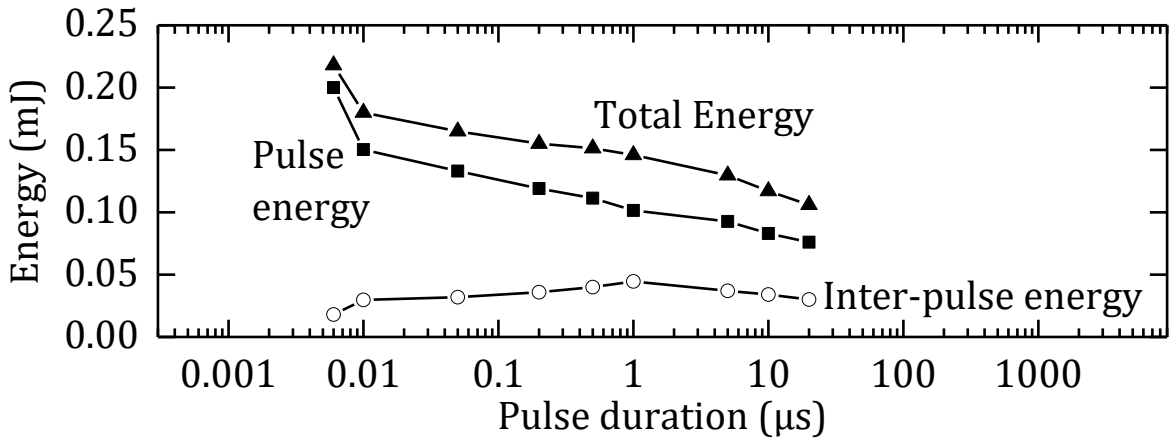

Figure 4.4 Output pulse, inter-pulse, and total energy *vs*. pulse duration for seed energy of ~3.5 μJ, PRF of 2 kHz, and launched pump power of 25 W (17 W absorbed).

Figure 4.5 (a) shows the temporal input and output profile of the 6-ns pulse that produced the highest energy of 0.2 mJ in Fig. 4.4. The output reaches 40 kW of peak power. Figure 4.5 (b) shows the average-power spectrum. With 40 kW of peak power, the nonlinear effect of four-wave mixing generates sidebands (e.g., [10, 18, 50]) containing ~44% of the energy. Sideband energy is included in all reported energies, but is negligible in most cases.

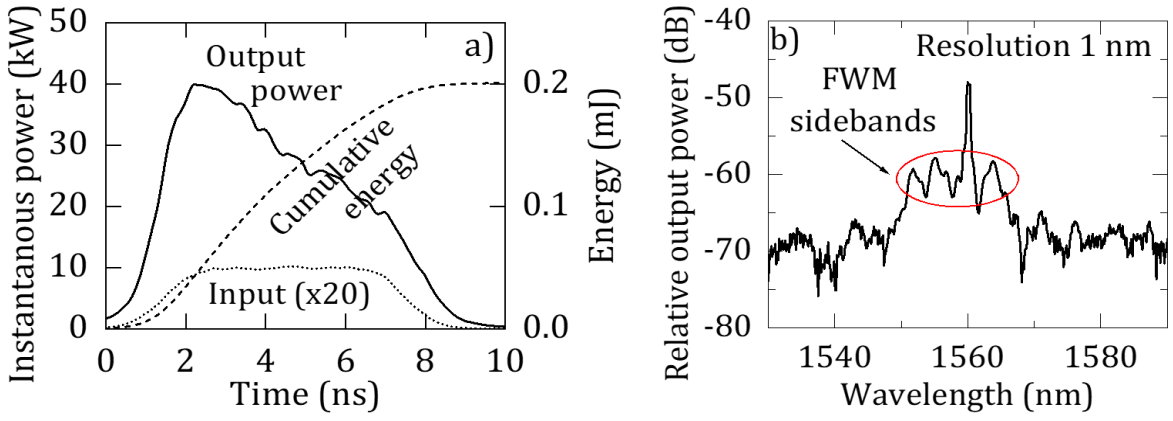

Figure 4.5 (a) Instantaneous signal input power (x 20) and output power and cumulative output pulse energy from the beginning of the pulse and (b) optical spectrum for 6-ns pulse duration at 17 W of absorbed pump power. Case (*a*) in Table 1.

When one takes into account the uncertainties resulting from possible differences between quenched and unquenched erbium cross-sections [37, 51] and in other experimental parameters, as well as the spectral broadening, Fig. 4.4 suggests that for sufficiently short pulses, it is possible to recover the energy gain of unquenched fibres, as described by the FNE, also in my quenched fibre. This is a key result of the experiments in this chapter. As outlined briefly above, this thesis proposes the following explanation: The dynamics of Er^{3+}-ions may be slow compared to the pulse duration. Then, all transitions during the pulse are negligible, compared to those induced by the high-energy signal pulse. This applies to unquenched as well as quenched ions, insofar as the quenching dynamics are slower than the pulse duration. Thus, even if the absorption of quenched ions (in the ground state) is effectively unsaturable in the CW regime, it behaves as a saturable absorber with a short pulse, just like unquenched ions in the ground state do. If other differences in the spectroscopy of quenched and unquenched ions are small, it no longer matters to the pulse if the ions in the absorbing ground state are quenched. Partly quenched and unquenched fibres should then yield similar output pulse energy for the same initial gain. By contrast, for longer pulses, a quenched ion that absorbs a signal photon has time to lose its energy through parasitic nonradiative processes during the pulse and return to the ground state. It can then absorb another signal photon in the same pulse, leading to lower output energy. Thus, the measured output energy recovers its unquenched value for shorter pulses in Fig. 4.4, but decreases significantly for longer pulses. Such dependence is not expected for unquenched fibres. I hypothesize that it also helps to maintain the ER for shorter pulses, but not for longer pulses (cf. Table 1), although further investigations would be needed to confirm that.

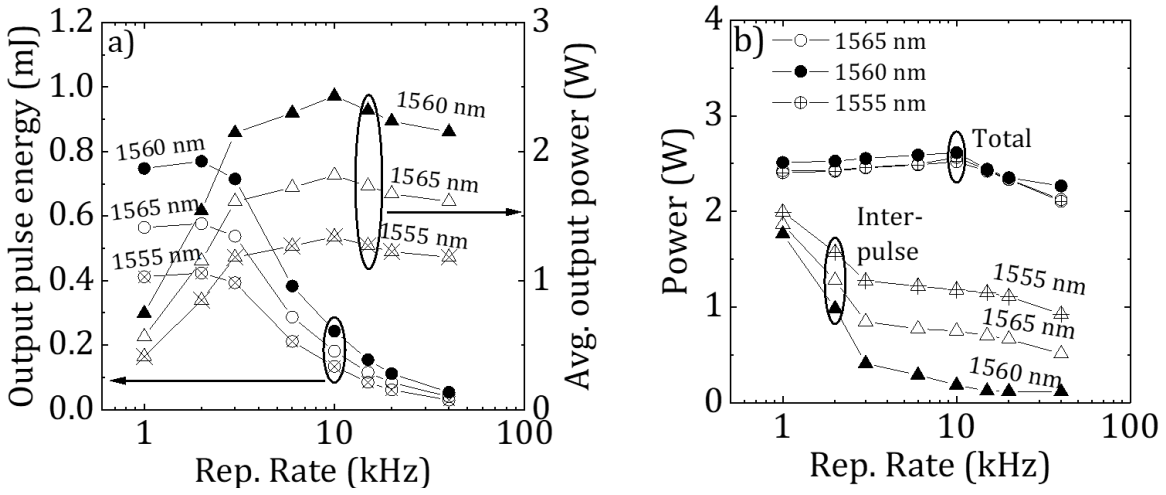

Figure 4.6 (a) Output pulse energy and average signal power *vs*. PRF at constant average signal input power of 45 mW in 1-µs pulses at three wavelengths, 1555 nm, 1560 nm and 1565 nm with 50 W of launched pump power (35 W absorbed). (b) Total output power (combined in pulses and between pulses) and inter-pulse power.

Although Fig. 4.4 shows higher output energy for shorter pulses, this was with pulse seed energy limited to ~3.5 μJ and with non-negligible inter-pulse seeding. Therefore, for the seeding used in Fig. 4.4, higher pump power than 17 W (absorbed) rapidly increased the energy between the pulses rather than in the pulses. Higher seed energy may lead to higher output energy, although this was beyond the capability of my seed source for the 6-ns case in Fig. 4.4 and 4.5. With longer pulses, however, the seed source can reach higher pulse energy with acceptable inter-pulse energy and power, thanks to the lower gain of the amplifiers. Thus, the FUT can be pumped with higher power and reach higher initial gain, which opens up for higher output pulse energy. Figure 4.6 (a) depicts the average output power and pulse energy *vs*. PRF for a constant average seed power of 45 mW in 1-μs seed pulses at three wavelengths, 1555 nm, 1560 nm and 1565 nm, with 50 W of launched pump power (35 W absorbed). The PRF varied from 1 to 40 kHz, so the corresponding seed energy varied from 45 μJ down to 1.1 μJ. The results across the three wavelengths show a ~6 dB increase in average output power for an increase in PRF from 1 kHz to 10 kHz. This is expected, because of decreasing energy saturation and inter-pulse ASE for higher PRF. For an unquenched system, one expects this trend to continue with a further increase in average output power also for PRF above 10 kHz, asymptotically towards a maximum for high PRF. Instead, Fig. 4.6 (a) shows a small drop in power. I propose this is another, more subtle, result of quenching. Even if a short pulse saturates the absorption of the quenched ions by exciting them for the duration of the pulse, the energy in the excited quenched ions is then rapidly dissipated through the quenching process. The saturation implies that the absorbed energy increases sub-linearly with pulse energy, so lower-energy pulses at higher PRF increase the fraction of the pulse energy, and thus the average power, deposited into the quenched ions. This reduces the average output power for higher PRF.

The decrease in power for higher PRF is confirmed in Fig. 4.6 (b), which shows the total output power as measured with a thermal power meter. It also shows the average inter-pulse power. In conventional fashion, the inter-pulse power is high at low PRF and lower for higher PRF. The inter-pulse power at 1555 nm and 1565 nm is significantly higher than at 1560 nm, especially at high PRF. This leads to an unusually strong wavelength dependence in Fig. 4.6 (a). For PRF lower than 3 kHz, the rapid increase in inter-pulse power hampers further pulse-energy growth, and the inter-pulse power reaches over 45% of the average signal power already at 2 kHz. Although ASE is generally bi-directional, the FUT is seeded in the forward direction by inter-pulse power from the seed laser (ASE as well as leaked signal). Compared to the forward inter-pulse energy, I expect backward-propagating inter-pulse power to be negligible.

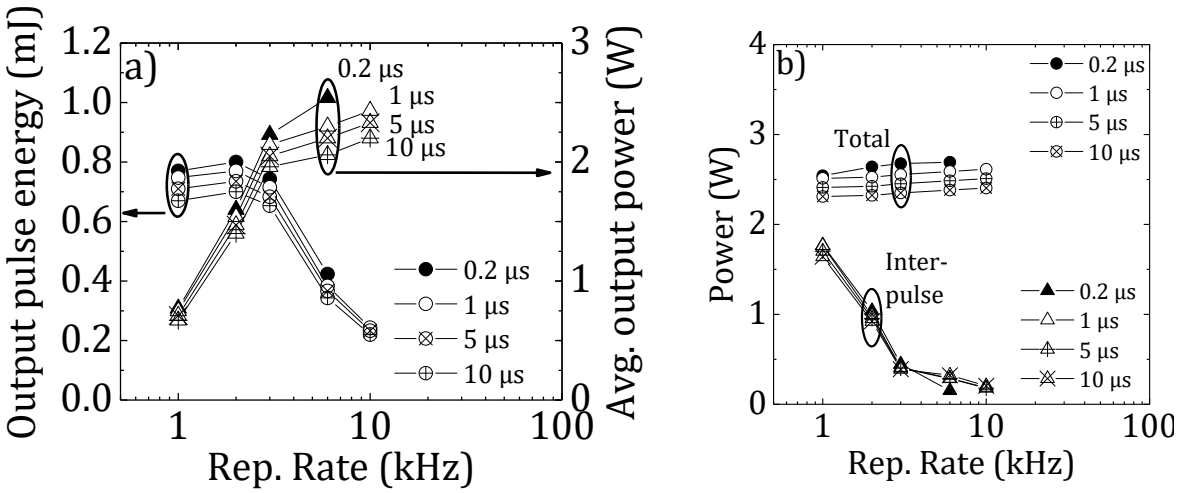

Figure 4.7 (a) Output pulse energy and average signal power *vs*. PRF at constant average signal input power of 45 mW at 1560 nm for different pulse durations with 50 W of launched pump power (35 W absorbed). (b) Total output power (in pulses plus between pulses) and inter-pulse power.

Next, let's consider the effect of pulse duration in this regime of high-energy seeding and extraction. For this, the parameters are the same as in Fig. 4.6, except that I seed at 1560 nm and vary the pulse duration from 0.2 µs to 10 µs with PRF in the range 1 to 10 kHz. The duty cycle varies between 2×10^{-4} (0.2 µs, 1 kHz) and 0.1 (10 µs, 10 kHz). The seed energy varies between 4.5 µJ at 10 kHz and 45 µJ at 1 kHz. The average power during the seed pulses varies between 0.45 W and 225 W (this is similar to the peak power of the seed pulses, but at high seed energy, saturation-induced pulse shortening can be significant already in the seed). The results are shown in Fig. 4.7. One can see that the trend with respect to PRF is the same as in Fig. 4.6. Furthermore, the trend with respect to pulse duration is the same as in Fig. 4.4, i.e., the shortest pulse of 0.2 µs leads to the highest energy, which is reached at 2 kHz rather than at 1 kHz, although the difference in output energy may be too small to be significant. Thus, with 2-kHz PRF seeding in 0.2-µs pulses (so with 22.5 µJ energy and 110 W average power and ~0.84×10^6 s^{-1} = $(1.2\ \mu s)^{-1}$ stimulated-emission rate during the seed pulse), the maximum pulse energy from the FUT reaches as high as 0.8 mJ, despite a conversion of no more than 4.6% of absorbed pump power. Figure 4.8 shows the corresponding input and output instantaneous power and cumulative pulse energy, and Fig. 4.9 shows the spectrum of the output pulses. The FWHM duration becomes 110 ns, and the actual peak power 6.2 kW, leading to a stimulated-emission rate of ~47×10^6 s^{-1} = $(21\ ns)^{-1}$. The energy between pulses becomes 53 µJ and the ER 36 dB. The spectral purity is relatively good, with 89% of the power at the signal wavelength. The energy gain reaches 15.5 dB. The energy of 0.8 mJ is 9.5 times the estimated saturation energy, and is 1.5 dB higher than the 0.57 mJ calculated with the FNE, with initial gain of 34 dB (estimated from Fig. 4.3) and seed energy of 22.5 µJ. Thus, as for the 6-ns pulse in Fig. 4.5, the agreement with the FNE is fair, but in contrast to the 6-ns pulse, the energy is now higher than that predicted by the FNE. Possible contributions to this difference include energy measurement errors, errors in the

estimate for the initial gain used in the FNE, the increased ability of a higher-energy seed pulse to extract energy also in the edges of the core where the signal intensity is relatively low as well as from any Er^{3+}-ions with atypically small cross-sections, and the increased ability of a higher-power pump to excite paired Er^{3+}-ions, which may have smaller cross-sections [37, 51] and thus store more energy for a given contribution to the gain. Note that measurements with the same seed energy and PRF on a low-quenched EDF (unsaturable absorption 4.5% at 1536 nm) agreed well with the FNE. This EDF was also fabricated by NRL but with nanoparticle-doping [44] and a lower Er-concentration (peak core absorption 33 dB/m) to avoid quenching.

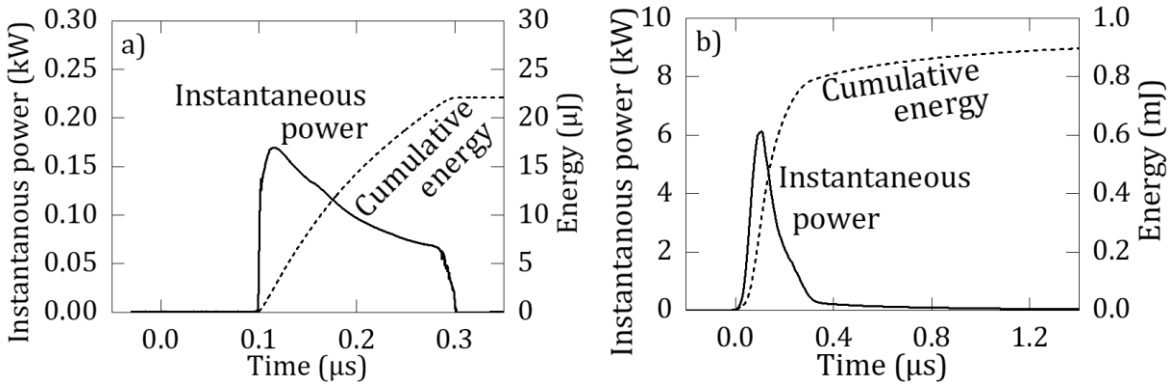

Figure 4.8 Instantaneous power and cumulative energy for highest achieved energy (case (*f*) in Table 1) for (a) input pulses and (b) output pulses.

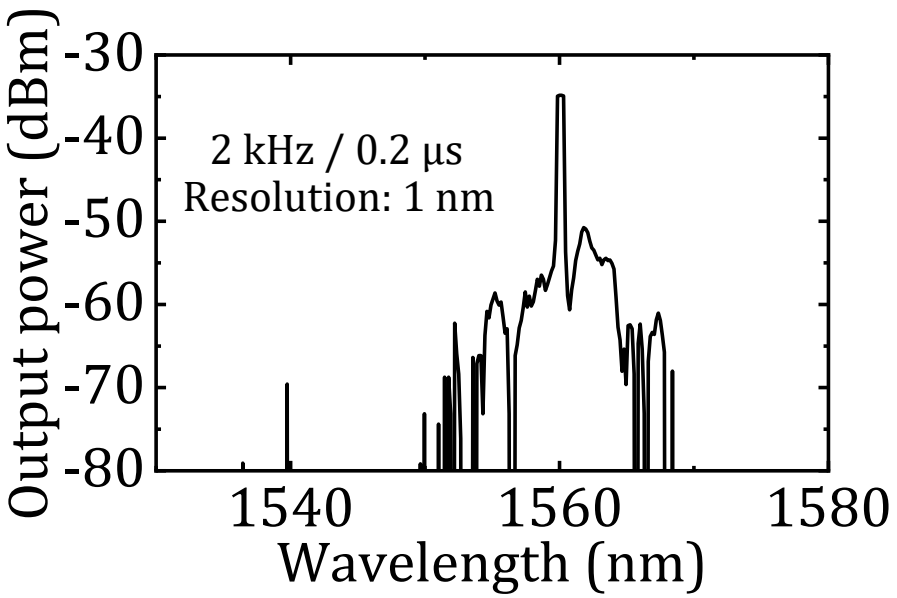

Figure 4.9 Output spectrum. Case (*f*) in Table 1.

Even if the effect of the quenching on the extraction process is small and the pulse energy is well described by the FNE, it is possible that the erbium excitation reached in the pumping process, and thus the initial gain, is more strongly affected by quenching. Based on the CW signal gain of 34 dB at 1560 nm for 35 W of absorbed pump power, one can roughly estimate that 55% of the Er^{3+}-ions are excited when a pulse arrives. This is a relatively low percentage, which may partly be a result of

quenching-induced degradation of the pumping process. Under the assumption of equal spectroscopic parameters for isolated and paired ions, one can estimate that 40% of the paired ions and 70% of the isolated ions are excited, as averaged over the fibre, when a pulse arrives. Still, even if the pumping is degraded, the 2.6-m long partly-quenched EDF outperforms unquenched silica EDFs (e.g., [4, 7]) in generation of energy per unit core area and length (0.98 μJ/μm^2/m) and gain per unit length (>5.9 dB/m) at 1560 nm. Although the conversion efficiency decreases, these results show that readily available pump power is more than enough to make the pulse energy limited by radiative losses to parasitic inter-pulse emission (including ASE) rather than by nonradiative quenching losses.

4.6 Influence of composition, cluster size and pump direction

It is interesting to compare my results to those reported from EDFs with lower quenching. Note first that similar Er^{3+}-concentrations as in my partly-quenched EDFs are possible with less quenching, as demonstrated with a P_2O_5:Al_2O_3:SiO_2 glass matrix [14] (I estimate the fraction of unsaturable absorption to be half of that in FUT #1). This allowed for pulse amplification with relatively high efficiency (8.4%) in a 1.7-m long EDF with a 35-μm core to 84 kW in 2-ns pulses [14] (energy extraction ~0.1 μJ/μm^2/m). Thus, it is clear that the relation between Er^{3+}-concentration, quenching, and unsaturable absorption is not unique. I also investigated a second partly-quenched EDF (FUT #6). Those investigations showed that the relation between the unsaturable absorption and the impact on high-energy pulse amplification is not unique, either. Although it had a lower fraction of unsaturable absorption (12% at 1536 nm) than the first partly-quenched EDF presented in this chapter, I could not extract high pulse energy. It is possible that it suffers from exceedingly fast quenching by direct exchange [22, 23]. This was an experimental nanoparticle-doped aluminosilicate EDF [44]. Nanoparticle-doping can reduce the quenching, but this EDF was selected for its unusually high quenching, and it is possible that also the quenching characteristics differ from those in EDFs fabricated in other ways. A hypothesis is that when the fabrication of a NP-doped fibre preform is unsuccessful, it leads to pairs or perhaps larger clusters of Er^{3+}-ions with very small separation and thus to fast quenching. Note here that for paired ions, according to the model of quenching, it is possible to excite half of the ions even if the quenching process occurs instantaneously (when both ions become excited). It is therefore possible to reach gain also in such paired ions for wavelengths longer than the zero-phonon wavelength of 1530 nm. At 1560 nm, this requires a 0.98-μm pump intensity of 0.13 mW/μm^2, to excite 36% of the paired ions, under the assumption of standard cross-sections and unquenched lifetime, and instantaneous quenching. This intensity translates to as little as 1.5 W of pump power in my fibre. Higher pump power as well as a non-zero quenching time are expected to increase the gain from paired ions, whereas larger

clusters would be expected to exhibit less gain (if any), under the assumption that only one ion per cluster can be excited. This suggests that EDFs that do not show any gain are quenched by larger clusters or other defects or impurities such as OH. Detailed spectroscopic studies beyond the scope of this work are needed to evaluate such factors and the impact on high-energy pulse amplification.

Finally, I mention that at low repetition rates, the gain that can be reached during the build-up phase between pulses is independent of the pump direction, if the inter-pulse leakage from the seed source and feedback from the fibre ends are negligible. Furthermore, insofar as the FNE is accurate, the energy extraction depends on the total gain, but not on its distribution. Thus, it may be possible to achieve similar pulse energy with co-directional pumping as I have reached with counter-pumping. However, more energy is normally extracted from the output end of the fibre than from the input end. Co-pumping then requires the pump light to travel further through the partly quenched EDF to replenish the energy, and is therefore likely to be less efficient (i.e., the stored energy will recover more slowly at a given pump power).

4.7 Conclusions

In summary, these results demonstrate that short pulses can efficiently extract high energy from a partly-quenched high-concentration erbium-doped fibre amplifier, even though the fibre exhibits significant unsaturable absorption in the CW regime. I reached up to 0.8 mJ of output energy from a short (2.6 m) EDFA, which is 9.5 times the estimated saturation energy. Although such results have not been reported before as far as I am aware, the high energy extraction in a short pulse can be readily understood in terms of the dynamics of the quenching process. Thus, one can attribute the high energy achievable in this regime to the rapid extraction of stored energy, on time scales faster than the quenching dynamics. Thereby, the short high-energy pulses can saturate the absorption of ions which are unsaturable in the CW regime. This implies that insofar as it is possible to reach a high small-signal gain, it is possible to generate pulse energies of several times the saturation energy. I reached output energies within 1.5 dB of those predicted by the Frantz-Nodvik equation for the unquenched case. Furthermore, in some pulse regimes, the average-power conversion efficiency increased in ways that would not be expected for an unquenched EDF. On the other hand, the impact of the quenching on the average-power conversion efficiency was large, and led to a 7-dB degradation in the CW regime. Furthermore, the amplification of high-energy pulses was severely compromised in another EDF with partial quenching, and it is hypothesized that the quenching timescale may be much faster in that fibre. Further studies of the details of different quenching and parasitic processes (which may involve higher-lying energy levels [3]) in different regimes are needed to better understand the impact on high-energy amplification, and how it may depend on composition and fabrication details. Particularly interesting is to what extent the

positive results of high-energy pulse amplification in partly-quenched EDFs reported here carry over to hosts and fabrication approaches known for low quenching, at even higher Er-concentration where significant quenching reappears also in such hosts.

Furthermore, the question now would be if it is possible to improve the performance of this system by using a pulse-pumping laser source instead of a CW-pump. Previously, it was stated that it is easier to obtain higher CW-pump power than pump pulse energy at 980-nm. However, there have been cases where mJ-level energy sources at 976-nm operating wavelength have been achieved with ytterbium-doped fibre amplifiers (YDFA), taking advantage of their three-level laser transition ("zero-level transition") [38]. Details of this pulse pumping study are presented in the following chapter.

4.8 References

1. P. Myslinski, J. Fraser, and J. Chrostowski, “Nanosecond kinetics of upconversion process in EDF and its influence to EDFA performance”, Institute for Information Technology, National Research Council, 100/ThE3-1 (1995).
2. J. Li, Z. Dai, Z. Ou, L. Zhang, Y. Liu, L. and Liu, “Modeling and optimizing of low-repetition-rate high-energy pulse amplification in high-concentration erbium-doped fibre amplifiers”, Optics Communications **282**, 3577-3582 (2009)
3. V. Kir’yanov, Y. O. Barmenkov, G. E. Romero, and L. E. Zarate, “Er^{3+} concentration effects in commercial erbium-doped silica fibres fabricated through the MCVD and DND technologies,” IEEE Journal of Quantum Electronics **49**, 511–521 (2013)
4. B. Desthieux, R. I. Laming, and D. N. Payne, “111 kW (0.5 mJ) pulse amplification at 1.5 µm using a gated cascade of three erbium-doped fiber amplifiers”, Appl. Phys. Lett. 63, 586-588 (1993).
5. V. Philippov, C. Codemard, Y. Jeong, C. Alegria, J. K. Sahu, J. Nilsson, and G. N. Pearson, “High-energy in-fiber pulse amplification for coherent lidar applications”, Opt. Lett. **29**, 2590-2592 (2004).
6. C. Codemard, C. Farrell, P. Dupriez, V. Philippov, J. K. Sahu, and J. Nilsson, “Millijoule, high-peak power, narrow-linewidth, sub-hundred nanosecond pulsed fibre master-oscillator power-amplifier at 1.55 µm”, Comptes Rendus Physique **7**, 170-176 (2006).
7. S. Desmoulins and F. Di Teodoro, “High-gain Er-doped fiber amplifier generating eye-safe MW peak-power, mJ-energy pulses,” Opt. Express **16**, 2431-2437 (2008).
8. E. Lallier and D. Papillon-Ruggeri, "High energy pulsed eye-safe fiber amplifier", in CLEO/Europe and EQEC 2011 Conference Digest, OSA Technical Digest (CD) (Optical Society of America, 2011), paper CJ1_5.
9. E.-L. Lim, S.-U. Alam, and D. J. Richardson, "Optimizing the pumping configuration for the power scaling of in-band pumped erbium doped fiber amplifiers," Opt. Express **20**, 13886-13895 (2012).
10. G. Canat, W. Renard, E. Lucas, L. Lombard, J. Le Gouët, A. Durécu, P. Bourdon, S. Bordais, and Y. Jaouën, “Eyesafe high peak power pulsed fiber lasers limited by fiber nonlinearity”, Opt. Fiber Technol. **20**, 678-687 (2014).
11. I. Pavlov, E. Dülgergil, E. Ilbey, and F. Ö. Ilday, "Diffraction-limited, 10-W, 5-ns, 100-kHz, all-fiber laser at 1.55 µm," Opt. Lett. **39**, 2695-2698 (2014).
12. L. Kotov, M. Likhachev, M. Bubnov, O. Medvedkov, D. Lipatov, A. Guryanov, K. Zaytsev, M. Jossent, and S. Février, "Millijoule pulse energy 100-nanosecond Er-doped fiber laser," Opt. Lett. **40**, 1189-1192 (2015).

13. J. W. Nicholson, A. DeSantolo, M. F. Yan, P. Wisk, B. Mangan, G. Puc, A. W. Yu, and M. A. Stephen, “High energy, 1572.3 nm pulses for CO_2 LIDAR from a polarization-maintaining, very-large- mode-area, Er-doped fiber amplifier”, Opt. Express **24**, 19961-19968 (2016).
14. M. M. Khudyakov, M. M. Bubnov, A. K. Senatorov, D. S. Lipatov, A. N. Guryanov, A. A. Rybaltovsky, O. V. Butov, L. V. Kotov, and M. E. Likhachev, "Cladding-pumped 70-kW-peak-power 2-ns-pulse Er-doped fiber amplifier," Proc. SPIE **10512**, Fiber Lasers XV: Technology and Systems, 1051216 (2018).
15. J. Nilsson and B. Jaskorzynska, "Modeling and optimization of low repetition-rate high-energy pulse amplification in cw-pumped erbium-doped fiber amplifiers", Opt. Lett. **18**, 2099-2101 (1993).
16. C. C. Renaud, H. L. Offerhaus, J. A. Alvarez-Chavez, J. Nilsson, W. A. Clarkson, P. W. Turner, D. J. Richardson, and A. B. Grudinin, “Characteristics of Q-switched cladding-pumped ytterbium-doped fiber lasers with different high-energy fiber designs”, IEEE J. Quantum Electron. **37**, 199-206 (2001).
17. L. M. Frantz and J. S. Nodvik, “Theory of pulse propagation in a laser amplifier,” J. Appl. Phys. 34, 2346–2349 (1963).
18. Y. Jaouen, G. Canat, S. Grot, and S. Bordais, “Power limitation induced by nonlinear effects in pulsed high-power fiber amplifiers”, Comptes Rendus Physique **7**, 163-169 (2006)
19. R. Wyatt, “Spectroscopy of rare earth doped fibres”, in Fiber Laser Sources and Amplifiers, Michel J. F. Digonnet, ed., Proc. SPIE 1171, 54-64 (1990).
20. B. J. Ainslie, “A review of the fabrication and properties of erbium-doped fibres for optical amplifiers”, J. Lightwave Technol. 9, 220-227 (1991).
21. W. J. Miniscalco, “Erbium-doped glasses for fiber amplifiers at 1500 nm,” J. Lightwave Technol. 9, 234–250 (1991).
22. D. L. Dexter, “A theory of sensitised luminescence of solids”, J. Chem. Phys. 21, 836-850 (1953).
23. M. Inokuti and F. Hirayama, “Influence of energy transfer by the exchange mechanism on donor luminescence”, J. Chem. Phys. 43, 1978-1989 (1965).
24. M. R. Brown, H. Thomas, J. M. Williams, R. J. Woodward, and W. A. Shand, “Experiments on Er3+ in SrF2. III. Coupled-ion effects”, J. Chem. Phys 51, 3321-3327 (1969).
25. F. E. Auzel, “Materials and devices using double-pumped phosphors with energy transfer”, Proc. IEEE 61, 758-786 (1973).
26. J. C. Wright, “Upconversion and excited state energy transfer in rare-earth doped materials”, in Radiationless Processes in Molecules and Condensed Phases (Topics in Applied Physics v. 15), F. K. Fong, ed. (Springer-Verlag, 1976), pp. 239-295.

27. V. P. Gapontsev and N. S. Platonov, "Migration-accelerated quenching in glasses activated by rare-earth ions", in Dynamical processes in disordered systems, W. M. Yen, ed. , Materials Science Forum 51, Aedermannsdorf, Switzerland (1989).
28. M. Shimizu, M. Yamada, M. Horiguchi, and E. Sugita, "Concentration effect on optical amplification characteristics of Er-doped silica single-mode fibers", IEEE Photonics Technol. Lett. 2, 43-45 (1990).
29. P. Blixt, J. Nilsson, T. Carlnäs, and B. Jaskorzynska, "Concentration dependent up-conversion in Er3+-doped fiber amplifiers: experiments and modeling", IEEE Photonics Technol. Lett. 3, 996-998 (1991).
30. Hiroji Masuda, Atsushi Takada, and Kazuo Aida, "Modeling the gain degradation of high concentration erbium-doped fiber amplifiers by introducing inhomogeneous up-conversion", J. Lightwave Technol. 10, 1789-1799 (1992).
31. E. Delevaque, T. Georges, M. Monerie, P. Lamouler, and J.-F. Bayon, "Modeling of pair-induced quenching in erbium-doped silicate fibers", IEEE Photonics Technol. Lett. 5, 73-75 (1993).
32. J. Nilsson, B. Jaskorzynska, and P. Blixt, "Performance reduction and design modification of erbium-doped fiber amplifiers resulting from pair-induced quenching", IEEE Photonics Technol. Lett. 5, 1427-1429 (1993)
33. J. L. Wagener, P. F. Wysocki, M. J. F. Digonnet, H.J. Shaw, and D. J. DiGiovanni, “Effect of concentration and clusters in erbium doped fiber amplifiers”, Opt. Lett. 18, 2014-2016 (1993).
34. M. K. Davis, M. J. F. Digonnet, and R. H. Pantell, “Characterization of clusters in rare earth-doped fibers by transmission measurements", J. Lightwave Technol. 13, 120-126 (1995).
35. E. Maurice, G. Monnom, B. Dussardier, and D. B. Ostrowsky, "Clustering-induced nonsaturable absorption phenomenon in heavily erbium-doped silica fibers," Opt. Lett. 20, 2487-2489 (1995).
36. P. Myslinski and J. Chrostowski, “Effects of concentration on the performance of erbium doped fiber amplifier”, J. Lightwave Technol. 15, 112–120 (1997).
37. B. N. Samson, W. H. Loh, and J. P. de Sandro, “Experimental evidence of differences in the absorption spectra of clustered and isolated ions in erbium-doped fibers”, Opt. Lett. 22, 1763-1765 (1997).
38. S. Tammela, M. Hotoleanu, K. Janka, P. Kiiveri, M. Rajala, A. Salomaa, H. Valkonen, and P. Stenius, "Potential of nanoparticle technologies for next generation erbium-doped fibers," in Optical Fiber Communication Conference, Technical Digest (CD) (Optical Society of America, 2004), paper FB5.

39. D. Boivin, T. Fohn, E. Burov, A. Pastouret, C. Gonnet, O. Cavani, C. Collet, and S. Lempereur, “Quenching investigation on new erbium doped fibers using MCVD nanoparticle doping process,” in Proc. SPIE 7580, 75802B–1 (2010).
40. B. J. Ainslie, S. P. Craig, S. T. Davey, and B. Wakefield, “The fabrication, assessment and optical properties of high-concentration Nd^{3+} and Er^{3+} doped silica-based fibres”, Mater. Lett. **6**, 139-143 (1988).
41. A. Le Sauze, C. Simonneau, A. Pastouret, D. Gicquel, L. Bigot, S. Choblet, A. M. Jurdyc, B. Jacquier, D. Bayart, and L. Gasca, "Nanoparticle Doping Process: towards a better control of erbium incorporation in MCVD fibers for optical amplifiers," in Optical Amplifiers and Their Applications, OSA Technical Digest Series (Optical Society of America, 2003), paper WC5.
42. A. Pastouret, C. Gonnet, C. Collet, O. Cavani, E. Burov, C. Chaneac, A. Carton, and J. P. Jolivet, "Nanoparticle doping process for improved fibre amplifiers and lasers", Proc. SPIE 7195, 71951X (2009)
43. I. Savelii, L. Bigot, B. Capoen, C. Gonnet, C. Chaneac, E. Burova, A. Pastouret, H. El-Hamzaoui, and M. Bouazaoui, “Benefit of rare-earth “smart doping” and material nanostructuring for the next generation of Er-doped fibers”, Nanoscale Res. Lett. 12:206 (2017).
44. C. Baker, E. J. Friebele, A. A. Burdett, D. L. Rhonehouse, J. Fontana, W. Kim, S. R. Bowman, L. B. Shaw, J. Sanghera, J. Zhang, R. Pattnaik, M. Dubinskii, J. Ballato, C. Kucera, A. Vargas, A. Hemming, N. Simakov, and J. Haub, “Nanoparticle doping for high power fiber lasers at eye-safer wavelengths”, Opt. Express 25, 13903-13915 (2017).
45. V. P. Gapontsev, S. M. Matitsin, A. A. Isineev, V. B. Kravchenko, "Erbium glass lasers and their applications", Optics and Laser Technol., pp. 189-196, August (1982).
46. A. I. Burshtein, "Energy transfer kinetics in disordered systems", J. Lumin. 34, 167-188 (1985).
47. Y. Feng, B. M. Zhang, J. Zhao, S. Zhu, J. H. V. Price, and J. Nilsson, “Absorption measurement errors in single-mode fibers resulting from re-emission of radiation”, IEEE J. Quantum Electron. 53, 6800611 (2017).
48. H. Zellmer, A. Tünnermann, H. Welling, and V. Reichel, "Double-clad fiber laser with 30 W output power," in Optical Amplifiers and Their Applications, M. Zervas, A. Willner, and S. Sasaki, eds., Vol. 16 of OSA Trends in Optics and Photonics Series (Optical Society of America, 1997), paper FAW18.
49. J. Nilsson, S. Alam, J. A. Alvarez-Chavez, P. W. Turner, W. A. Clarkson, and A. B. Grudinin, “High-power and tunable operation of erbium-ytterbium co-doped cladding-pumped fiber lasers,” IEEE J. Quantum Electron. **39**, 987–994 (2003).
50. S. P. Singh, and N. Singh, “Nonlinear effects in optical fibers: origins, management and applications”, Prog. Electromagnetics Res. 73, 249-275, (2007).

51. J. Li, Z. Dai, Z. Ou, L. Zhang, Y. Liu, L. Liu, “Modeling and optimizing of low-repetition-rate high-energy pulse amplification in high-concentration erbium-doped fiber amplifiers”, Opt. Commun. 282, 3577-3582 (2009).

Chapter 5 High Pulse Energy Extraction with Pulsed 0.98-µm Cladding-Pumping

This chapter discusses and presents simulations of 0.98-µm pulse-pumping of an EDF, and quantitatively compares this approach to CW-pumping. Motivation for this is provided by the exciting prospects suggested by the analysis of 1.53-µm cladding-pumping in Chapter 3 and the results obtained with 0.98-µm CW pumping in Chapter 4. It was also noted that cladding pumping at 1.53-µm presented some additional requirements on the EDF, compared to the more established 0.98-µm pumping. It is interesting to explore to what extent the advantages in those two regimes can be maintained with 0.98-µm cladding-pumping. Core-pumping is in principle interesting, too, but is not considered because of the lack of practical single-mode sources with high pulse energy at 0.98 µm. This is a consequence of the low saturation fluence at 0.98 µm, of Yb-doped fibre sources, which I consider to the most realistic pump option in this regime. of the Even with cladding-pumping, which allows for energy-scaling through the use of multimode pump sources, it is far from obvious that sufficient pump energy can be obtained. Another potential issue with 0.98-µm pulse-pumping is the possibility of bottlenecking in the pump-level ($^4I_{11/2}$).

As stated in Chapter 3, in a pulse-pumped system, when the pump pulses passes through the signal fibre amplifier (i.e., FUT), at the beginning of each pump pulse, the excitation level in the FUT starts rising quickly, then suffers a sudden short loss of excited ions at the end of the pump pulse as short-lived (quenched) ions relax. After that, the excitation decreases more slowly as normal ions relax until the next pump pulse arrives and the excitation levels quickly rise once again, repeating the process. The advantage over CW pumping is that the time-averaged excitation level is much lower, so quenching-losses to rapid nonradiative relaxation can be smaller. Furthermore, it may be possible to extract energy also from the (nominally) quenched ions, insofar as the pump pulses are able to excite them. Additionally, pulse-pump with low duty cycle helps to alleviate the heat load that could otherwise cause damage to the FUT at high PRF and pulse energy.

However, on the downside, a pulsed pump laser is normally more challenging and complex than a CW-pump laser. Pump pulse energy on the mJ-level or higher translates to pump peak powers from 100 W to those approaching MW-level. While the former is within the practical reach of pump diode lasers, the latter is not. Furthermore, for high-energy pump pulses at 0.98 µm, a fraction of Er^{3+}-ions would be in the pump-level ($^4I_{11/2}$) for a non-negligible amount of time, causing a significant fraction of these Er^{3+}-ions to remain in that level. This bottlenecking reduces the absorption efficiency of the EDF, requiring a longer fibre to compensate and it can also lead to pump-ESA.

In order to understand 0.98-µm pulse pumping of a highly doped erbium fibre, I simulated the following configurations:

A signal-EDF cladding-pumped at 0.98 µm with 2 mJ and 4 mJ, 10-µs-duration pump-pulses at 5-kHz PRF. The input signal energy is 10 µJ at 1560 nm in 1-µs pulses, synchronized with the pump pulses. The results were compared to those obtained with CW-pumping of the same average power (10 and 20 W).

An obvious choice for a pulsed pump source at 0.98 µm is an Yb-doped fibre laser. However, although ytterbium ions (Yb^{3+}) have an emission peak at around 0.98 µm, the gain peak and emission normally occurs at wavelengths in the range 1.03 – 1.1 µm. By contrast, reabsorption at 0.98 µm in combination with competing quasi-four-level emission at longer wavelengths makes scaling of the average power at 0.98 µm much more limited. In addition, its low saturation fluence at 0.98 µm (less than 0.1 µJ/µm^2) limits the pulse energy. Therefore, pulsed sources based on YDFAs have been limited to around 1 mJ [1], and generally at average powers that are closer to 10 W than 100 W. Therefore, for these simulations, limited pump energies of 2 and 4 mJ at 0.98 µm are reasonable starting points for this investigation into pulsed cladding-pumping at 0.98 µm.

The simulated FUT is a double-clad EDF, assumed D-shaped, with a 10-µm core diameter and an inner cladding / core area ratio (i.e., A_{clad}/A_{core}) of 16 to 36. The FUT has an Er-concentration of 5×10^{25} ions / m^3. The lifetime of quenched Er-ions (i.e., the time for energy transfer between two excited ions that are close) is assumed to be 1 µs for all cases, unless otherwise specified. The pump-level lifetime is assumed to be 0.5 µs, which is short compared to the pump pulse duration. The simulations model quenching dynamics as arising from Er^{3+}-ions in pairs. As such, for example, "50% Er-quenching" means that 50% of Er^{3+}-ions are treated as paired-ions).

The pump source is investigated in the next chapter. Here, it suffices to note that experimentally, a double-clad ytterbium doped fibre (YDF), with a 300 µm core diameter and a 400-µm diameter shaped cladding did reach the assumed pump parameters. This is based on the recently developed large-core fibres (e.g., XLMA fibres up to 300 µm core diameter), which are currently being used to reach higher pulse energies in the range 1.03 – 1.1 µm. At 0.98-µm, the large core will help to compensate for the low saturation fluence at the 0.98 µm wavelength, at the expense of beam quality.

5.1 Results of Simulations and Discussion

Figure 6.1 shows the FUT performance in pulse-pumping and CW-pumping configurations, where only the fiber length and pump wavelength were optimized for best performance for each case.

The "energy ratio" is calculated by Eq. 5.1, where "pulse-pump energy" represents the signal output energy extracted on the pulse-pumping configuration, and the "CW-pump energy" represents the signal output energy extracted on the CW-pumping configuration.

$$Energy\ ratio = {Pulse - pump\ \ energy}/{CW - pump\ energy} \tag{5.1}$$

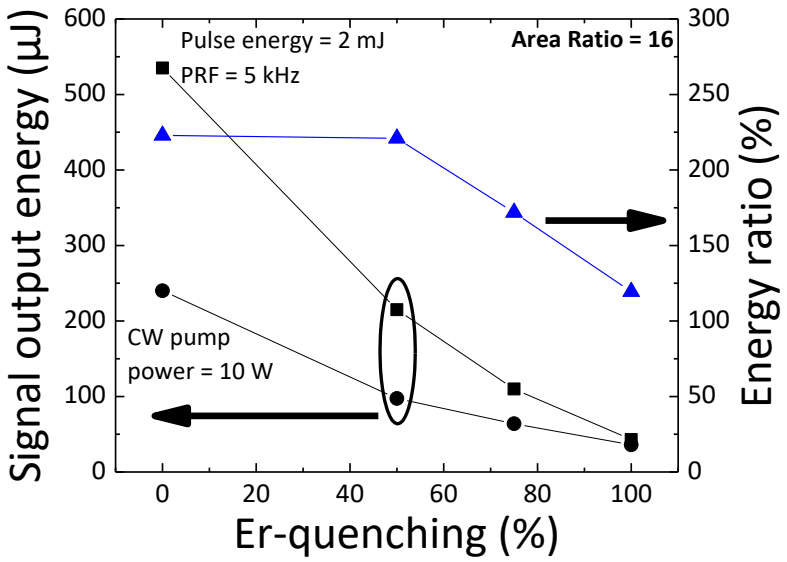

Figure 5.1 Signal output energy at 1560-nm at different percentage of Er^{3+}-ions suffering from "concentration quenching" using a 2-mJ pump pulse energy and a CW-pump power of 10-W.

From Fig. 5.1, the pulse-pumping achieved 2.2 times (i.e., 220% energy ratio) the extractable energy compare to the CW-pump system at 50% quenched ions, as well as 1.2 times the extractable energy at 100% quenched ions.

The improvement at quenched ions 100% seems marginal. This could be partly attributed to the lack of pump energy (e.g., 2 mJ), which cannot build up enough gain amongst the quenched ions.

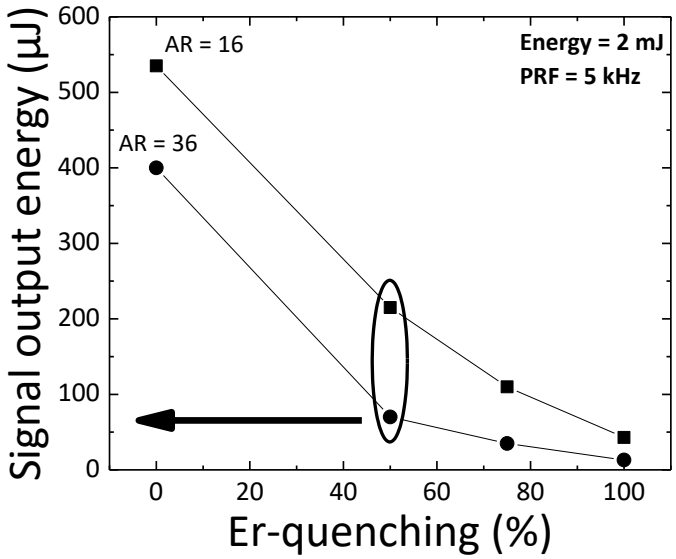

Figure 5.2 Signal output energy at 1560-nm at different percentage of paired Er^{3+}-ions (thus affected by "concentration quenching") using area ratios of 16 and 36.

In addition, the area ratio is significant. See Fig. 5.2. A pump-pulse energy of 2 mJ may work reasonably well for an area ratio of 16, but not for 36 or higher.

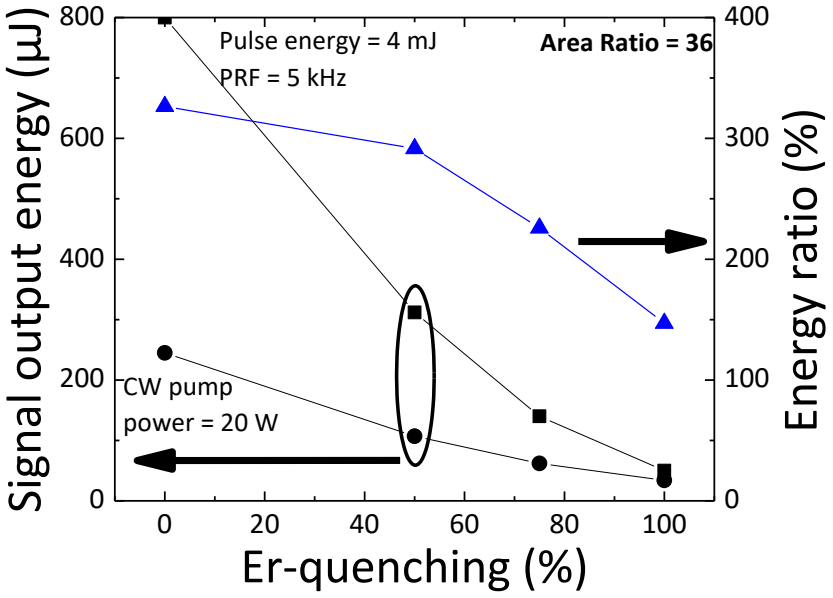

Figure 5.3 Signal output energy at 1560-nm at different percentage of Er^{3+}-ions suffering from "concentration quenching" using a 4-mJ pump pulse energy and a CW-pump power of 20 W.

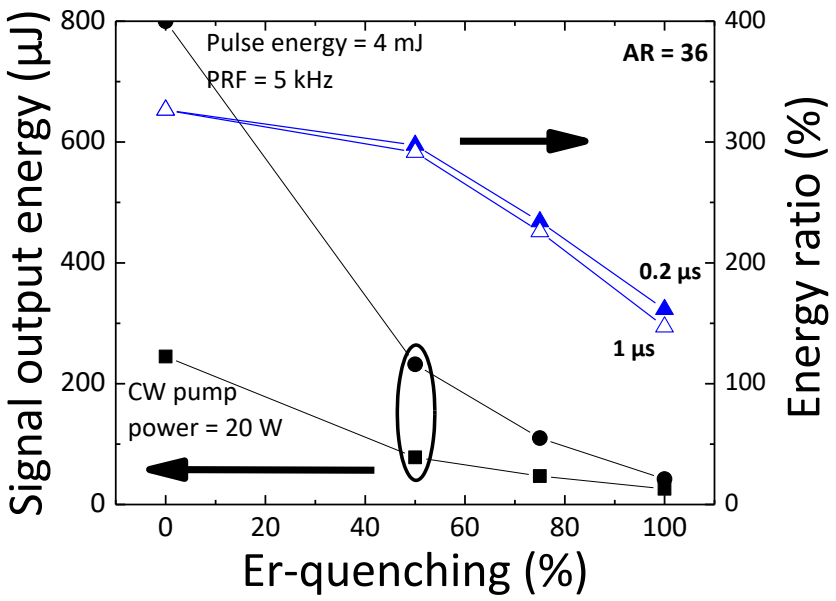

Figure 5.4 Performance of the pulse-pump and CW-pump systems at different quenching time scales (e.g., 1 and 0.2 µs)

Fig. 5.3 shows results with an area ratio of 36 with 4 mJ-pumping, as well as the corresponding CW-pumping. At an area ratio of 36, the increase of CW-pump power from 10-W to 20-W does not show significant improvement, whereas the pump pulse energy of 4 mJ performs much better, achieving 1.5 times the extractable energy of the 20-W CW-pumping case at 100% quenched ions.

Next, from Fig. 5.4, the extractable energy with 100% quenched ions for pulse pumping decreases from 50-µJ to 42-µJ when the quenching time scale is reduced from 1-µs to 0.2-µs. By contrast, it increased from 1.5 to 1.6 times higher extractable energy compare to CW-pumping. This suggests that pulse-pumping remains seemingly unaffected by faster lifetime quenching. Even though this will not be true for other choices of parameters, nor in fully optimized systems, it is still surprising.

Following up from the results in Chapter 4, using the FUT #1 (NRL-160415) characteristics as a template for the simulations, the results in Fig. 5.5 and 5.6 show the performance between the CW-pump and pulse pumping at different fraction of ion pairs and lifetime quenching (e.g., quenching time scales), which are reported to be in the range of 50 ns – 10 µs [2].

For the CW-pumping configuration, the launched pump power is 60 W when seeded by 0.2 µs, 25 µJ pulses at 2 kHz PRF. For the pulse-pumping configuration, the launched pump energy is 7 mJ, 10 µs pulses when seeded by 0.2 µs, 25 µJ pulses at 5 kHz PRF (a reasonably high pump energy that seemed theoretically plausible using an XLMA YDFA).

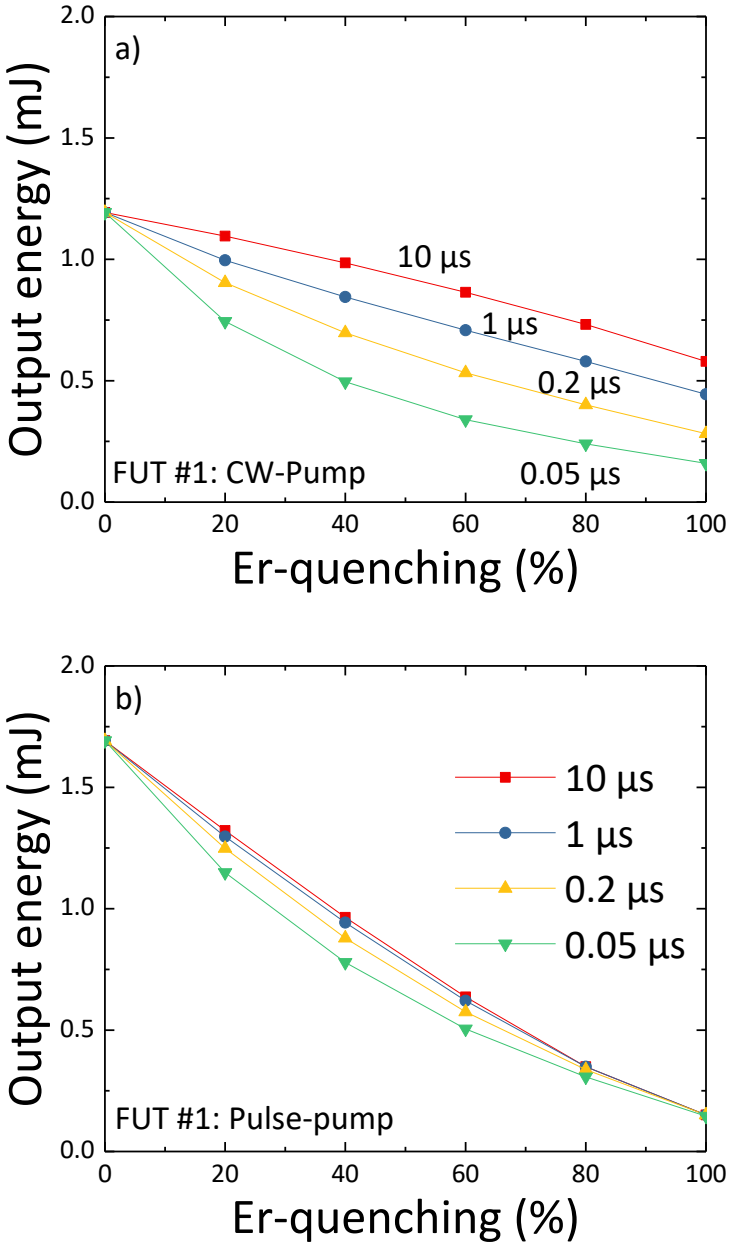

Figure 5.5 Performance of the pulse-pump and CW-pump systems at different quenching time scales (e.g., from 10 to 0.05 µs) on the FUT #1.

The results presented in Chapter 4 (i.e., 0.8 mJ of pulse energy at 2 kHz PRF, 0.2 µs pulse duration) are shown in Fig. 5.5 (a), assuming a lifetime quenching of 1 µs and 50% quenched ions in the FUT #1. Fig. 5.5 (a) shows significant changes in the output energy at 1560 nm depending on the lifetime quenching. According to these results, for the same lifetime quenching (i.e., 1 µs) at 50% Er-quenching, the pulse pumping system reached around 0.9 mJ of output pulse energy at 1560 nm in the FUT #1, a marginal improvement over the CW-pump performance (i.e., 0.8 mJ).

Additionally, it is clear that the CW-pumping configuration strongly depends on the lifetime quenching for energy extraction. The gain losses comparing the output energy at 10 µs and 0.05 µs (or 50 ns) lifetime quenching is over 5.5 dB, whereas pulse pumping has a maximum 1 dB loss.

5.2 Conclusions

In summary, the results of my simulations indicate a significant improvement in the extractable energy by using pulse-pumping instead of CW-pumping. However, previous results discussed in Chapter 4 demonstrated that short signal pulses can efficiently extract high energy from a partly-quenched (e.g., 20% quenched ions) high concentration erbium-doped fibre amplifier, reaching up to 0.8 mJ of output energy which corresponds to 9.5 times the estimated saturation energy in the FUT #1. Furthermore, the pulse pumping system is expected to reach up to 0.9 mJ of output energy, which could be considered a marginal improvement over the current CW-pump system presented in Chapter 4. From these simulations, it is safe to assume that the current FUT #1 has already been optimized in terms of extractable energy with the CW-pump system. However, the results also indicate that CW-pumping is more susceptible to short lifetime quenching, whereas pulse-pumping performance remains significantly ineffective by it.

In other words, the CW-pumping setup described in Chapter 4 have essentially stored (and subsequently extracted) high energy with the partly quenched, highly erbium-doped fibre pumped at 0.98-µm. Despite the constant losses of energy in the CW-regime and the low average power efficiency, which is further degraded by concentration quenching.

Even if pulse-pumping turns out not to be able to offer significantly higher extractable energy from FUT #1, pulse-pumping can offer an improvement in terms of lower inter-pulse ASE, alleviation of heat load and lower inter-pulsed ASE in regards on the quenching dynamics (e.g., 10 µs), by making the pumping time much shorter (e.g., comparable to the lifetime quenching). This could in turn improve the low average power efficiency of the system.

However, it is not clear if there is any real advantage on using pump pulses shorter than 10 µs. Part of the issue is because when pumping with 0.98-µm, a lot of Er^{3+}-ions remain in the $^4I_{11/2}$ energy level for a non-negligible amount of time (e.g., µs-level). The lack of clarity in the spectroscopy, in both quenching and high-power regime, could potentially hinder additional claims for the pulse pumping simulations without experimental data to go along with the simulations.

In summary, although obtaining higher pump energy at 0.98-µm may present more challenges compare to reach higher CW-pump powers, pulse pumping may still become more efficient in terms of alleviate heat load on the FUT, in addition to reducing the inter-pulse ASE and concentration quenching losses. Furthermore, it is possible to achieve higher pump energy at 0.98-µm (e.g., mJ-level) through the use of an ultra large core, ytterbium-doped fibre amplifier configuration [1].

5.3 References

1. Johan Boullet, Romain Dubrasquet, Capucine Médina, Ramatou Bello-Doua, Nicholas Traynor, and Eric Cormier, "Millijoule-class Yb-doped pulsed fibre laser operating at 977 nm," Opt. Lett. 35, 1650-1652 (2010).
2. P. Myslinski, J. Fraser, and J. Chrostowski, “Nanosecond kinetics of upconversion process in EDF and its influence to EDFA performance”, Institute for Information Technology, National Research Council, 100/ThE3-1 (1995)

Chapter 6 Millijoule-level Ytterbium-Doped Pulsed Fibre Amplifier Operating at 0.98-µm

This chapter demonstrate the advantages of using a large core ytterbium doped fibre. The amplifier configuration uses a co- and core-pumping scheme, on a 1-meter fibre length, delivering microsecond pulses (e.g., 10 µs) at adjustable pulse repetition frequency (e.g., 1 kHz) on an ultra-large core (i.e., 300-µm core diameter) ytterbium doped fibre.

6.1 Ytterbium Doped Fibre Amplifier Configuration

Ytterbium-doped fiber amplifiers (YDFAs) and lasers are renowned for their superb efficiency and power-scalability [1, 2], and have reached over 100 mJ of pulse energy and MW-level of peak power [3] in the pulsed regime. However, although ytterbium ions (Yb3+) have an emission peak at around 980 nm µm, these results are generally obtained at wavelengths in the range 1030 – 1100 nm. By contrast, reabsorption at 980 nm in combination with competing quasi-4-level emission at longer wavelengths makes scaling of the average power at 980 nm much more limited [4]. In addition, pulse-energy scaling is hampered by the low saturation fluence at 980 nm (~0.05 µJ/µm2 at the 980-nm emission peak in aluminosilicate, compared to, e.g., ~0.2 µJ/µm2 at the secondary peak at 1030 – 1040 nm, and ~0.4 µJ/µm2 at 1064 nm). This is a consequence of the large peak absorption and emission cross-sections. Therefore, to date, pulsed sources based on Yb-doped fibres (YDFs) have been limited in power to 78 W with 0.4-mJ pulse energy [5]. Nearly 1 mJ could be reached at lower repetition rates, but then with large levels of amplified spontaneous emission (ASE) [5]. These results were obtained from an YDFA with an 80-µm diameter core which although large, generated a high beam quality (M2 = 1.3) thanks to a rod-type fiber design with a low NA. On the other hand, recently-developed large-core fibres (including so-called XLMA fibres with up to 300-µm core diameter) are currently explored as a route to high pulse energy at [6], albeit at the expense of beam quality. Materials processing is the most prominent application of such sources. As the precise wavelength is not critical, they generally emit at wavelengths in the 1000 – 1100-nm range. However, although 980-nm operation much more challenging, it is also an attractive pump wavelength, e.g., for erbium, Although those are normally pumped by continuous-wave (CW) diode-lasers (DLs), pulse-pumping may be attractive for generation and amplification of high-energy pulses for erbium-doped fiber devices that suffer from quenching. For this, DLs are limited by their relatively low instantaneous power.

In this chapter, I use a XLMA YDFA with a 290-µm diameter aluminosilicate core to amplify pulses from a DL at 980 nm. The YDFA is pumped by another DL, at. Thanks to the large core of the YDF and the high brightness of the 915-nm pump, it is possible to core-pump the YDFA, to enable high pump intensity, absorption, and ultimately efficiency.

6.1.1 Design of the pulsed-YDFA

The YDF we consider is a commercial fiber (Nufern, XLMA-YTF-300/400/480), with a 0.11-NA Yb: aluminosilicate core measured to 290-µm diameter, inside an octagonal first (inner) cladding with a 400-µm flat-to-flat diameter and 0.22 NA and a second cladding of 480-µm flat-to-flat diameter. This was coated by a low index polymer and has an NA of 0.46. Thus, light can propagate throughout the glass structure, but we will use core-pumping. Although the absorption and emission cross-section spectra we use for design and simulations both peak at 976 nm, the gain peak is shifted to 977 nm. The saturation energy E_{sat} of the fiber is calculated to ~3.22 mJ at 977 nm and ~4% lower at 976 nm. With a fluorescence lifetime of 0.8 ms for Yb^{3+}:aluminosilicate, the (intrinsic) saturation power at 977 nm becomes 4.02 W. From this, a gain slope of 1.08 dB/W (with respect to absorbed pump power) can be calculated. The core absorption was measured with white light to 115.5 dB/m at 915 nm and 165 dB/m at the peak at ~976 nm, although at least the higher of these values seems reduced by nonuniform absorption effects. Insofar as the 915-nm absorption is accurate, the Yb^{3+}-concentration becomes ~4.32×10^{25} m^{-3}. Gain at ~976-nm (the zero-phonon wavelength) requires that at least 50% of the Yb-ions are excited. At this minimum excitation, the power lost to becomes 387 W/m, as recalculated to the pump wavelength. This indicates that it is important that the fiber is not overlength. More generally, for any fiber, the fluorescence power at the excitation level that leads to transparency is proportional to the fiber length, and becomes much higher for 980-nm amplification than for 1060 nm The pump intensity should be at least 0.943 mW/µm^2 at 915 nm to reach 50% excitation everywhere in the fiber. This translates to 62.3 W of power across the core, everywhere along the fiber.

Our pump source is a 915-nm DL with a 200/220-µm, 0.22 NA pigtail (nLight model e24i). The maximum output power is 400 W, 95% of which is specified to propagate within an NA of 0.15. The resulting beam parameter product of 150 mrad × 0.1 mm = 15 mm mrad is well matched to the 110 mrad × 0.145 mm = 15.95 mm mrad of the core of the YDF. Thus, we assume that pump launch efficiency can reach 90% for a launched pump intensity of around 5.45 mW/µm^2. Thus, we will target a pump leakage of 62.3/360 = 17.3%, or –7.62 dB.

A high gain is required for amplification of high-energy pulses, since the extractable energy is proportional to the product of the saturation energy, which is low in a fiber, and the initial

logarithmic gain $G_{dB}^{initial}$. The initial gain may be limited by available pump power as well as parasitic emission such as spurious lasing amplified spontaneous emission (ASE). The power lost to ASE grows approximately exponentially with $G_{dB}^{initial}$, and the spontaneous emission that is captured by the core and thus seeds the ASE grows with the square of the NA. According to simulations, a pump intensity of 5.45 mW/µm^2 allows for ~40 dB of gain. However, spurious lasing may well occur at such high gain, and furthermore it is reached only asymptotically. Furthermore, spurious lasing is a distinct possibility at such high gain. Thus, although our calculations suggest that our pump intensity does not limit the achievable gain and thus the pulse energy, we choose to design the system for $G_{dB}^{initial}$ = 20 dB. This reduces the likelihood for spurious lasing and allows for a higher PRF and average power, through reduced losses to parasitic emission. The extractable energy becomes E_{sat} $G_{dB}^{initial}$ / 4.343 = 14.8 mJ.

A pump leakage of 7.783 dB at 915 nm and a gain of 20 dB at 977 nm fixes the average fractional excitation n_2 to 62.10%, when a pulse arrives, and the length of 0.145 m. We also note that at this excitation level, the logarithmic gain at the secondary peak at 1030 – 1040 nm is ~60% of that at. This suggests that parasitic emission need not be a problem.

6.2 Experimental setup

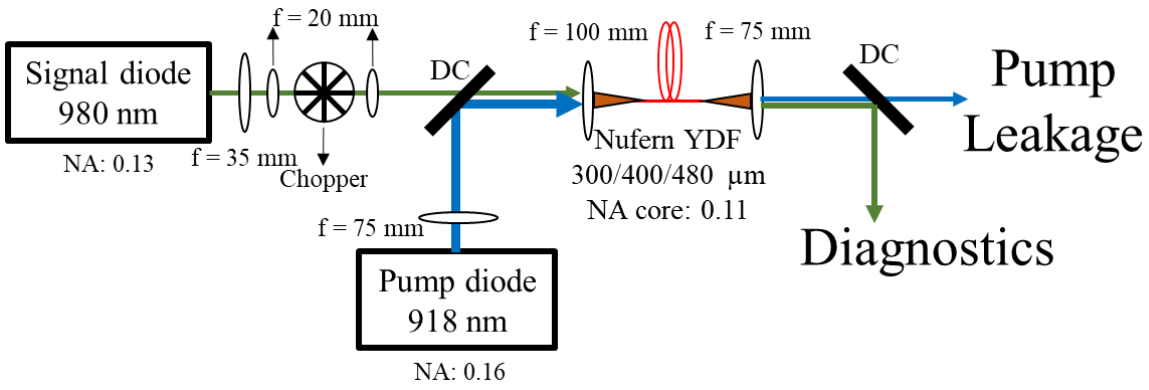

Figure 6.1 Experimental layout of the YDFA, co-directionally core-pumping

The experimental setup as shown in Fig. 6.1 (a) comprises a pump-DL at 915 nm as described above, a 980-nm DL to seed the amplifier, dichroic mirrors and lenses for coupling signal and pump light into and out of a 1-m-length of the YDF, in a co-pumped amplifier configuration, fibre length selected after experimental analysis, achieving the highest performance in terms of energy extraction. The output end of the YDF was angle-cleaved (~12°) to suppress feedback. This angle suffices to largely suppress feedback from the core into the first cladding, too, but signal light reflected at the output facet will be guided by the second cladding, since we did not attempt to strip this light. However, at sufficiently low gain in the core (e.g., 20 dB), the reduced overlap of

light guided by the second cladding is expected to suppress lasing on cladding-modes. The seed-DL (IPG PLD-70-974) is pigtailed with a 105/125-µm diameter fiber. It emits a CW beam with an NA of 0.13 and a maximum power of 50 W. This can be on-off-modulated by a mechanical chopper at kHz-level PRF. The pump-DL is driven quasi-CW by a power supply (TDK Lambda GEN50-30). Throughout, this is asynchronously on-off modulated by a waveform generator (Tektronix AFG1022) to produce 130-ms pump pulses at 1 Hz (duty cycle 13%). This mitigates the heat-load that could otherwise damage the YDF with CW operation. Quoted average powers compensate for the pump-modulation, i.e., they are averaged only for the time which the pump is on. Thus, reported average powers are nearly an order-of-magnitude higher than actual average powers. We used an InGaAs lightwave power meter (8153A model mainframe, 81533B module and InGaAs head 81525A, Hewlett-Packard) to measure power via the analog signal provided by the power meter. This was fed to an oscilloscope and calibrated., it was possible to measure the corresponding optical power in the temporal domain with a response time of 20 ms. For higher-bandwidth measurements, traces were captured with a photodetector connected to the oscilloscope. The traces were calibrated and pulse energies determined through integration (See Chapter 2.2).

I measured 70% of the pump power in the core at the output end, while 30% resided in the inner-cladding, out of overall launching efficiency of 90%. The pump leakage was measured to be 20%. I measured 70% of the leaked pump power as emerging from the core at the output end, by imaging the output as captured by a lens onto a camera. This captures also cladding-guided rays that are traversing the core at the output facet, so the fraction of the leaked power that is guided by the core is smaller. The other 30% emerged from the inner cladding. When we take the light outside the core into account, the pump power needed for 50% excitation at a fiber cross-section increases from 62.3 W to 89 W.

6.3 Results and Discussion

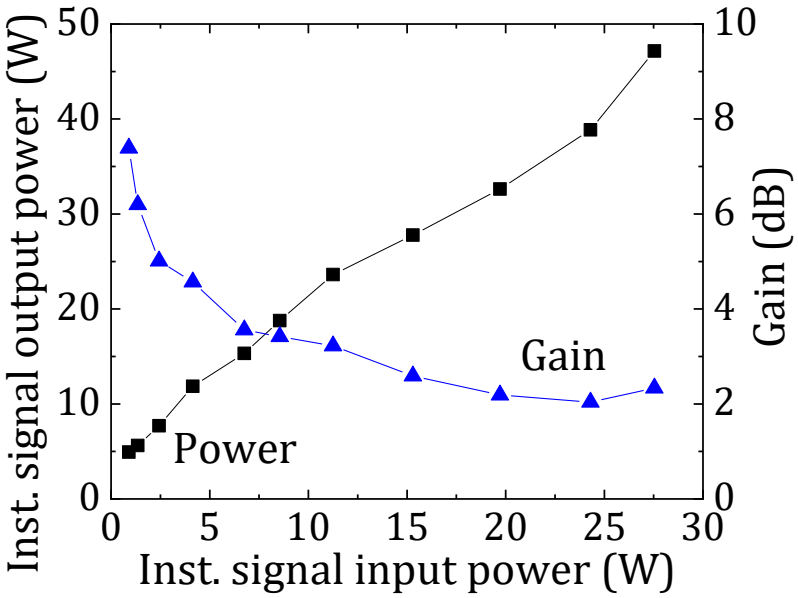

Figure 6.2 Instantaneous output power and gain at 980 nm as a function of launched input power (CW)

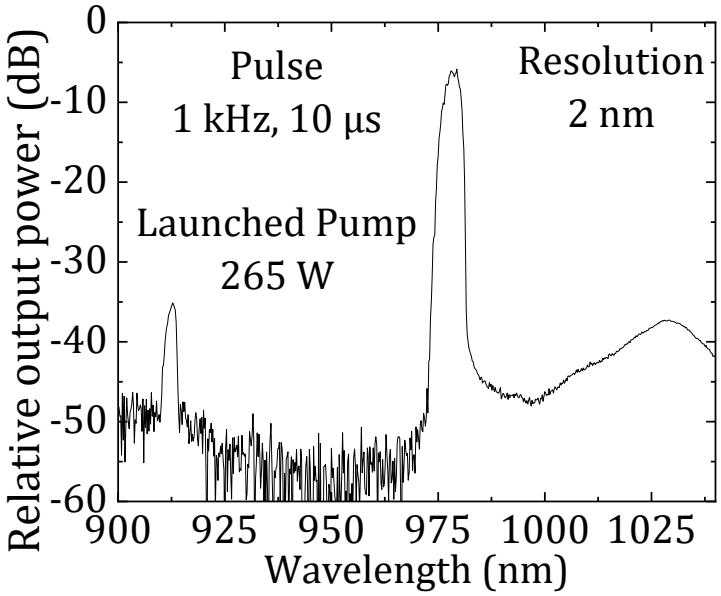

Figure 6.3 Optical spectra of signal pulse at 1 kHz repetition rate , 10 µs pulse duration , and launched constant quasi-CW pump instantaneous power of 265 W.

First, I assessed the efficiency with a CW seed signal of varying power. As always in this chapter, the pump was on-off modulated. The fiber reached transparency for 120 W of launched on-power. The power was then increased to 175 W. Then, the gain reaches 7.5 dB at a seed power of 0.9 W. The gain slope becomes 0.136 dB/W with respect to launched pump power (most of which is absorbed).

The signal output power reaches 47 W for 28 W of seed power, corresponding to 2.2-dB gain. The 19-W increase in signal power represents a pump conversion efficiency of 10.9%.

I then turned to pulsed seeding. Fig. 6.4 and 6.5 show results with 10-µs, 0.8-mJ seed pulses at 1 kHz PRF. The average seed power becomes 0.8 W and the peak power 80 W. From the optical spectra shown in Fig. 6.3, for a pump-on power of 265 W, we can observe that most of the power resides within the signal wavelength 980 nm (OSNR > 25 dB, spectral width of ~5 nm). The pulse output energy was 4.4 mJ, corresponding to 5.5 dB of high-energy gain.

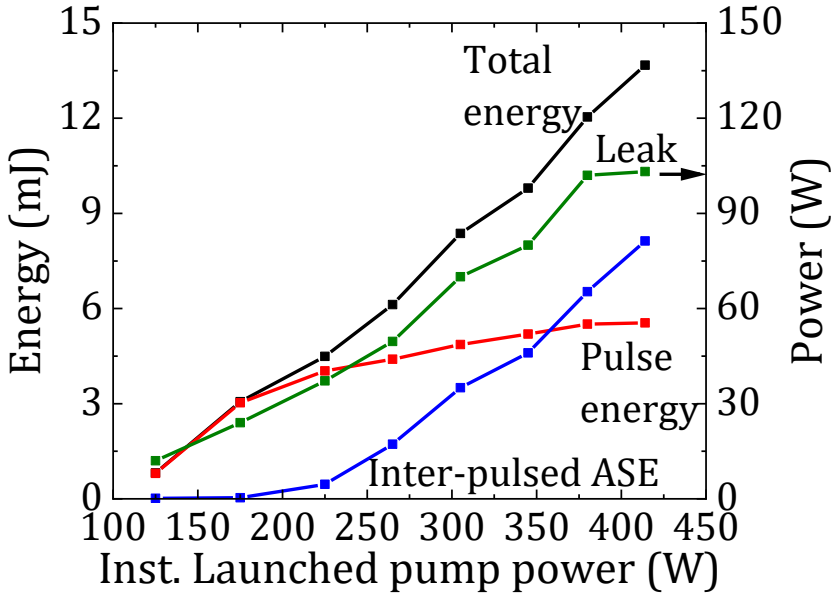

Figure 6.4 Output energy and leakage power at 0.98 µm at different launched pump powers.

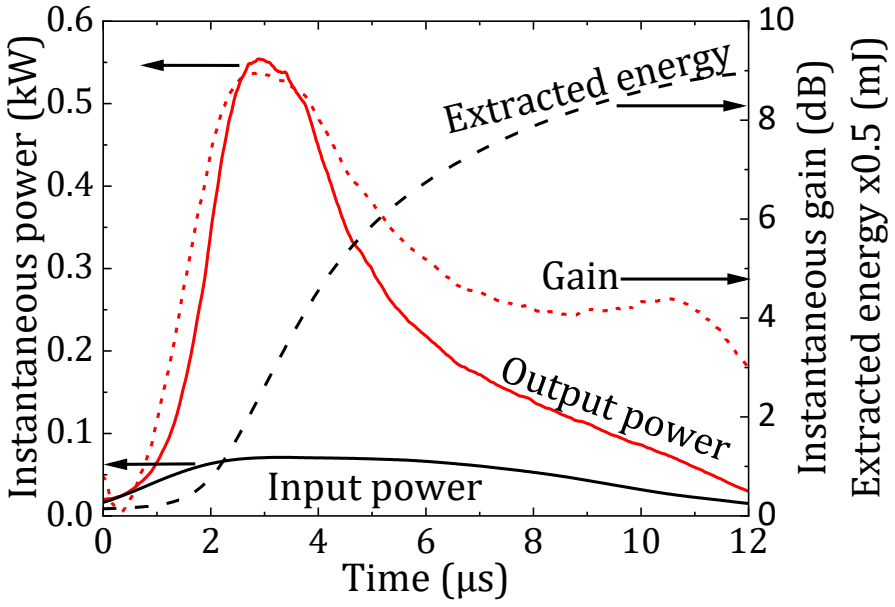

Figure 6.5 Instantaneous signal power and extracted output energy at maximum energy of 0.8 mJ.

Fig. 6.4 shows the total energy (measured based on the total average power measured with the power meter), output energy (measured based on the temporal traces and the average power within the pulse), inter-pulse ASE energies (energy between pulses) on left y-axis and pump leakage on the right y-axis at a constant seed avg. power of 0.8-W, at 1kHz, 10-µs signal pulses, as a function of launched instantaneous pump power. The maximum extracted energy becomes 4.7-mJ, for launched pump-on power of 414 W, which corresponds to a 17% pump conversion efficiency, despite the possible strong re-absorption at 0.98 µm expected from high-power YDFAs [1, 2].

The leakage shows that 103-W instantaneous launched pump power (i.e., ~20% of the launched pump power) is not being absorbed by the fiber. Additionally, at instantaneous launched pump power higher than 250-W, the inter-pulsed ASE becomes an issue (e.g., >20%). A higher PRF is expected to allow for lower ASE with only a minor drop in pulse energy.

Fig. 6.5 shows the instantaneous signal power and gain with the same signal seeding and launched pump-on power of 265 W. The highest achievable peak power is ~0.55-kW. Furthermore, the instantaneous gain drops by ~5 dB (or 1.15 Np) after reaching its peak gain (i.e., 9 dB), which implies that the YDFA configuration should have extracted at least ~6.5 mJ. Yet, the YDFA extracted 72% of the maximum extractable energy. This discrepancy is most likely due to the very strong inter-pulsed ASE (i.e., ~60%). Another explanation would be imperfect extinction between the pump power and signal power by the dichroic mirror used in the experiment, which could imply that a fraction of the extracted energy (~15%) is being neglected, and due to the much higher pump energy in the leakage output, an accurate calculation of the neglected signal energy may not be entirely accurate.

6.4 Conclusions

In summary, at the time of writing, these results demonstrated the advantage of an XLMA YDF, achieving over 5.5-mJ of pulse energy, at 1-kHz PRF, 10-µs pulse duration at 980 nm, using a 1-m fiber length. This simple core-pumping, amplifier configuration reached over 17% pump conversion efficiency at the pulsed-regime, and 27% at the CW-regime.

Additional experimental work at shorter fibre lengths, signal pulse duration and the PRF may prove to be of utmost important to reach even higher pulse energies and peak powers (e.g., kW-level) in the near future. Said YDFA configuration could make an efficient, high-power, pulse-pumping laser source in order to further study future partly quenched, highly doped erbium fibres with mJ-level pulse pump energies.

6.5 References

1. Y. Jeong, J. K. Sahu, D. N. Payne, and J. Nilsson, "Ytterbium-doped large-core fibre laser with 1.36 kW continuous-wave output power," Optics Express **12**, 6088-6092 (2004).
2. A. Liem, J. Limpert, H. Zellmer, A. Tunnermann, V. Reichel, K. Morl, S. Jetschke, S. Unger, H. R. Muller, J. Kirchof, T. Sandrock, and A. Harschak, "1.3 kW Yb-doped fibre laser with excellent beam quality," in Conference on Lasers and Electro-Optics, Vol. 96 of OSA Trends in Optics and Photonics Series (Optical Society of America, 2004), post deadline paper CPDD2.
3. F. D. Teodoro and C. D. Brooks, "Multistage Yb-doped fibre amplifier generating megawatt peak-power, sub nanosecond pulses," Optics Letters **30**, 3299-3301 (2005).
4. J. Boullet, Y. Zaouter, R. Desmarchelier, M. Cazaux, F. Salin, and E. Cormier, "Single mode fibre laser emitting 94 W at 977 nm," in Advanced Solid-State Photonics, OSA Technical Digest Series (CD) (Optical Society of America, 2009), paper TuA3.
5. J. Boullet, R. Dubrasquet, C. Médina, R. Bello-Doua, N. Traynor, and E. Cormier, "Millijoule-class Yb-doped pulsed fibre laser operating at 977 nm," Optics Letters **35**, 1650-1652 (2010).
6. R. Selvas, J. K. Sahu, L. B. Fu, J. N. Jang, J. Nilsson, A. B. Grudinin, K. H. Ylä-Jarkko, S. A. Alam, P. W. Turner, and J. Moore, "High-power, low-noise, Yb-doped, cladding-pumped, three-level fibre sources at 980nm," Optics Letters **28**, 1093-1095 (2003).

Chapter 7 Conclusions and Future Works

For this final chapter, I will summarize the results presented in this thesis, provide additional discussion and future research directions.

7.1 Summary

Chapter 3 investigated quenching dynamics and compared core-pumped amplifiers with pulses at 1535 nm based on a homemade, highly doped erbium fibre A0735-L10420 (FUT #3) and a commercial fibre I-12 (980/120) HC (FUT #4). The EDFs have a 14.4-µm (FUT #3) and 5.2-µm (FUT #4) core diameter respectively, both with a 125-µm-diameter cladding and a high-index polymer coating. The core absorption reached 130 dB/m for FUT #3 and 20 dB/m for FUT #4 at 1.53 µm.

Benefits of pulse-pumping of a highly-quenched erbium doped fibre (i.e., FUT #3) were demonstrated in an amplifier configuration, reaching a signal gain (i.e., 1.45-dB) 2.4 times higher through pulse-pumping compared to CW-pumping. However, a marginal increase of 1.45 dB is far from good. Much better results were demonstrated by the commercial erbium doped fibre I-12 (980/120) HC (i.e., FUT #4). This is not only attributed to the concentration quenching effects being negligible in low concentration fibres, but also the small core area increased the gain efficiency and compensated for the low pump pulse energy available (i.e., 25-µJ), leading to an improvement of the system.

Alternatively, one can conclude that the pump pulse energy and the core area need to be reasonably well matched. In this regard, FUT #4 was a better match to the core-pumping system than FUT #3. And while one of the aims of this research is to overcome the impact of concentration quenching, it is worth pointing out that an unquenched fibre will always win in terms of extractable energy. However, the final goal is not only overcoming quenching effects, but also keeping the fibre short in order to prevent optical nonlinearities that can appear in high-power regime.

Due to the lack of pulse energy, the predicted gain from the simulations are far from optimal, and it is unsure if pulse pumping would have been able to counteract the effects of quenching. Even with optimization of the pump source (e.g., larger core pump fibre to extract higher pump energy, and smaller core signal fibre to increase the gain efficiency), it was still unknown if I could achieve good results in the high power regime, as core-pumping system are usually limited to W-level pump powers. To move forward, simulations presented in Chapter 3 suggested that CW cladding-pumping at 0.98- µm with power up to ~50 W is a viable way to store the pump energy within the signal fibre amplifier despite the concentration quenching effects. This was also attractive because suitable

pump sources and EDFs were readily available. The results in Chapter 4 obtained with this approach demonstrate that short pulses can efficiently extract high energy from a partly-quenched high-concentration erbium-doped fibre amplifier at the cost of low pump conversion efficiency. This implies that insofar as it is possible to reach a high small-signal gain, it is possible to generate pulse energies of several times the saturation energy. The results showed up to 0.8-mJ of output energy from a short (2.6-m) EDFA, which is 9.5 times the estimated saturation energy. The high energy achievable in this regime is attributed to the rapid extraction of stored energy, on time scales faster than the quenching dynamics. By contrast, the CW and average-power conversion efficiency were low, although in some pulse regimes, the average-power conversion efficiency increased a little, which would not be expected for an unquenched EDF.

A further question is if it would be possible to improve the performance of this system by using a pulse-pump laser source instead of a CW-pump. Simulations explored the performance of pulse-pumping and CW-pump at different percentage of ions suffering from ETU and at different lifetime quenching range (i.e., 0.005 to 10 μs). Assuming I can reach high pulsed energy at 0.98 μm in a YDFA, simulations clearly show that in the presence of strong quenching dynamics, pulse-pumping reaches higher efficiency compare to CW-pumping. In a sense, pulse pumping shows > 1 dB gain loss while CW-pumping leads to > 5.5 dB loss.

Therefore, I designed and constructed an YDFA for the 0.98-μm wavelength to operate as the pump source for the EDFs. Thanks to the ultra-large core area from the YDF (which allowed for high energy extraction despite the low saturation fluence at the 0.98-μm), the core-pumping configuration (enabling high excitation level on shorter fibre length), the YDFA reached 5.5 mJ of pulse energy, which translated to 0.55 kW peak powers at 0.98-μm.

7.2 Future Works

At the time of writing, the CW-pump system presented in Chapter 4 shows the highest performance to date from a partly-quenched, highly doped erbium fibre. Additionally, according to the simulations presented in Chapter 5, this current system appears to have reached the maximum efficiency in terms of extractable energy from the FUT #1 (NRL-160415). Even with a pulse pumping system, the increase of output energy from 0.8 mJ to 0.9 mJ at 1.56-μm could be considered marginal.

Simulations have shown that the efficiency is strongly affected by the lifetime quenching (i.e., quenching time scales). Therefore, further studies of assessing the lifetime quenching in different highly doped erbium fibre may be vital to understand and estimate their performance. A viable way to achieve this is by continuing the study of ETU at 0.98-μm that can be observed at high Er-

concentrations (e.g., Fig. 2.8). By using a pulsed seed source at around 1.53-µm, with pulses shorter or close to the quenching time scale, it is possible to measure the upconversion lifetime at 0.98-µm and categorize EDFs in terms of lifetime quenching. Said lifetime could have different distribution of quenching time scales in a given fibre, depending not only on the Er^{3+}-concentration but also on the fabrication method (e.g., solution doping, nano-particle doping). This is particularly important, since it is unknown if the results reported in this thesis carry over to hosts and fabrication methods known for diminishing or lowering the effects of concentration quenching.

Additionally, to better understand the impact on high-energy amplification, further studies regarding different quenching and other parasitic processes, which may involve higher-lying energy levels (e.g., above $^4I_{11/2}$) are required.

Appendix A List of Publications

1. **P. G. Rojas Hernández**, C. Baker, S. Pidishety, M. Belal, Y. Feng, E. J. Friebele, A. Burdett, D. Rhonehouse, L. B. Shaw, J. Sanghera, and J. Nilsson, “High energy pulse amplification in partly quenched highly Er3+-doped fibre”, in Advanced Solid State Lasers 2018, OSA Technical Digest (online) (Optical Society of America, 2018), paper AM6A.16.
2. **P. G. Rojas Hernández**, C. Baker, S. Pidishety, M. Belal, Y. Feng, E. J. Friebele, A. Burdett, D. Rhonehouse, L. B. Shaw, J. Sanghera, and J. Nilsson , “Study of quenched Er^{3+}-ions in the high-power regime at CW and pulse pumping configurations. Northrop Grumman Mission Systems Research Symposium [Poster presentation in Baltimore, USA].
3. **P. G. Rojas Hernández**, C. Baker, S. Pidishety, M. Belal, Y. Feng, E. J. Friebele, A. Burdett, D. Rhonehouse, L. B. Shaw, J. Sanghera, and J. Nilsson, “Efficient extraction of high pulse energy from partly quenched highly Er3+-doped fibre amplifiers”, Opt. Express **28**, 17124-17142 (2020)

Other publications

1. Yutong Feng, **Pablo G. Rojas Hernández**, Sheng Zhu, Ji Wang, Yujun Feng, Huaiqin Lin, Oscar Nilsson, Jiang sun, and Johan Nilsson, "Pump absorption, laser amplification, and effective length in double-clad ytterbium-doped fibres with small area ratio," Opt. Express 27, 26821-26841 (2019)
2. Shankar Pidishety, Pranabesh Barua, Peter C. Shardlow, **Pablo G. Rojas Hernández**, Mohammad Belal, Yutong Feng, Naresh Kumar Thipparapu, Jayanta K. Sahu and Johan Nilsson, “Short-wavelength near-diffraction-limited beam, 792 nm cladding pumped efficient thulium-doped fibre laser in a power-scalable fibre design”, CLEO/EUROPE-EQEC 2019, 23-27 June 2019, Munich, Germany

Appendix B List of Fibres

Fibre under tests (FUTs):

Fibres ID	Dopant	Peak absorption (dB/m)	Core diameter (μm)	Cladding diameter (μm)	Pumping scheme
NRL-160415 FUT #1	Erbium	95 (@1.5 μm)	20	125	Cladding
NRL-170525 FUT #2	Erbium	36 (@1.5 μm)	45	264	Cladding
A0735-L10420 FUT #3	Erbium	130 (@1.5 μm)	14.4	125	Core
I-12 (980/125) HC FUT #4	Erbium	20 (@1.5 μm)	5.2	125	Core
XLMA-YTF-300/400/480 FUT #5	Ytterbium	13.4 (@0.915 μm)	300	400	Cladding

Appendix C Summary

CORE-PUMP

	980 nm	**1530 – 1550 nm (In-band pumping)**
CW	Perhaps interesting for devices (with tandem-pumping) Bottle-necking and pump-ESA in / from pump level are issues. Not studied.	Seems interesting for devices, especially if quenched ions can be excited. Possible pump source: EDFL @ 1530 – 1550 nm, fibre Raman laser @ 1480 nm. May be less interesting than 980-nm CW cladding-pumping because of the need for a more complex pump source without clear benefits. Not studied.
Pulsed	Tandem-pumping. Very limited pump pulse energy; uninteresting for devices. Not studied.	Tandem-pumping. Very limited pump pulse energy; achieved. My studies provide insight into potential performance of 15xx-nm pulsed cladding-pumping, which seems more interesting for devices.

CLADDING-PUMP

	980 nm	**1530 – 1550 nm (In-band pumping)**
CW	Interesting, has been studied and good results were obtained but with low power conversion efficiency (PCE). Diode-pumping possible (preferred). Polymer outer cladding is possible. Attractive for simplicity.	Seems interesting for devices, but advantages over 980-nm pumping are not clear. Possible pump sources: Diode laser, EDFL @ 1530 – 1550 nm, fibre Raman laser @ 1480 nm. Loss in polymer → polymer-free pump waveguiding needed. May be less interesting than 980-nm CW cladding-pumping because of the need for a worse or more complex pump source & fibre without clear benefits. Not studied.
Pulsed	Interesting to improve PCE. Tandem-pumping required to reach adequate pulse energy. Polymer outer cladding should be possible. Bottle-necking and pump-ESA in / from pump level are issues. In progress.	Perhaps most interesting. Tandem-pumping with EDFL required. 1530 nm likely to be best pump wavelength. All-glass pump waveguide & large pump overlap likely to be required. Not studied but I would like to.